ABSTRACT

SEDIMENTOLOGY AND STRATIGRAPHY OF DIATOMACEOUS SEDIMENTS IN THE CASMALIA HILLS AND ORCUTT OIL FIELDS IN THE SANTA MARIA BASIN, CALIFORNIA

By

Daniel Torn

May 2014

Two industry acquired diatomite cores (Sisquoc Formation) from the Orcutt (Newlove 76-RD1) and Casmalia Hills (Stokes A-30804) oil fields were analyzed by core descriptions, laboratory analysis (XRD and SEM), and gamma ray logs. Based on these data, five distinct lithofacies, nine sedimentary features and compositional trends of both cores were established. Newlove 76-RD1 and Stokes A-30804 record an upward-shallowing succession at different depositional positions on the Pliocene paleo-slope of the Santa Maria basin. Stokes A-30804 reflects slope deposition on a lower flank of a paleo-bathymetric high receiving higher detrital influx from inter-ridge troughs. Slope deposition of Newlove 76-RD1 was closer to a paleo-bathymetric high where purer diatomaceous sediments accumulated. Within Stokes A-30804, purer opal-A dominant lithofacies contain the highest oil saturations. The diagenesis and precipitation of opal-CT and abundance of phyllosilicate significantly hinders oil saturation within lithofacies.

SEDIMENTOLOGY AND STRATIGRAPHY OF DIATOMACEOUS SEDIMENTS IN THE CASMALIA HILLS AND ORCUTT OIL FIELDS IN THE SANTA MARIA BASIN, CALIFORNIA

A THESIS

Presented to the Department of Geological Sciences

California State University, Long Beach

In Partial Fulfillment

of the Requirements for the Degree

Master of Science in Geology

Committee Members:

Richard J. Behl, Ph.D., (Chair)
Tom Kelty, Ph.D.
Robert D. Francis, Ph.D.

College Designee:

Robert D. Francis, Ph.D.

By Daniel Torn

B.S., 2011, San Diego State University

May 2014

WE, THE UNDERSIGNED MEMBERS OF THE COMMITTEE,

HAVE APPROVED THIS THESIS

SEDIMENTOLOGY AND STRATIGRAPHY OF DIATOMACEOUS SEDIMENTS IN THE CASMALIA HILLS AND ORCUTT OIL FIELDS IN THE SANTA MARIA BASIN, CALIFORNIA

By

Daniel Torn

COMMITTEE MEMBERS

Richard Behl, Ph.D. (Chair)	Geological Sciences
Tom Kelty, Ph.D.	Geological Sciences
Robert D. Francis, Ph.D.	Geological Sciences

ACCEPTED AND APPROVED ON BEHALF OF THE UNIVERSITY

Robert D. Francis, Ph.D.
Department Chair, Department of Geological Sciences

California State University, Long Beach

May 2014

ACKNOWLEDGEMENTS

Dr. Rick Behl--There are no words to describe how much you have affected my life and future. Thank you for the opportunity to work with you. You are passionate, intelligent, and you make the world a much better place. I will forever be in your debt.

My Family (Kim Torn, Sam Torn, Touphie Torn, Toulip Torn, and Vanessa Torn) --To be where we are today from where we started is nothing short of a miracle. From escaping the Khmer Rouge concentration camps to our survival in America is a story of its own. Education, hard work, and our love for each other were our only hopes to attain the American dream. I am beyond astonished by our collective achievements and even more enthusiastic for our futures. I am so proud, blessed, and honored to have the opportunity to continue our legacy for the future generations.

CSULB Geology Staff Members--Thank you for your support. Special thanks to Dr. Francis and Dr. Kelty for your roles as members of my thesis committee.

MARS Consortium Affiliates--I appreciate all of your support in our research. Special thanks to Jon Kuespert at BreitBurn and Mark Wilson at Santa Maria Energy for giving us the opportunity to use and publish the data from your cores.

Lastly, thank you to all who supported and believed in me throughout my young and developing years. You all know who you are and I appreciate every one of you.

TABLE OF CONTENTS

Page

CHAPTER Page

LIST OF TABLES

TABLE Page

LIST OF FIGURES

FIGURE Page

FIGURE Page

FIGURE Page

CHAPTER 1

INTRODUCTION

Unconventional petroleum plays (for example, low permeability, organic-rich shale) have become vital to maintain or expand hydrocarbon production as most conventional accumulations have been discovered and exploited (United States Geological Survey [USGS], 2012). A rare type of unconventional reservoir --diatomite-- has been exploited exclusively in California. Yet, diatomaceous sedimentary deposits are not unique to this region and a greater understanding of the depositional environments, facies, and related variations in physical properties of these diatomaceous sediments is important for further development and exploitation in California and elsewhere.

Diatomaceous sediments in general are highly porous (~50-75%), biosiliceous, and organic-rich deposits that are primarily composed of diatom frustules, silicoflagellates, and radiolarians, and may contain calcareous microfossils and detrital minerals. These deposits primarily formed on coastal upwelling zones situated within cold high-latitude settings (Ingle, 1981b). Diatomaceous sediments are found all over the world (i.e., Iceland, Turkey, Namibia, and Antarctica) (Ingle, 1981b; Mahood and Barron, 1996; Pole, 1996; Mees, 2002; Durham, 1973; Gürel and Yildiz, 2007; USGS, 2012), but a conspicuous deposit of these sediments occurred as a belt of Neogene diatomaceous strata along the Pacific Rim including the Sea of Japan, Bearing Sea, Gulf of Alaska, Guyamas Basin, coast of Peru and down to the coast of northern Chile (Ingle,

1981b). In California, diatomaceous deposits are chiefly found within Miocene to lower Pliocene strata throughout numerous basins (i.e., Los Angeles, Ventura, Santa Barbara, Salinas, and San Joaquin); however, these deposits vary in terms of depositional environment, thickness, and composition (Bramlette, 1946; Ingle, 1981a; Gorsline, 1992; Isaacs and Ruellkötter, 1999). This study will aid in understanding these aspects within of the Santa Maria basin.

The Santa Maria basin is one of the most prolific petroleum provinces in California (onshore and offshore) with over one billion barrels of produced oil (California Division of Oil, Gas, and Geothermal Resources, 2010). Historically, the main oil producing zone was within naturally fractured reservoirs of the Miocene Monterey Formation (Woodring and Bramlette, 1950). Recently, there have been increasing quantities of oil recovery from diatomaceous sediments within the Miocene upper Monterey and upper Miocene to lower Pliocene Sisquoc formations due to the development of enhanced oil recovery techniques such as cyclic steam injection. These methods allow production of heavy oil from low permeability, but highly porous diatomite facies. Consequently, there is growing interest in, and focus on, previously non-producible diatomaceous sediments.

The Santa Maria basin diatomite facies (highly porous biosiliceous deposits) varies in clay and other detrital content, sedimentary fabric, and interbedded lithologies because of the complex and irregular bathymetry during its deposition on a tectonically deformed active continental margin (Behl, 1999). These variations in depositional environment of the Sisquoc (Ramirez and Garrison, 1995) and upper Monterey

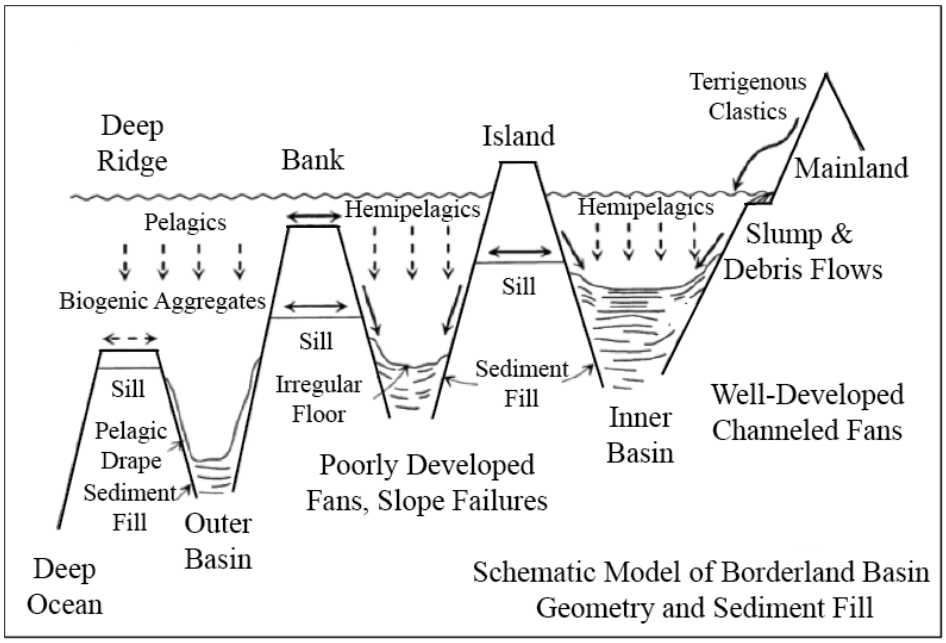

FIGURE 1. Schematic model of borderland basin geometry and fill. This model represents the various components of the depositional environment of the California borderland (modified from Gorsline and Emery, 1959).

Formations directly control the reservoir properties of these sediments. These include: proximity to source (inner and outer basins), centers of upwelling, variations in paleobathymetry, variations in sill depth (oxic or dysoxic environments), variations in detrital influx, and others (Figure 1) (Gorsline and Emery, 1959; Isaacs, 1983; Gorsline, 1992). Understanding the different deposits related to these environments may provide insight to better understand the petroleum system in a diatom-rich margin, and consequently to aid in targeting petroliferous diatomaceous facies in other basins.

Objective and Location of Study

This study will investigate the sedimentologic and stratigraphic variability in two proprietary cores from the Orcutt (Newlove 76-RD1) and Casmalia Hills (Stokes A-

30804) oil fields by visual, laboratory, and petrophysical analysis. The Casmalia Hills and Orcutt oil fields are located within the Santa Maria basin on the central California coast, situated approximately 30 miles northwest of Santa Barbara. Both oil fields are coast, situated approximately 30 miles northwest of Santa Barbara. Both oil fields are located on the Casmalia-Orcutt anticlinal trend (Figure 2).

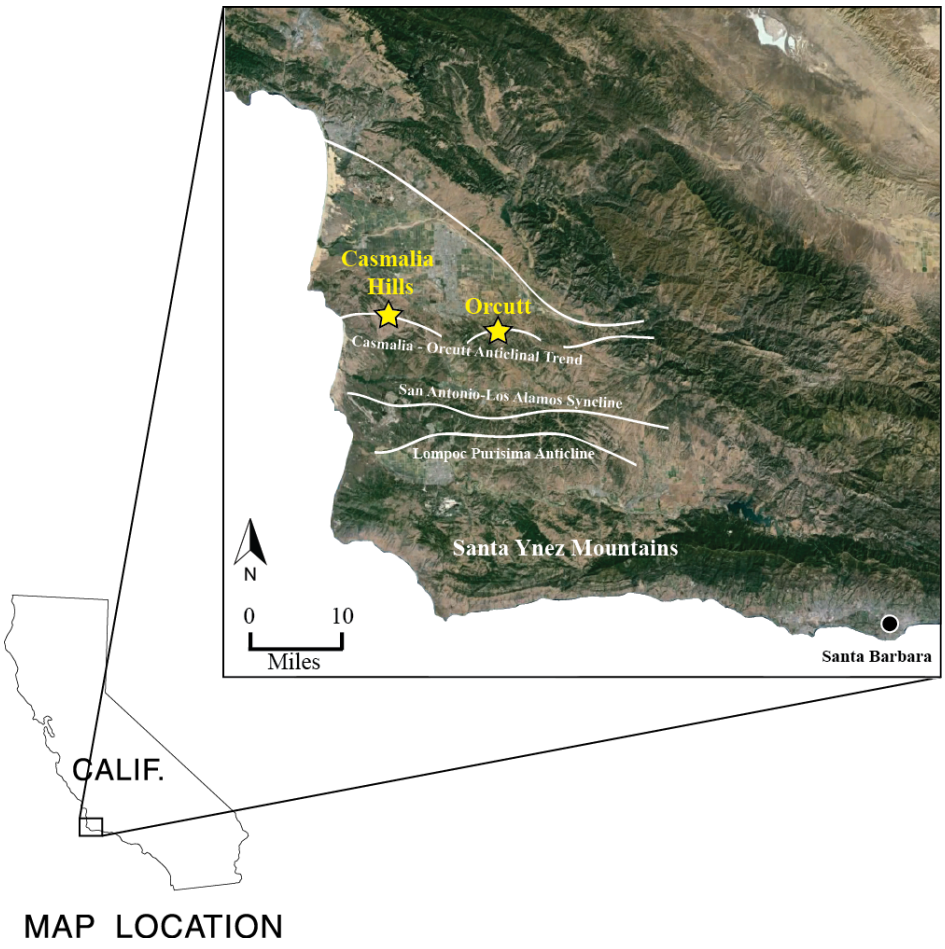

FIGURE 2. Regional map displaying the Casmalia Hills and Orcutt oil fields. Yellow stars represent both oil fields. This map also displays the surrounding structural trends (structure from Namson and Davis, 1990).

Regional Geology and Tectonic History

The triangular onshore sedimentary Santa Maria basin is situated between the junction of the Western Transverse Ranges and Coast Ranges. The basin is structurally bounded offshore by the Hosgri fault zone to the west, the Santa Ynez River fault to the south, and the Santa Maria River fault to the north (Figure 3). The Santa Maria basin was formed in a geologically complex location that records a geologic and tectonic history of extension and shortening and basin inversion due to rotation of the Transverse Ranges (McCrory et al., 1995; Behl and Ramirez, 2000).

The pre-Mesozoic history of the Santa Maria basin is undistinguished and most of the Mesozoic and early Tertiary geologic history is obscure (Woodring and Bramlette, 1950). The better-documented history of the basin began in the early Miocene with initial subsidence of the Santa Maria basin at about 18 Ma (Stanley et al., 1996). The exposed Mesozoic basement rocks of the Franciscan assemblage, Great Valley Sequence and Coast Range Ophiolite rifted apart closely followed with the capture of the partially subducted Monterey microplate by the Pacific plate (Nicholson et al., 1994). Clockwise rotation of the Western Transverse Ranges initiated shortly thereafter (Hornafius, 1985; Luyendyk et al., 1985; Crouch and Suppe, 1993). Regional transtension, continued rotation of the Western Transverse Ranges and rapid subsidence resulted in dip-slip, oblique-slip, and large displacement strike-slip faulting throughout the region (Figure 4) (Stanley et al. 1996; Behl and Ramirez, 2000). Paleomagnetic data suggest that the entire western Transverse Ranges rotated approximately 50° to 60° clockwise during the middle Miocene (Figure 4) associated with a minimum of 200 km of distributed dextral shear

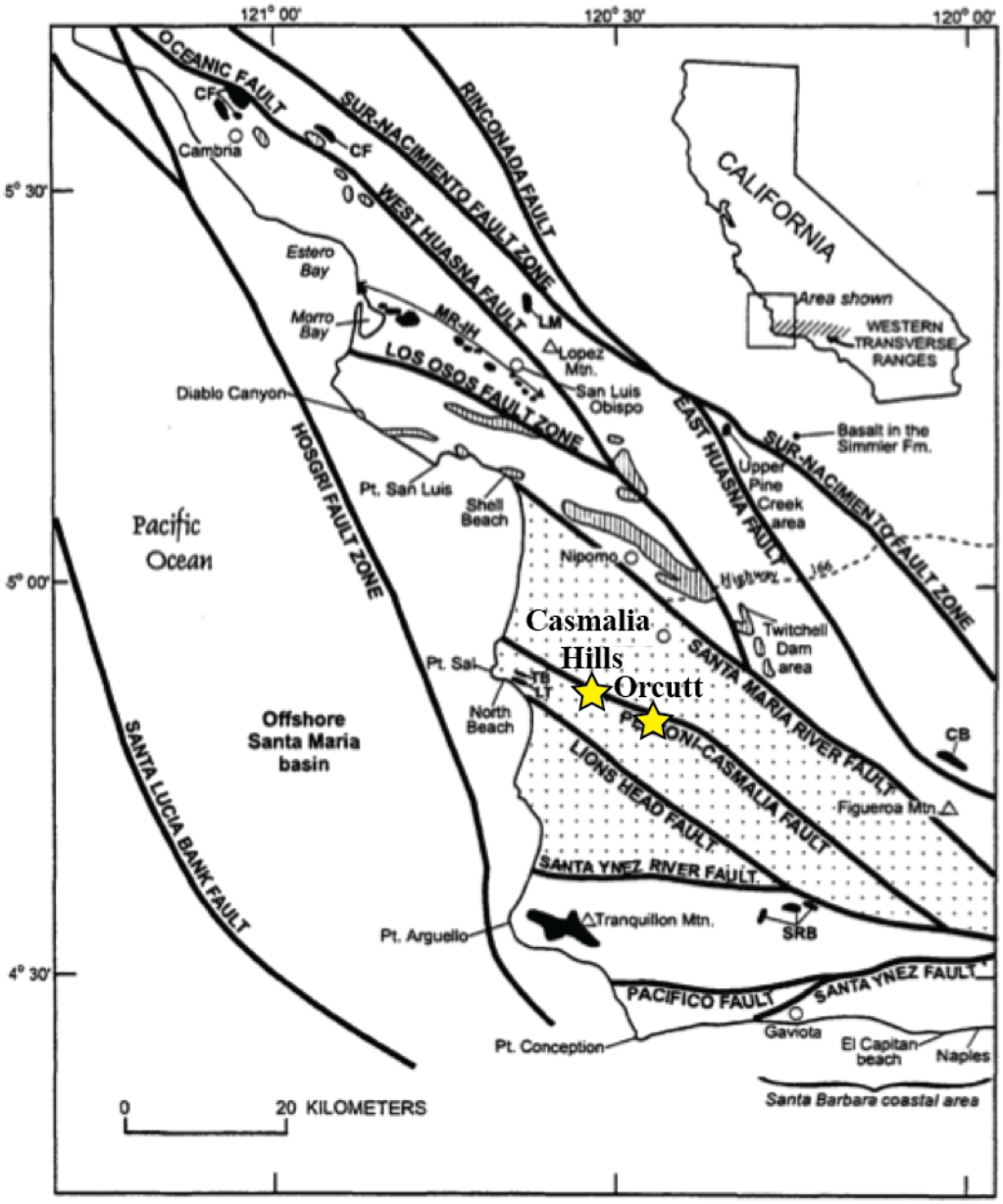

FIGURE 3. Fault map of the Santa Maria basin. This map illustrates the major faults surrounding the Santa Maria basin (Modified from Cole and Stanley, 1998). Yellow stars represent the localities of the Casmalia Hills and Orcutt oil fields.

FIGURE 4. Tectonic models illustrating shortening within the Santa Maria province. Tectonic movement caused regional uplift and shortening shown in the models (A) Overview location map of the central California. (B) Post position of blocks (C) Termination of right-lateral faults with no vertical-axis block rotation (D) Same as C except faults terminate into clockwise-rotating block with shortening decreasing to the east between fault intersections (E) Non rotating faults bounding clock-wise rotating slats terminating into clockwise-rotating Santa Ynez Mountain block. Amberjack high (AH); Coast Ranges (CR); Diablo Canyon nuclear power plant (D); Hosgri Fault (HF); Point Sal block (PSB); Shell Beach (SB); Morro Bay (MB); Santa Barbara Channel (SBC); Santa Maria Basin (SMB); San Rafael Mountains (SRM); San Simeon fault (SSF); Santa Ynez Mountains (SYM); Vandenberg Air Force Base (V); Inferred right-lateral sheer zone (SZ) (Sorlien et al., 1999).

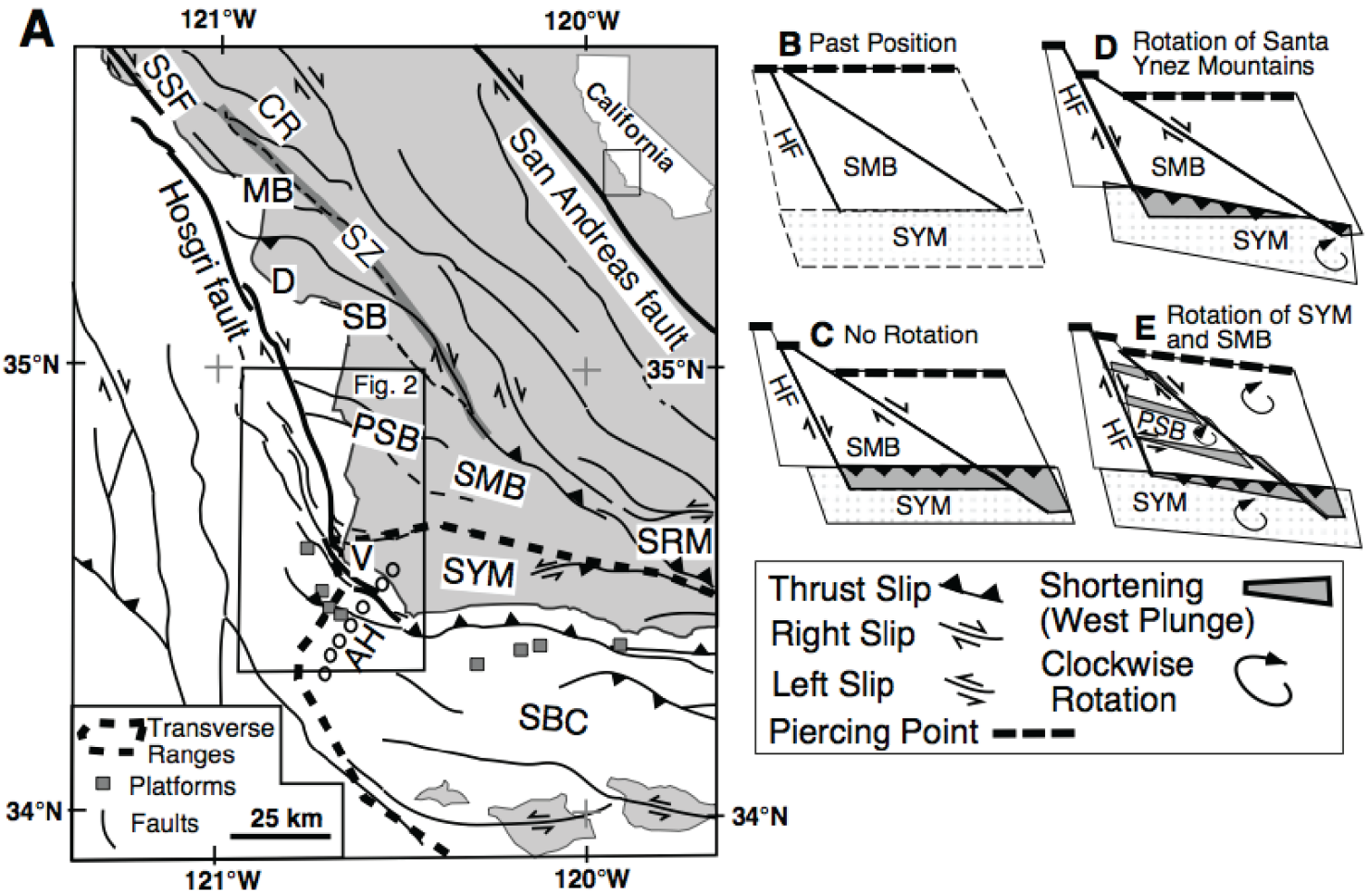
A
121°W
120°W
35°N
34°N
SSF
CR
MB
SZ
D
SB
Hosgri fault
San Andreas fault
California
Fig. 2
PSB
SMB
SRM
SYM
V
AH
SBC
Transverse Ranges
Platforms
Faults
25 km
B Past Position
HF
SMB
SYM
C No Rotation
D Rotation of Santa Ynez Mountains
E Rotation of SYM and SMB
Thrust Slip
Right Slip
Left Slip
Piercing Point
Shortening (West Plunge)
Clockwise Rotation

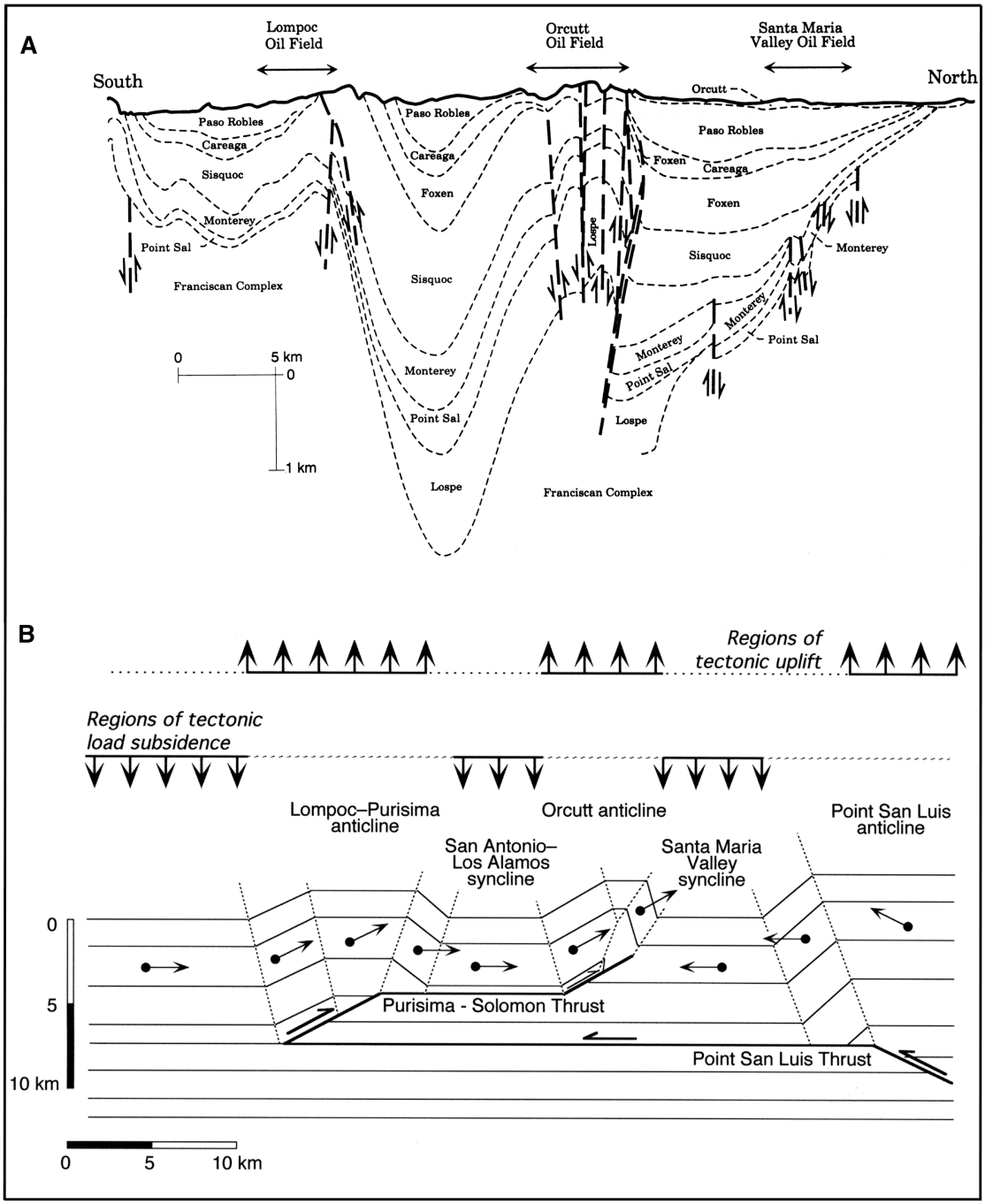

FIGURE 5. Cross section though the Santa Maria Valley, Orcutt, and Lompoc. This north-south cross section displays the anticline and syncline sequences though the Santa Maria basin (A) with a structural interpretation by Namson and Davis (1990) and Behl and Ingle (1995) emphasizing the regions of tectonic uplift over thrust ramps and tectonic load subsidence due to regional crustal thickening (B).

along the California coast and offshore Santa Maria basin (Hornafius et al., 1986). Further rotation of the Western Transverse Ranges led to an episode of structural inversion as extension turned into shortening in the late Miocene to Pliocene (McCrory et al., 1995; Behl and Ramirez, 2000) (Figure 5). Dip-slip, oblique-slip, and thrust faults formed across the Santa Maria basin during the tectonic reorganization of the Transverse and Coast Ranges (Namson and Davis, 1990). Fault-bend and fault-propagation folds associated with thrust ramps formed the dominant series of large Pliocene to Quaternary anticlinal structures (i.e., Lompoc-Purisima trend, Point San Luis anticline, Casmalia-Orcutt trend, La Panza Range anticlinorium and the Santa Lucia Range anticlinorium (Namson and Davis, 1990) illustrated in Figure 5. Continued clockwise rotation of the western Transverse Ranges during the Pliocene-Pleistocene contributed to an additional 30-60 km of distributed dextral shear across the southern California Coast Ranges (Hornafus et al., 1986). Crustal shortening continued to the present-day (Woodring and Bramlette, 1950; Canfield, 1939; Feigl et al., 1990).

Generalized Stratigraphy

The igneous and metamorphic basement rocks of Santa Maria basin consist of the Franciscan assemblage and Point Sal Ophiolite. Overlying these units is the Knoxville Formation that is chiefly composed of shale, thick conglomerate beds, and thin fine-grained to moderately coarse-grained calcareous sandstone (Woodring and Bramlette, 1950). Unconformably overlaying the Knoxville is the oldest Neogene unit – the lower Miocene Lospe Formation. This terrestrial to nearshore, nonfossiliferous deposits is subdivided into upper and lower members (Woodring and Bramlette, 1950). The lower

member consists of coarse-grained sandstones and conglomerates, whereas the upper member consists of sandstone, siltstone and mudstone (Woodring and Bramlette, 1950). Turbiditic, hemipelagic, and bathyal sediments make up the overlying Miocene Point Sal Formation (Behl and Ramirez, 2000). The Point Sal Formation is dominantly composed of siltstone, mudstone, and thin beds of sandstone (Woodring and Bramlette, 1950).

Maximum basin subsidence occurred concurrently with deposition of the highly organic-rich, siliceous, and hemipelagic deposits of the Miocene Monterey Formation (Woodring and Bramlette, 1950; Behl and Ramirez, 2000). In most locations of the Santa Maria basin, water depth gradually shoaled during deposition of the Monterey Formation. (McCrory et al., 1995). The Monterey Formation contains an unusual abundance of biogenic silica, carbonates, phosphates, and organic matter (Behl, 1999). This basinal succession exhibits three distinct units over broad areas of California: a lower calcareous facies, a middle phosphatic facies, and an upper siliceous facies (Woodring and Bramlette, 1950; Pisciotto and Garrison, 1981). The lower calcareous facies (up to 300 meters thick) is characterized by massive to thinly bedded mudstone, claystone, calcareous shale, limestone and dolostone (Pisciotto and Garrison, 1981; Behl and Ramirez, 2000). The condensed middle phosphatic facies of the Monterey Formation is starved of siliciclastic material and reflects slow accumulation rates during the time of deposition (Pisciotto and Garrison, 1981). The upper siliceous facies represents the thickest facies within the Monterey Formation, comprised chiefly of diatomite, diatomaceous mudrocks, siliceous mudstone, porcelanite, and chert (Pisciotto and Garrison, 1981).

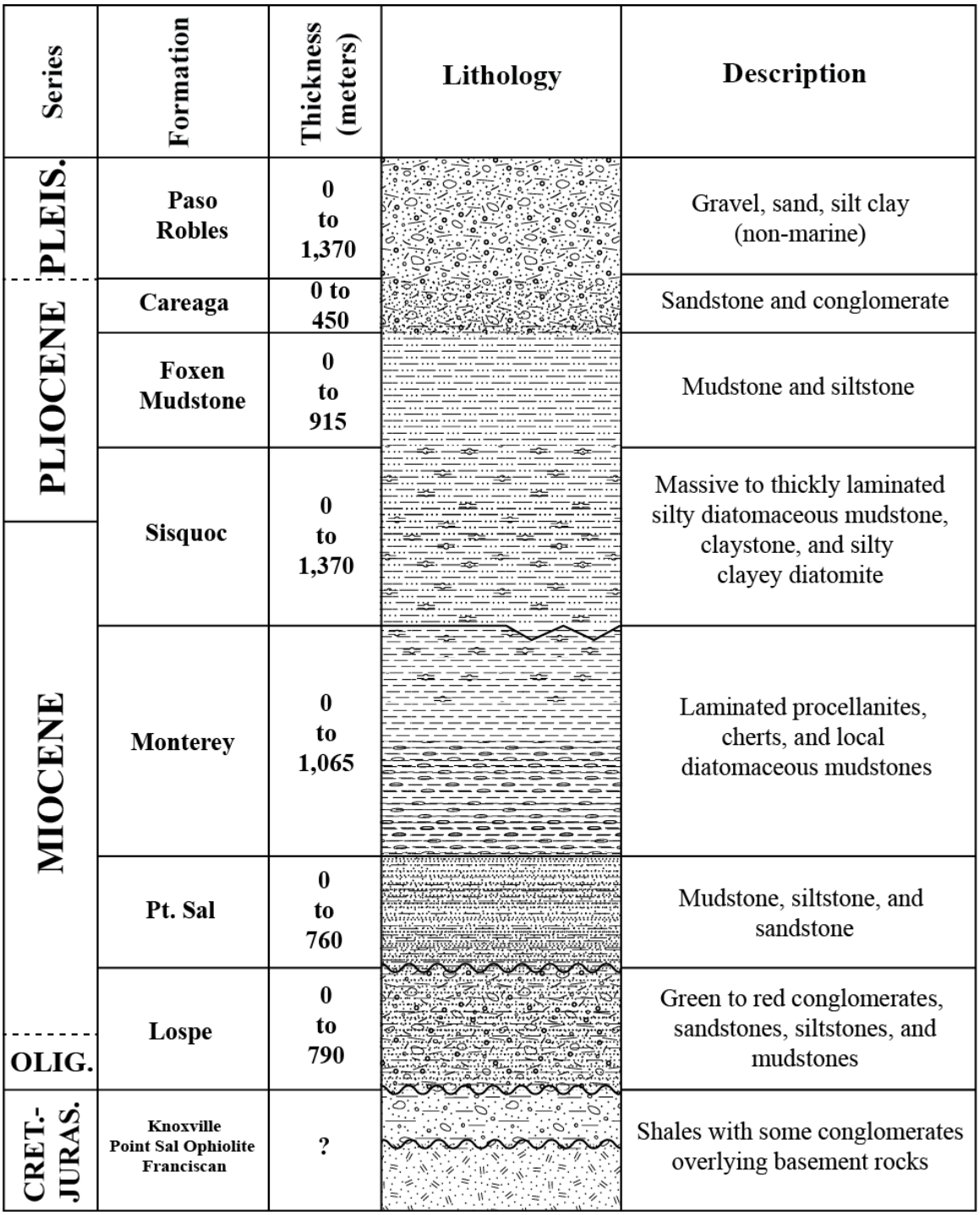

FIGURE 6. Generalized stratigraphic column of the Santa Maria basin. This figure was modified from Ramirez, 1990.

The highly siliceous and reactive components of the Monterey Formation underwent diagenesis as temperatures increased during burial (Behl, 1999). In general, silica diagenesis takes place in two distinct steps involving dissolution and reprecipitation of silic polymorphs. The two transitions consist of the alteration of biogenic opal-A (amorphous hydrous silica) to diagenetic opal-CT (hydrous silica with crystalline structure of cristobalite and tridymite) and finally opal-CT to diagenetic quartz

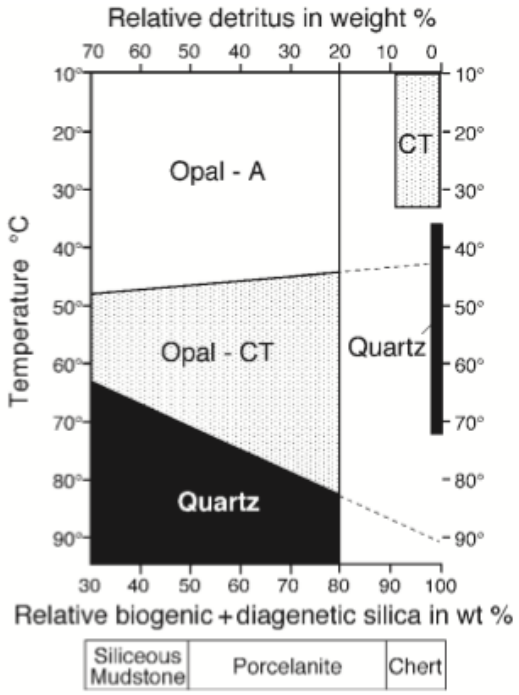

FIGURE 7. Diagram displaying timing and temperatures of silica diagenesis. (Behl, 1992; Behl and Garrison, 1994, modified from Keller and Isaacs, 1985).

(cryptocrystalline, chalcedonic, and microcrystalline forms). The timing of transformation of these sediments is controlled by the original bulk composition (relative abundance of detritus and silica), temperature and burial depth (Murata and Nakata, 1974; Murata and Larson, 1975; Isaacs, 1981; Pisciotto, 1981; Isaacs, 1982; Behl and Garrison, 1994; Behl, 1998; Eichhubl and Behl, 1998; Behl, 1999). Figure 7 illustrates the relative timing and temperatures of the silica phase changes for sediments of varying compositions.

The overlaying Sisquoc Formation represents a continuation of similar Monterey Formation deposits of moderately organic-rich, but still highly siliceous hemipelagic deposits. However, the Sisquoc contains higher amounts of terrigenous detritus and lower concentrations of silica due to basin shoaling (Henderson and Ramirez, 1990; Behl and Ramirez, 2000). The contact between the Monterey and Sisquoc Formations can range from gradational to unconformable making it difficult to physically distinguish the two formations in certain localities (Behl and Ramirez, 2000). Some researchers place the Monterey-Sisquoc contact at the opal-A to opal-CT boundary; however, in several sections the diagenetic change varies within either the Monterey or the Sisquoc Formations (Behl and Ramirez, 2000). In several outcrop localities (i.e., Mussel Rock, Naples Beach, and Jalama Beach), the Sisquoc and Monterey Formations are divided by a thick and distinct clast-supported conglomerate bed composed of transported phosphate and sometimes other Monterey-derived clasts (Föllmi et al., 1991). In other outcrops (i.e., Sweeny Road, Pedernales and Lompoc Hills), the boundary between the Sisquoc and Monterey Formation is completely gradational and difficult to physically distinguish.

In the Casmalia Hills, the Monterey-Sisquoc contact is established by a fine-grained somewhat porcelaneous claystone facies named the Todos Santos Claystone member (Woodring and Bramlette, 1950). In most cases, the Monterey-Sisquoc contact is determined by one or more of the following: lithological changes, compositional changes (chemical differences distinguished by laboratory data), and diatom biostratigraphy (Ramirez, 1990). Differences between locations reflect a complex and varied Sisquoc Formation depositional environment. High-resolution diatom biostratigraphy within the Santa Maria basin (Harris Grade Section) indicates that the Sisquoc Formation was deposited from approximately 6.0 Ma (*Thalassiosira miocenica/Nitzschia miocenica* interval zone) to 3.8 Ma (*T. oestrupii* interval zone*)*. But this duration varies with location, especially where unconformities or condensed sections bound the formation.

Overall, the Sisquoc Formation is chiefly composed of light gray, massive to thickly laminated, silty diatomaceous claystone or silty clayey diatomite (Behl and Ingle, 1995). Depending on the locality, the diatomaceous strata of the Sisquoc Formation can range from virtually pure white laminated diatomite (up to 70% biogenic silica) to massive mudstone (90% detritus) (Ramirez, 1990; Woodring and Bramlette, 1950). Weathered diatomaceous outcrops are generally very light in color, whereas subsurface samples are somewhat darker. Typically, massive strata are commonly darker, denser, and more detrital-rich, whereas laminated strata are typically richer in silica with reduced detrital abundance (Ramirez, 1990). Other Sisquoc lithologies include conglomerate, breccia, dolomite, phosphorites, and silty to sandy mudstones (Ramirez, 1990). Many researchers have interpreted the Sisquoc Formation to have been deposited on an unstable

slope, moderate to upper bathyal depths, and below active wave base (Woodring and Bramlette, 1950; Ingle, 1981b; Henderson et al., 1984; Henderson and Ramirez, 1990).

Following a brief and local episode of tectonic subsidence and paleobathymetric deepening, the continuation of basin-infilling and increased rate of siliciclastic deposition led to the generally non-diatomaceous Foxen Mudstone (Behl and Ingle, 1995; Ramirez and Garrison, 1995; Behl and Ramirez, 2000). The upward-shoaling slope to outer-shelf deposits of the Foxen Mudstone are mainly composed of thick mudstone and clayey siltstone (Woodring and Bramlette, 1950; Ramirez, 1990).

The Careaga Sandstone overlies the Foxen Mudstone and is the youngest fully marine formation within the Santa Maria basin (Woodring and Bramlette, 1950). The shallowing- and coarsening-upwards deposits of the Careaga Sandstone are primarily composed of sandstone, sand, and gravel conglomerate (Woodring and Bramlette, 1950). The Careaga Sandstone is divided into two members: (1) a lower fine-grained sandstone designated as the Cebada fine-grained member and (2) an upper coarse-grained sandstone and conglomerate designated as the Graciosa coarse-grained member (Woodring and Bramlette, 1950). Thereafter, nonmarine deposition formed the conformably overlying Paso Robles Formation. This formation is chiefly composed of fluvial and gravel deposits (Woodring and Bramlette, 1950). Continued nonmarine deposition characterizes the unconformably overlying Orcut Sand (Woodring and Bramlette, 1950) that blanketed the now uplifted Santa Maria basin (Behl and Ramirez, 2000).

Santa Maria Basin Petroleum System

The onshore Santa Maria basin has been an area of intense hydrocarbon exploration and exploitation since the early 1900s (Woodring and Bramlette, 1950). The uplift of sea floor anticlinal ridges from latest Miocene to middle Pliocene formed various anticlinal structural and stratigraphic traps where numerous oil deposits developed throughout the Santa Maria Basin (Woodring and Bramlette, 1950; Behl and Ingle, 1995; Behl and Ramirez, 2000). Oil fields of the onshore and offshore Santa Maria basin include: Guadalupe, Santa Maria Valley, Cat Canyon, Zaca, Barham Range, Los Alamos, Lompoc, Jesus Maria, Orcutt, Casmalia Hills, San Miguel, Point Pedernales, Bonito, Rocky Point, Point Arguello, and Sword. Figure 8 illustrates the proven oil fields within the region.

The Monterey Formation is considered the major source rock within the Santa Maria basin (Woodring and Bramlette, 1950). Production of heavy, low American Petroleum Institute (API) gravity oil is chiefly from fractured rocks (i.e., chert, porcelanite, dolostone) within the Monterey Formation (Canfield, 1939; Woodring and Bramlette, 1950). However, there has recently been increasing production from the diatomaceous Sisquoc Formation, facilitated by higher oil prices and technological advances in enhanced oil recovery techniques. In addition to the reservoir rocks of the Monterey and Sisquoc Formations, limited oil has been recovered from the Point Sal Formation, Lospe Formation, Foxen Mudstone, and the Knoxville Formation (Woodring and Bramlette, 1950).

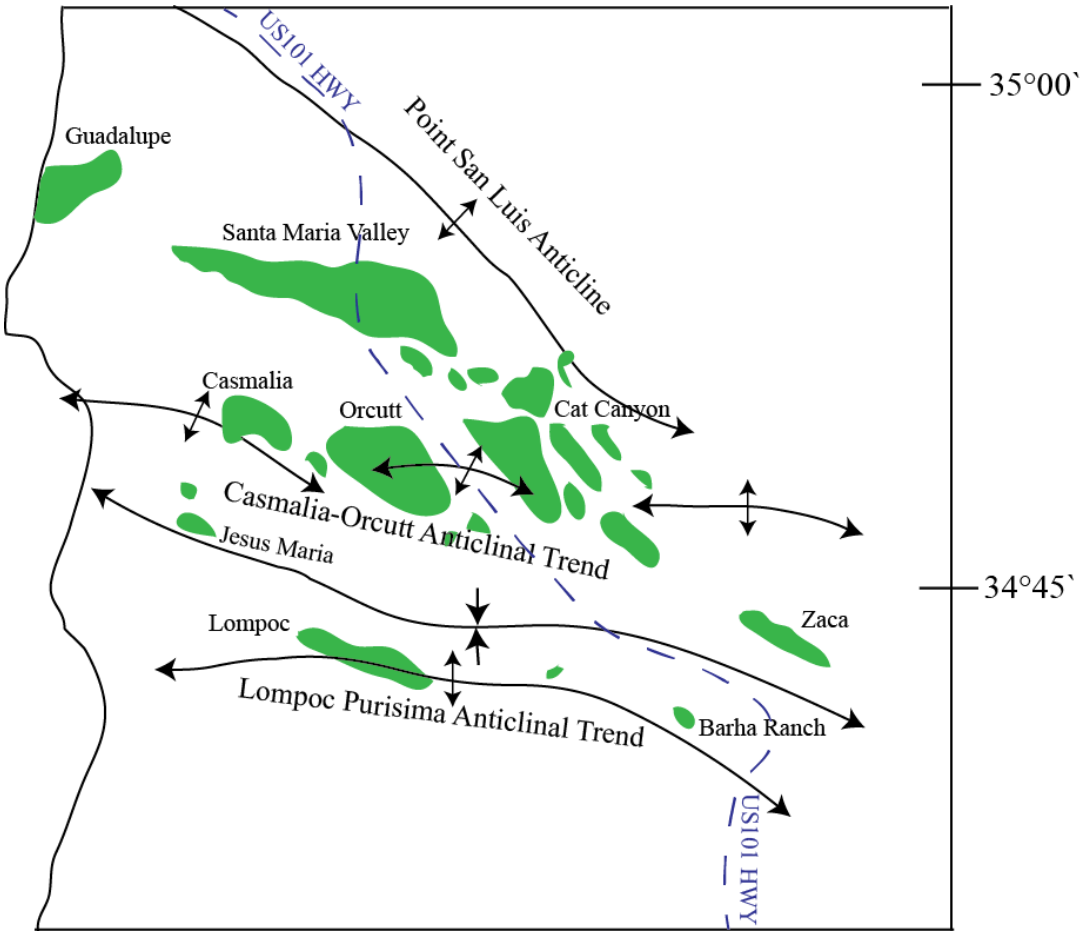

FIGURE 8. Regional map of oil fields and structural trends of the Santa Maria basin. This figure was modified from Namson and Davis, 1990.

Previous Studies of Diatomaceous Sediments

The Santa Maria basin has been studied for over 100 years since the discovery of oil in the Orcutt field in 1901. A majority of the data in previous studies that will be discussed in this section derived predominantly from outcrop data (Woodring and Bramlette, 1950; Ramirez 1990; Henderson and Ramirez, 1990; Ramirez and Garrison,

1995) but several studies encompassed data from cores (Canfield, 1939; Henderson et al., 1984; Farley and Wilson, 1983). Several of these published studies are especially pertinent to this research and are discussed in greater detail within this section.

Outcrop Studies

Woodring and Bramlette (1950) established a comprehensive framework of the stratigraphy, geologic history, paleontology, and petroleum system of the Santa Maria basin. This study provided detailed descriptions of the stratigraphy, lithology and paleontology of the Franciscan Formation, lower and upper Lospe Formation, Point Sal Formation, Monterey Formation, Sisquoc Formation, Foxen Mudstone, Careaga Sandstone, Paso Robles Formation, Orcutt Sand, and Quaternary terrace deposits. Relative ages were provided for each unit based on biostratigraphy. In addition, small to large-scale structural features were identified and the structural geologic history was interpreted. This geologic framework was used by all following studies in varied subdisciplines.

Ramirez's (1990) PhD dissertation established a stratigraphic, sedimentologic, geochronologic, and paleoceanographic framework for the Sisquoc Formation from outcrop data from various localities in the Santa Maria basin. In this study, Ramirez analyzed small-scaled sedimentary features, sedimentary composition and biostratigraphy to interpret depositional processes and environment at the following outcrops: Mussel Rock, Pt. Pedernales, Sweeny Road, and Casmalia Hills. He identified a variety of sedimentary structures and fabrics, including: planar lamination, grading, trace fossils, sandstone laminations, scour surfaces, angular discontinuities, microfaults, slump folds,

intraformational breccia, phosphorites, cross bedding, ripples, and channel structures. With these plus microfossil assemblages, Ramirez concluded that the Sisquoc was deposited in a slope to shelf-edge environment. Ramirez's descriptions and interpretations of sedimentary structures played a significant role in my analyses, as many of his outcrops are proximal to the field area for this thesis research.

Subsurface and Core Studies

In general, outcrops and surface exposures in the Santa Maria basin of the diatomaceous sediments of the Sisquoc Formation and upper Monterey are highly weathered, masking sedimentary features, lithology, and bedding relationships. Thus, core data can reveal sedimentologic details of these diatomaceous sediments difficult to determine in outcrop (Henderson and Ramirez, 1990).

Henderson et al. (1984) from Union Oil conducted a study of the relationship of diagenetic dolomite to depositional facies in the upper Sisquoc Formation using nine cores from the Casmalia Hills--approximately 1 mile from the Stokes A-30804 core studied for this thesis research. Analyses of these cores included detailed core descriptions, thin-section petrography, X-ray diffraction and stable isotopes. Eleven different rock types were identified: claystone, diatomaceous claystone, mudstone, diatomaceous mudstone, opal-CT bearing claystone, opal-CT bearing mudstone, pebbly mudstone, pebbly conglomerate, sandstone, dolomite and vitric tuff. The cores were divided into six lithostratigraphic units that were interpreted for their depositional environments. Classification schemes in my thesis research were modified from their study. Henderson et al. (1984) concluded that the cores represented an overall upward

succession from a nearly anoxic basin or outer slope environment to an aerobic upper slope or outer shelf environment. Unfortunately, the published paper lacks high-quality core photos.

Farley and Wilson (1983) from Gulf Mineral Resources Co. conducted a core study of the lithology, sedimentary features, and mineralogy of the Airox oil-saturated diatomite located 10 km southwest of Santa Maria within the Casmalia Hills. This is also very close to the Stokes A-30804 core. Farley and Wilson collected several samples for bulk mineralogy (X-ray diffraction) and geochemical analysis. In addition, they also analyzed the physical character of oil saturation and fracture systems. Farley and Wilson concluded that oil saturation is a function of lithology as more porous rocks contained higher oil saturation compared to less porous mud-rich rocks.

Henderson and Ramirez (1990) studied four cores that penetrated approximately 1,300 ft. within the Sisquoc Formation in the Casmalia Hills. This study focused on the pebbly lithologic units that were highly oil-saturated. Lithofacies from their cores consist of distinct intervals of laminated and bioturbated to massive porcellaneous and diatomaceous mudstone. Henderson and Ramirez noted that the pebbly units were likely deposited via debris-flows based on their poor sorting, lack of sedimentary structures, and poor grading. Additionally, the heavy oil-saturated pebbly units suggest that the pebbly units may have been conduits for oil migration from the underlying Monterey Formation.

Henderson et al. (1984), Farley and Wilson (1983), and Henderson and Ramirez (1990) established a valuable foundation for this research based on their analyses of cores that were less than 10 miles from the data used in this research. The integration of the

studies on core and surface/outcrop data contributed to the understanding of the rocks studied in this research as the two data sets provide different advantages. The subsurface samples are unweathered, but limited to the width of the core barrel, whereas the surface exposures can be highly weathered, but provide wider perspectives and more unequivocal identification of sedimentary structures and depositional processes.

CHAPTER 2

METHODOLOGY

Core Data

Data for this study derive from two cores from the Casmalia Hills and Orcutt oil fields in the Santa Maria basin. Both cores are interpreted to represent the Sisquoc Formation. Through the generosity of Santa Maria Energy and BreitBurn Energy, the two cores were made temporarily available to sample and analyze for this thesis research.

The first core, from well Stokes A-30804 (34.889572°N, -120.554016°W) is located in the northeast-dipping, northwestern region of the Casmalia Hills oil field (Figure 9). Stokes A-30804 (operated by Santa Maria Energy) was drilled in 2005 to a total depth of 1,350 ft. with 406 ft. cored. The cores were stored at the oil field until 1/3-volume slabs of the cores were transported to California State University, Long Beach for analysis. Additional acquired data from Stokes A-30804 included core photos (with normal and UV light), sparse x-ray diffraction (XRD) (bulk and clay mineralogy at depths 288 ft., 336 ft., 582 ft., 607 ft., 787 ft., 1153 ft.), sparse scanning electron microscope (SEM) data (SEM photos from depths 607 ft. and 336 ft.), petrophysical data (gamma ray, spontaneous potential, and resistivity curves), porosity and fluid saturation data (oil and water).

The second core is from well Newlove 76-RD1 (34.832481°N, -120.405438°W), located on the anticlinal structure of the Orcutt oil field (Figure 9). Newlove 76-RD1

FIGURE 9. Geologic map of the Casmalia Hills and Orcutt oil fields. Stokes A-30804 and Newlove 76-RD1 are approximately 9 miles apart (modified from Dibblee, 1989a and Dibblee, 1989b).

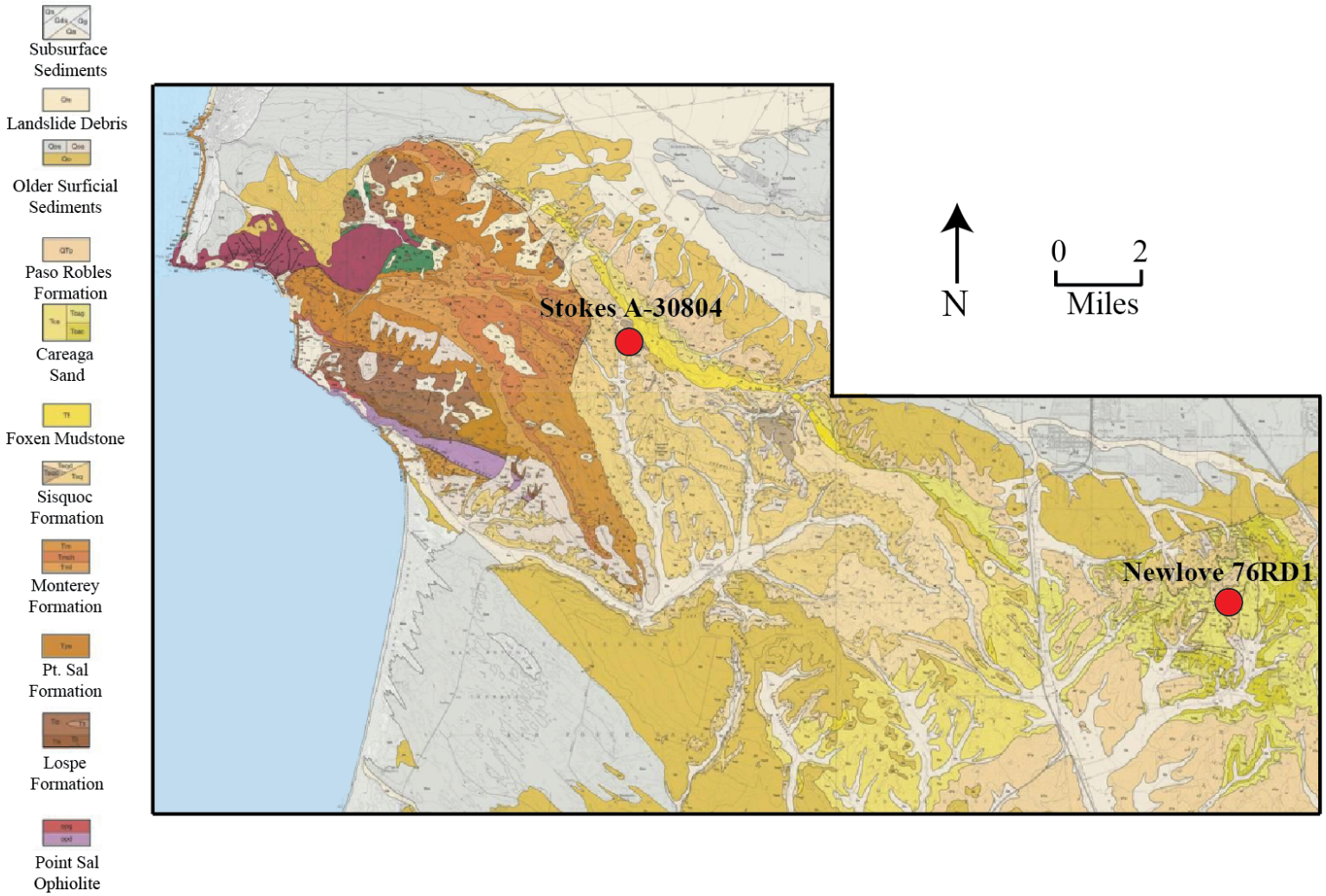
Subsurface Sediments
Landslide Debris
Older Surficial Sediments
Paso Robles Formation
Careaga Sand
Foxen Mudstone
Sisquoc Formation
Monterey Formation
Pt. Sal Formation
Lospe Formation
Point Sal Ophiolite
Stokes A-30804
Newlove 76RD1
N
0
2
Miles

(operated by BreitBurn Energy) was drilled and discontinuously cored in 2005 to a total depth of 893 ft. A total of 282 ft. of 2/3-slab cores were made available for this study. After the completion of drilling, the cores were stored in Core Laboratories in Bakersfield, CA. Unfortunately, by the time of initiation of this research, the cores were highly desiccated and damaged; however, high-resolution foot-by-foot photos (with normal and UV light) of the cores had been taken shortly after recovering and slabbing the cores. These photos were instrumental in acquiring the observational data used in this research. Samples from Newlove 76-RD1 were collected from the cores at Core Laboratories in Bakersfield, California. Additional data that were acquired for Newlove 76-RD1 included gamma-ray, spontaneous potential, and resistivity well logs.

Core Descriptions

Lithofacies and sedimentary structures were documented and recorded at every foot of both cores. General core descriptions include: color, contacts, bed thickness, stratal geometry, texture, stacking patterns, sorting, fossil content, faults, degree of bioturbation, presence of laminations, other sedimentary structures, and degree of oil saturation. These descriptions of both cores provided an initial basis for subdivision into lithofacies units. The subdivided units were further refined with laboratory data from core samples at various depths.

Core Sample Collection at Selected Depths

Samples were collected at an average of every 3 ft. throughout both cores. A total of 176 samples were collected from Stokes A-30804 and 115 samples from Newlove 76-RD1. Of these, 65 were chosen for compositional and textural analysis by XRD and

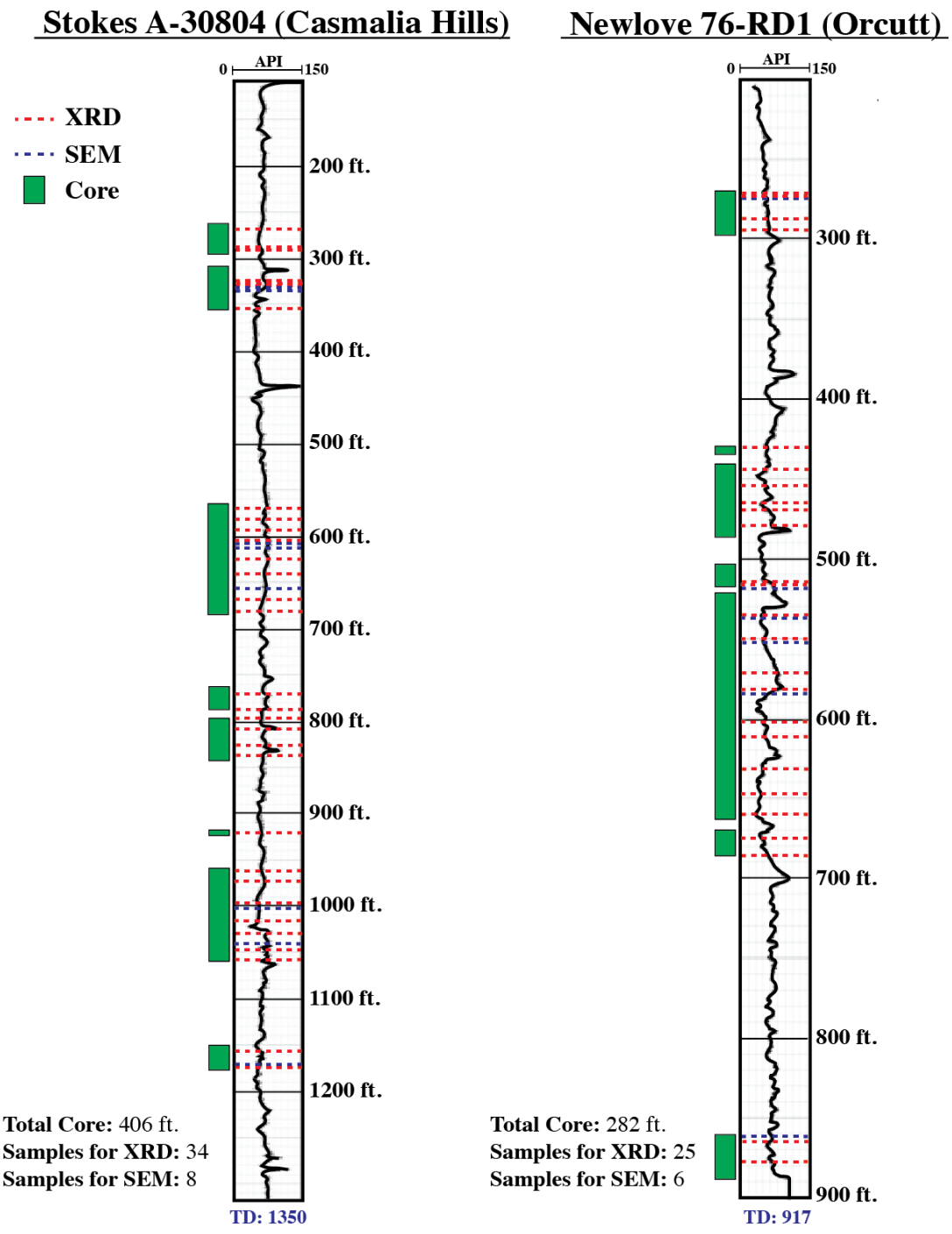

FIGURE 10. Gamma-ray logs, available core data, and samples of Stokes A-30804 and Newlove 76-RD1. This figure displays the available core data and depths of samples chosen (dotted lines) for XRD and SEM analysis. Both cores are interpreted to represent the Sisquoc Formation.

SEM (Figure 10). These samples were strategically chosen to provide adequate stratigraphic data for major lithofacies and for specific intervals in both wells.

For Stokes A-30804, 28 samples were analyzed by XRD and 6 samples were prepared for SEM investigation (specific depths available in appendices). XRD data that were previously acquired by Core Laboratories from samples at 6 depths (288 ft., 336 ft., 582 ft., 607 ft., 787 ft., 1,153 ft.) and SEM images from 2 depths (336 ft. and 607 ft.) were integrated in this research. In total, characterization of the Stokes A-30804 well was supplemented by data from 34 XRD and 8 SEM stratigraphic reference points. For Newlove 76-RD1, 25 samples were analyzed by XRD and 6 samples were imaged by SEM (specific depths available in appendices).

Conventional Core Analysis Data

Porosity and fluid saturation (oil and water) data were acquired for Stokes A-30804 from 32 samples (specific depths available in appendices). Methods are unknown for these data as they were conducted by Core Laboratories prior to the start of this thesis. Nonetheless, Core Laboratories generally uses helium and Boyle's Law relationships to measure pore volume and grain volume from 1" diameter plugs. Fluid saturation is measured by distillation extraction. First water is boiled and the vapor collected to determine water volume. Then toluene solvent is run through the sample to collect oil for at least two days to extract oil from the effective porosity of the sample.

X-Ray Diffraction

Acquisition parameters are unknown for the two samples previously analyzed by Core Laboratories. X-ray diffraction (XRD) analyses of new samples for this study were

completed by K-T GeoServices, Inc. (Gunnison, Colorado) for whole rock and clay fraction analyses to quantitatively determine mineralogical composition. Samples were initially cleaned of contaminants and hydrocarbon. Samples were then transferred into distilled water and pulverized. Dried powders were loaded into a metal sample holder for randomly oriented mounts for whole-rock analysis. A separate sample split was used for clay mineral analysis by dispersing the sample in distilled water using a sonic probe. Suspensions were size fractionated by centrifugation to separate clay-size material (<4 micron equivalent spherical diameter) for analysis. The suspensions were vacuum deposited on nylon membrane filters and exposed to ethylene glycol vapor for 12 hours to fully expand swelling clays.

XRD diffractograms were obtained with a Siemens D500 automated powder diffractometer equipped with a copper X-ray source (40kV, 30mA) and a scintillation X-ray detector. The whole rock samples were evaluated from 5-60° two-theta at 1° per minute, whereas the clay analyses were analyzed from 2-36° two-theta at 1° per minute. The analytical program, NEWMOD, was used to distinguish and quantify clay mineralogy. Whole pattern fitting and Rietveld refinement processes were used by MDI Jade software for all other quantitative and whole rock mineralogical analysis of the XRD data.

Scanning Electron Microscope

A FEI Quanta 200 Environmental Scanning Electron Microscope was used to capture digital images of selected samples at high magnification. The instrument was operated in the secondary electron imaging mode, which is optimal for textural

investigation. These images were used to characterize the degree of biofragmentation based on the preservation of observed diatoms.

Degree of biofragmentation was classified into three categories: (1) no to low degree of biofragmentation (>90% intact diatoms), (2) moderate degree of biofragmentation (70-89% intact diatoms), and (3) high degree of biofragmentation (<70% intact diatoms) shown in Figure 11.

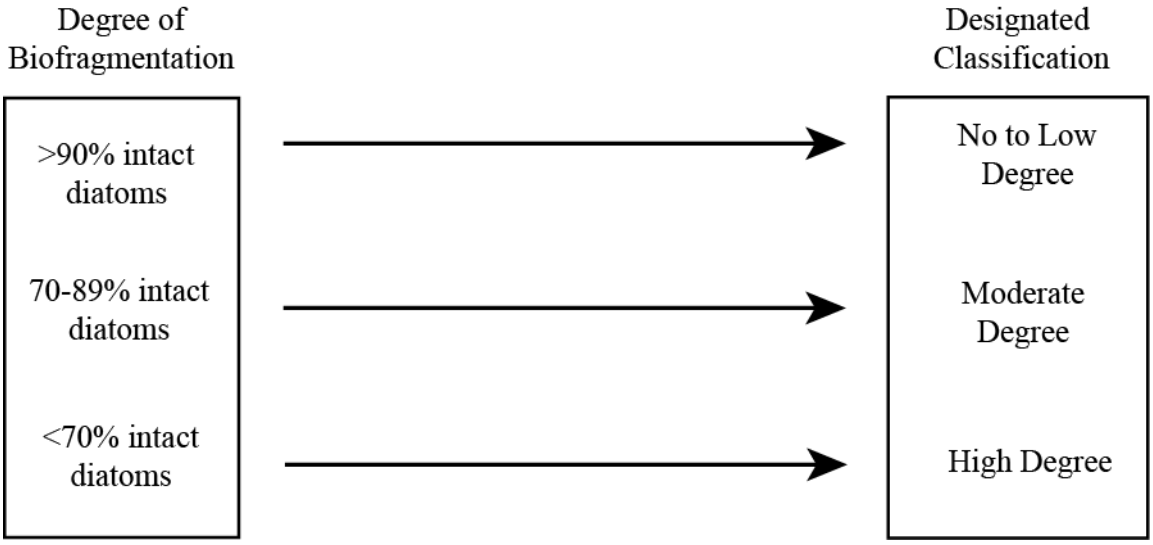

FIGURE 11. Classification scheme for degree of biofragmentation.

All samples were carefully broken by hand or a rock hammer to uncover a clean exposure of the sample mitigating possible contaminants and weathering on the surface. These newly exposed surfaces were then inserted into the instrument for textural analysis. Diatoms were commonly abundant and easier to identify within samples in opal-A phase;

meanwhile, diatoms and degree of biofragmentation were difficult to distinguish within samples in opal-CT phase (due to their dissolution and precipitation of opal-CT). This made it impossible to confidently distinguish the degree of biofragmentation in several samples resulting in non-classification.

Classification Scheme

The general classification schemes employed within this research are primarily based on visible characteristics and XRD data. These datasets are integrated and formalized into the scheme below. This general classification scheme is modified from (Schnurrenberger et al., 2003) (Figure 12).

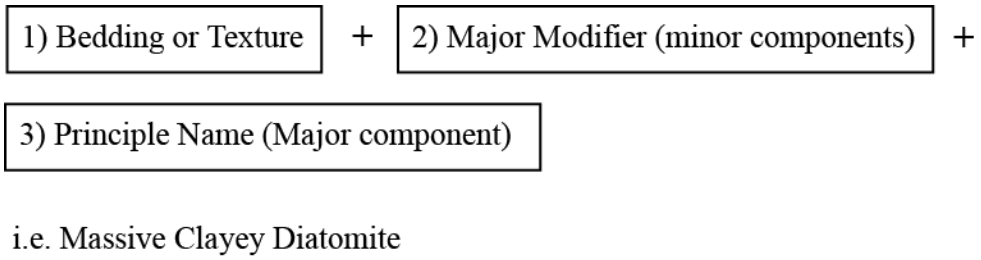

FIGURE 12. Classification scheme for nomenclature of lithofacies. This method was modified from Schnurrenberger et al., 2003.

Term "1" describes observable physical features from the cores (i.e., massive, laminated, brecciated, ripple, cross-laminated, pebbly, porcelaneous, or sandy). Terms "2" and "3" describe minor and major mineralogical components chiefly determined from XRD data.

A major modifier is a component of secondary abundance that is not the primary composition and typically makes up from 10-49% of the total rock. The nomenclature of the minor components designated in this research is shown below (Figure 13):

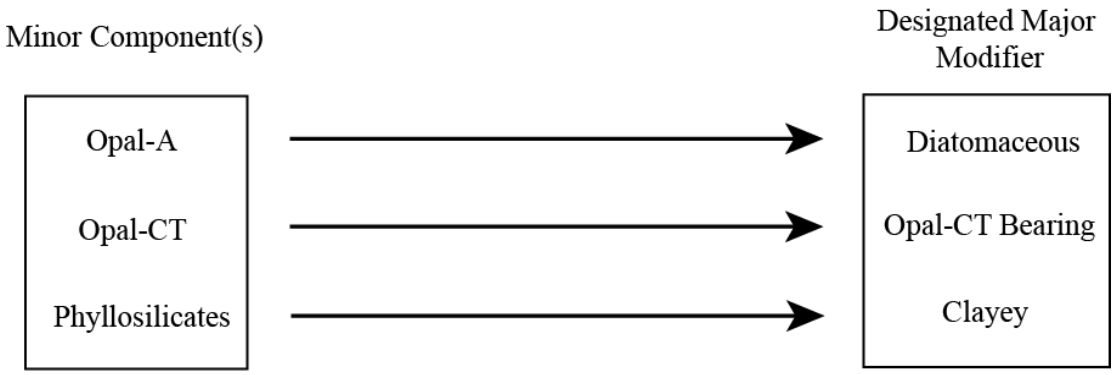

FIGURE 13. Classification scheme for major modifiers.

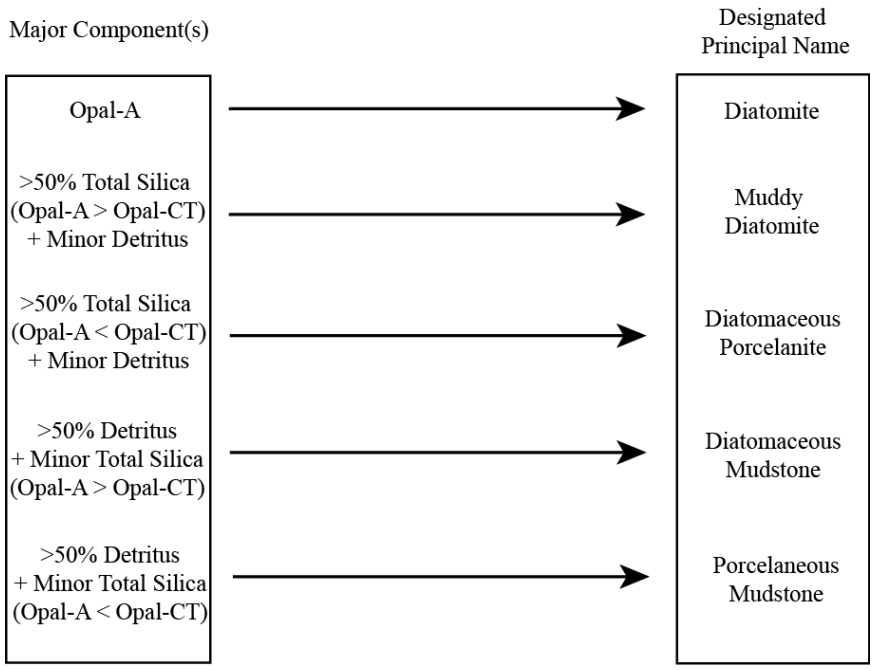

FIGURE 14. Classification scheme for principal name.

To be classified as a principal name, the component must be the major component of the total rock composition (i.e., the principal name is designated as a diatomite if the unit is dominantly composed of total opal-A). Total silica is defined to consist of the total bulk percentage of opal-A and opal-CT.

In more deeply buried rocks, some of the quartz would also be diagenetic and formed from originally diatomaceous sediments, but in the case of these shallowly buried rocks, most quartz is detrital. Total detritus include the bulk percentage of quartz, feldspars, micas, and phyllosilicates. The nomenclature of the major components designated in this research is shown in Figure 14.

Sedimentary Features

Sedimentary structures in fine-grained sediments provide clues about the depositional process or environment. Thus, all sedimentary structures and other bedding features visible in core or core photos from the Newlove 76-RD1 and Stokes A-30804 wells (i.e., slump folds, discontinuities, truncation surfaces, faults, burrows, scoured surfaces, hardgrounds, intraformational breccia, and fossils) were logged.

Petrophysical Data

Well logs provide petrophysical data used to distinguish subdivided lithofacies units within the Stokes A-30804 and Newlove 76-RD1 wells. Gamma-ray signatures (based on the sum of potassium, uranium and thorium) were a key tool for identification, analysis, and differentiation of units. The software program Neurolog was used for display and analysis.

CHAPTER 3

RESULTS

The stratigraphy and sedimentology of Newlove 76-RD1 and Stokes A-30804 were characterized by using a combination of direct observation, laboratory analysis (x-ray diffraction and scanning electron microscope), and subsurface gamma-ray logs. The various lithofacies, sedimentary features and compositional trends of these two cores are described within this section.

Newlove 76-RD1 Results

Lithofacies

Muddy Diatomite

Muddy diatomite is the dominant lithofacies of Newlove 76-RD1. This lithofacies is characterized as massive to laminated, light-to-dark brown with fossils, erosional surfaces, hardgrounds, and breccia. The average mineralogic composition consists of 69.4% opal-A, 0% opal-CT, 26.8% total detritus (7.7% phyllosilicates and 19.1% quartz and feldspars), and no pyrite. SEM images reveal that this lithofacies has a low to high degree of biofragmentation containing fragmented to fully preserved diatoms (Figure 16, A, B, D and E). Gamma-ray values average ~60 API units and ranges from ~30-80 API.

Diatomaceous Mudstone

Diatomaceous mudstone lithofacies represents a minor portion of the core (535-539 ft.) and is distinct as it is characterized by a dark brown massive muddy texture that lacks sedimentary features (Figure 15, C). Compositional averages consist of 45% opal-A, 0% opal-CT, 53.4% total detritus (10.9% phyllosilicates and 42.5% quartz and feldspars), and little to no pyrite (<1%). SEM images of this lithofacies exhibit a low degree of biofragmentation, as distinct intact diatoms are visible (Figure 16, C). Overall, gamma-ray values average ~45 API units.

Diatomaceous Porcelanite

Diatomaceous porcelanite dominates the lower section of Newlove 76-RD1 displayed in the available core (from 865' to 892'). This lithofacies is massive to discontinuously laminated, light-to-dark brown, and contain discontinuous to continuous sandstone/siltstone laminations (Figure 15, D) that exhibit cross-laminations, breccia, and faults. X-ray diffraction reveals that this lithofacies contains an average of 19.5% opal-A, 53% opal-CT, 24.9% total detritus (8.7% phyllosilicates and 16.2% quartz and feldspars), no pyrite, and is within the opal-A to opal-CT transition zone as it contains both opal-A and opal-CT.

Primary depositional microfabric and degree of biofragmentation within this lithofacies are difficult to discern due to the digenesis of opal-CT (Figure 16, F), but it appears that porosity loss is substantial within this lithofacies in comparison to opal-A phase rocks within Newlove-76RD1. The gamma-ray values average ~65 API units and ranges from ~50-85 API units.

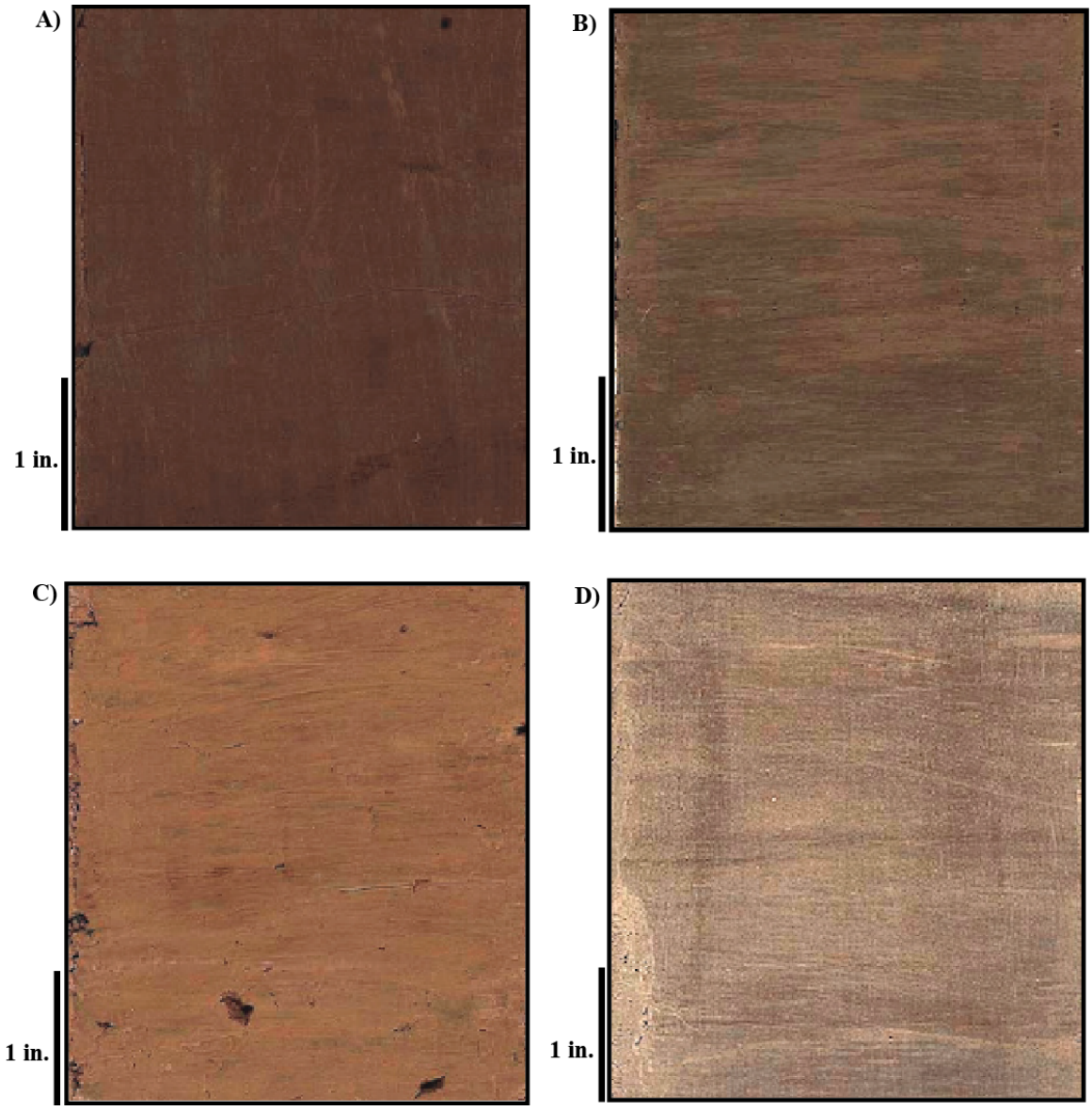

FIGURE 15. Core photos of lithofacies within Newlove 76-RD1. The images of the three lithofacies shown above are (A) muddy diatomite (massive) at 294’ (B) muddy diatomite (discontinuously laminated) at 618’ (C) diatomaceous mudstone at 535’ and (D) diatomaceous porcelanite (discontinuously laminated) at 994’.

FIGURE 16. SEM images of lithofacies within Newlove 76-RD1. The images shown are (A) full centric diatoms within muddy diatomite (massive) at 275' (B) fragmented diatoms within muddy diatomite (massive) at 518' (C) full centric diatoms within diatomaceous mudstone (massive) at 535' (D) full centric diatoms within muddy diatomite (discontinuously laminated) at 553' (E) fragmented diatoms within muddy diatomite (massive) at 585' and (F) diatomaceous porcelanite (discontinuously laminated) at 865'.

A)

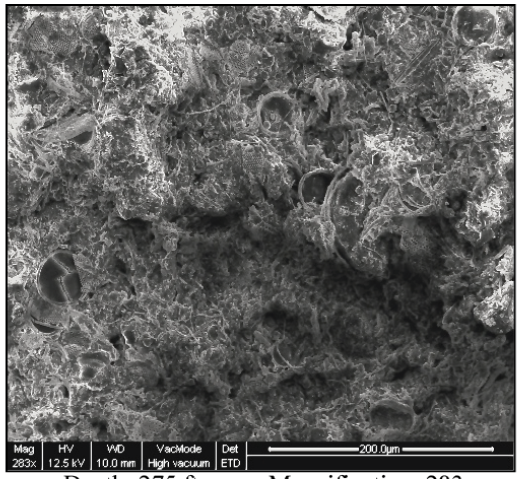

Depth: 275 ft. Magnification: 283x

B)

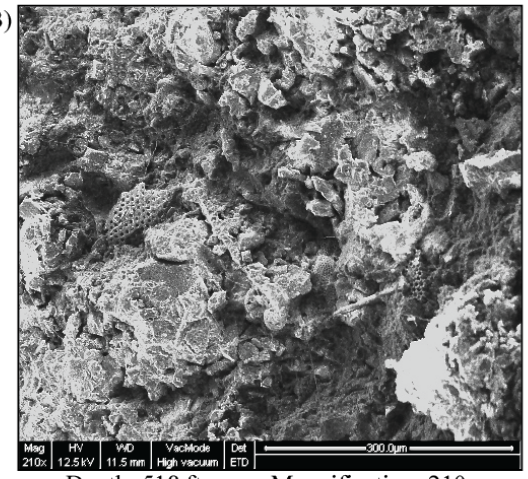

Depth: 518 ft. Magnification: 210x

C)

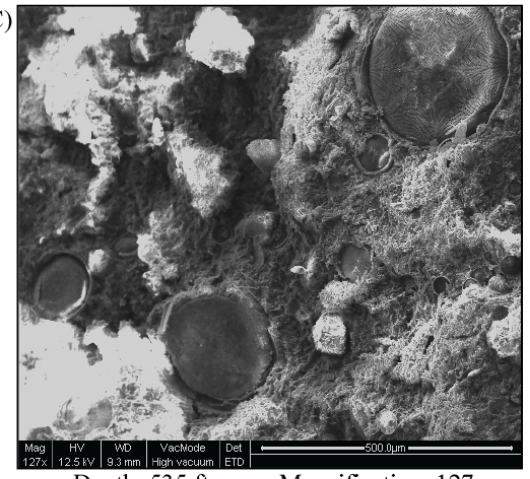

Depth: 535 ft. Magnification: 127x

D)

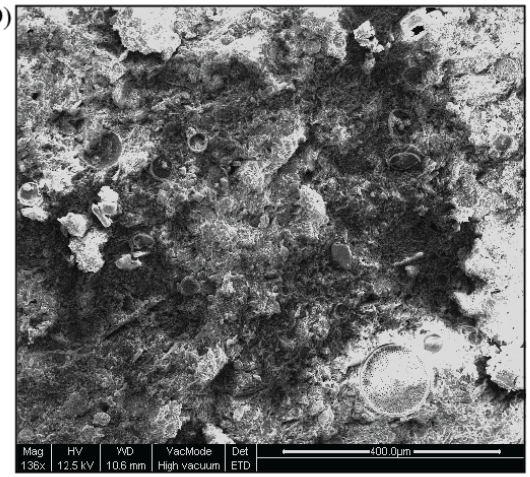

Depth: 553 ft. Magnification: 136x

E)

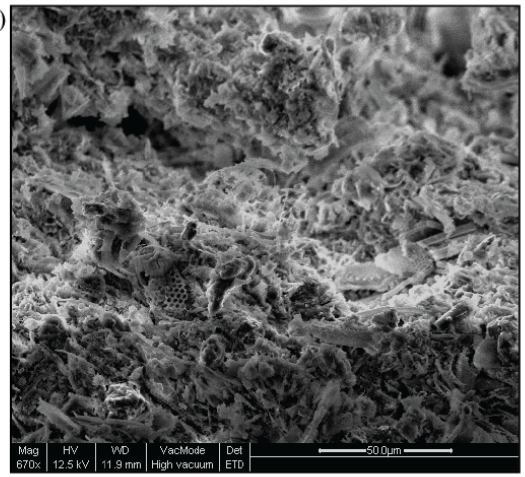

Depth: 585 ft. Magnification: 370x

F)

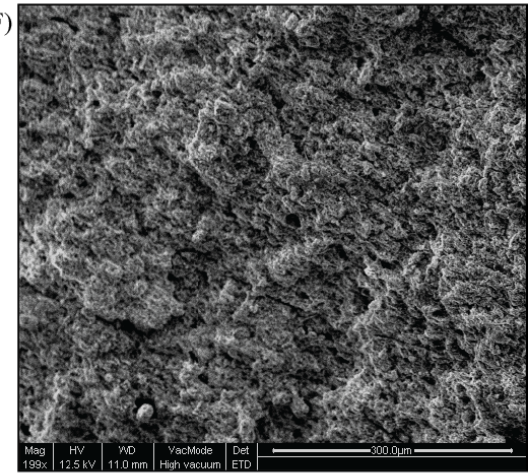

Depth: 865 ft. Magnification: 199x

TABLE 1. Summary of lithofacies within Newlove 76-RD1

Lithofacies	Description
Muddy Diatomite	- Light-to-dark brown - Massive to discontinuously laminated - Fossils, faults, erosional surfaces, breccia, and hardgrounds are common - Debris-flow deposits present in some portions of core - Average 69.4% opal-A, 0% opal-CT, 26.8% total detritus (7.7% phyllosilicates and 19.1% quartz and feldspars), and no pyrite - Gamma-ray values average 60 API units (ranges from 30-105 API units) - Low to high degree of bioturbation (fragmented to fully intact diatoms present)
Diatomaceous Mudstone	- Distinct dark brown massive muddy texture - Average 45% opal-A, 0% opal-CT, 53.4% total detritus (10.9% phyllosilicates and 42.5% quartz and feldspars) and <1% pyrite - Lack of sedimentary features - Low degree of biofragmentation (fully intact diatoms present) - Low gamma-ray values average of 45 API units
Diatomaceous Porcelanite	- Light-to-dark brown - Massive to discontinuously laminated - Sandstone and siltstone cross laminations - Minor breccia and small-scale faults - Average 19.5% opal-A, 53% opal-CT, 24.9% total detritus (8.7% phyllosilicates and 16.2% quartz and feldspars), and <1% pyrite - Gamma-ray values average 65 API units (ranges from 50-85 API units)

Descriptions of identified lithofacies within Newlove 76-RD1 (muddy diatomite, diatomaceous mudstone, and diatomaceous porcelanite) are summarized in Table 1.

Sedimentary Features

Slump folds observed within Newlove 76-RD1 are typically less than ~3 inches in height and are frequently found adjacent to erosional surfaces, breccias, and faults. Slump folds are usually identified by distinct sand laminations (typically ~0.5 inches in thickness) that exhibit a different color and texture compared to surrounding sediments. In addition, slump fold limbs typically vary in thickness (Figure 17, A).

Small to large-scale erosional surfaces and faults are common throughout Newlove 76-RD1. These features are chiefly associated together with debris flow deposits. Erosional surfaces are typically angular (up to ~45 degrees) and sharp, but may be irregular. Sharp contacts commonly exhibit little to no observed deformation between their divided units (Figure 17, B and C). The resolution of cores limits the lateral coverage of larger scale faults; however, mapped surface faults (Namson and Davis, 1990) within Orcutt suggest that large separation is probable. Nearly 90% of laminated strata (discontinuous to continuous) in Newlove 76-RD1 exhibit small-scale (<0.5 inches) microfaulting. In addition, high concentrations of faults are commonly associated with visually apparent elevated oil saturation.

Cores from Newlove 76-RD1 display abundant amounts of fossils, burrows, and hardgrounds (Figure 18). Fossils and burrows can range from less than 0.1 inches to ~2 inches and are closely associated with hardgrounds. Hardgrounds range from less than 1 inch to approximately 1.5 inches in thickness and are easily distinguishable as they are

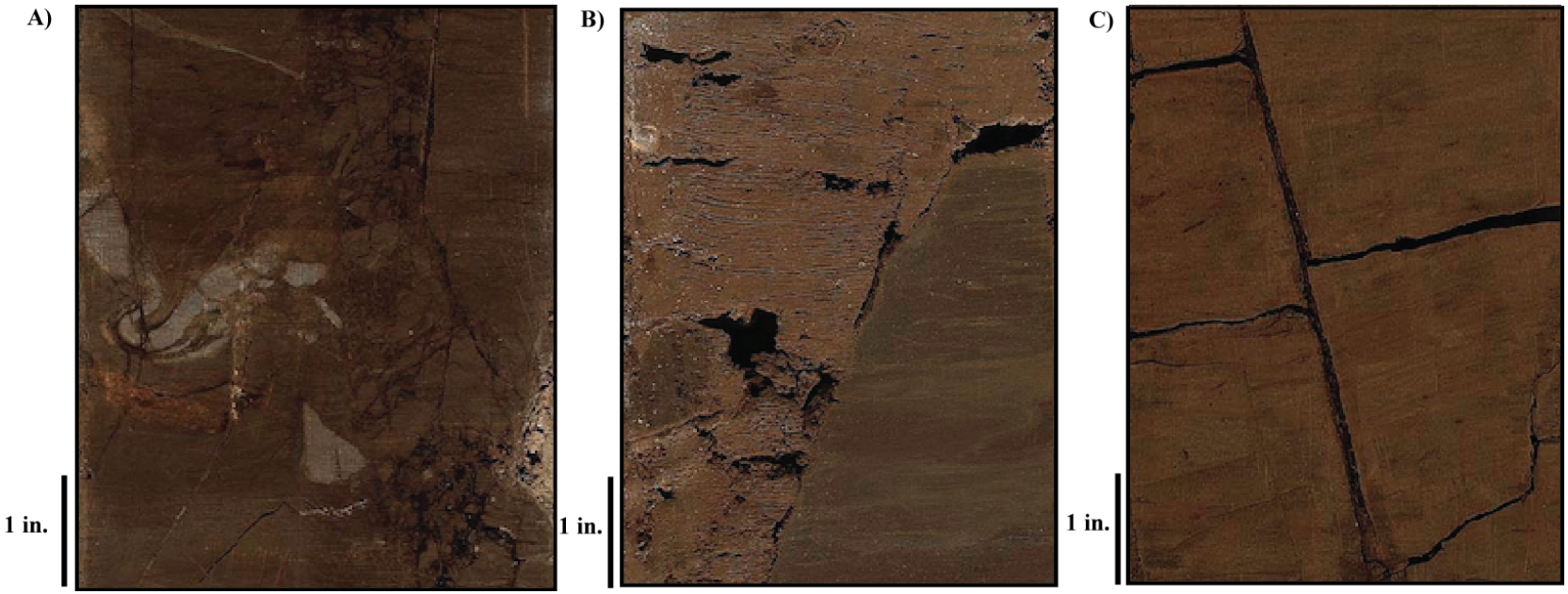

FIGURE 17. Core photos of sedimentary features within Newlove 76-RD1: slump fold, erosional surface, and faults. The images shown are (A) slump fold at 510' (B) erosional surface at 522' and (C) fault at 281'.

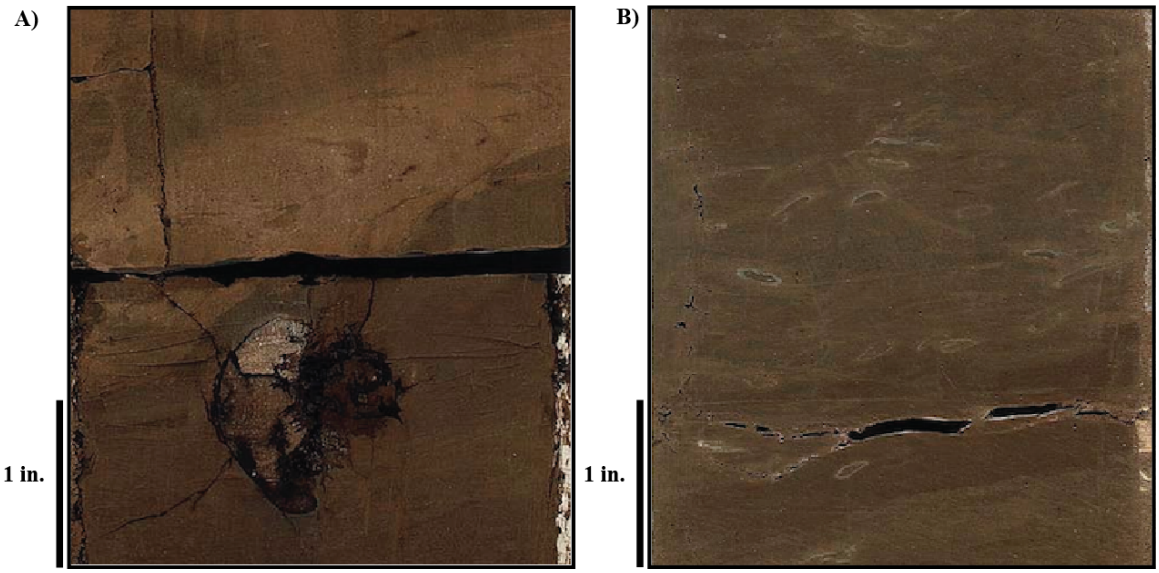

FIGURE 18. Core photos of sedimentary features within Newlove 76-RD1: fossil, hardbround, and burrow. The images above show (A) sediment-infilled mollusk fossil underlying a hardground at 289' and (B) burrows at 529'.

commonly lighter colored, denser, and contain a dissimilar texture compared to their surrounding sediment. The contacts of hardgrounds with their surrounding sediment are frequently irregular and gradational, but may also be sharp.

Thin to thickly bedded debris-flow deposits ranging from inches to feet in scale are present at scattered depths throughout Newlove 76-RD1. Debris-flows typically consists of polymictic conglomerate clasts (granule to cobble) and are matrix supported (Figure 19). X-ray diffraction from selected depths confirms that the compositions of these clasts are phosphatic and dolomitic. Cyclic debris-flow deposits reoccur approximately every 30-70 ft. throughout the middle portion of the cored interval (378' to 700'). In addition, debris-flow deposits throughout Newlove 76-RD1 are commonly

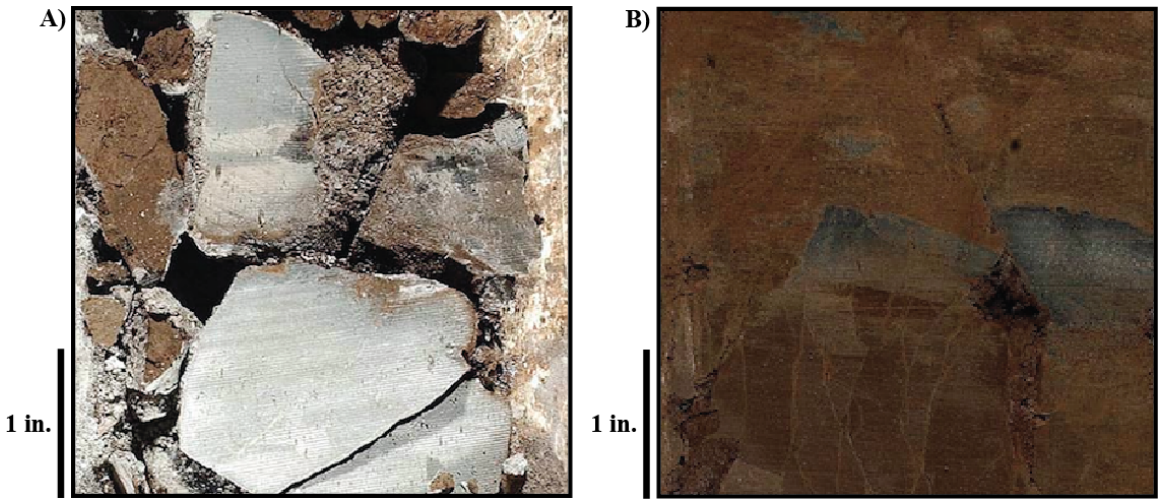

FIGURE 19. Core photos of sedimentary features within Newlove 76-RD1: conglomerate and phosphate debris-flow deposit. Images above show (A) thick conglomerate deposit at 519' and (B) phosphate debris flow deposit at 529'.

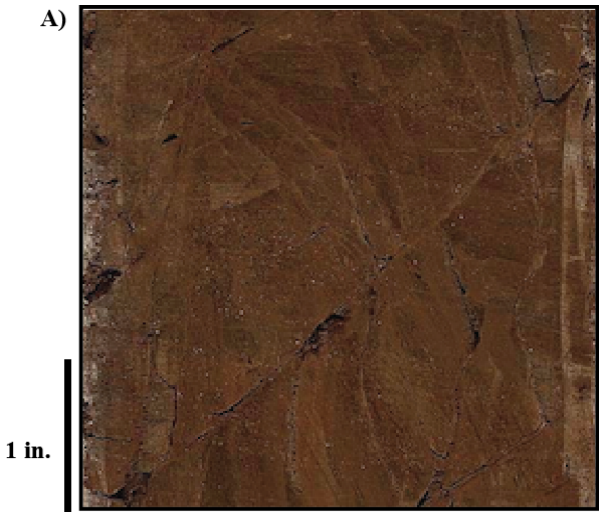

FIGURE 20. Core photo of a sedimentary feature within Newlove 76-RD1: breccia. Image above show a breccia at 629' within a muddy diatomite in Newlove 76-RD1.

associated with observed elevated oil saturation.

Localized, small to thick (<0.25 to 36 inches) intraformational breccias are present throughout Newlove 76-RD1. These breccias are commonly found in association with erosional surfaces, slump folds, and debris-flow deposits. Brecciated fragments can range from smaller (<0.25 inch) to larger clasts (~1 inch) and are typically found with no separation or matrix between fragments (Figure 20).

Discontinuous sandstone and siltstone laminations are prominent within the deeper intervals of Newlove 76-RD1 (865'-892') (Figure 21). These laminations are approximately <0.1 inch in thickness, fine grained, commonly graded, and are easily identified by their oxidized light orange to tan color.

FIGURE 21. Core photo of sedimentary features from Newlove 76-RD1: sandstone and siltstone laminations. Image above show discontinuous to continuous sandstone and siltstone laminations at 888'.

Compositional Trends

Overall, combined samples of Newlove 76-RD1 averaged 65.4% opal-A, 4.8% opal-CT, 26.6% total detritus (7.8% phyllosilicates and 18.9% quartz and feldspars), and <1% pyrite. X-ray diffraction results indicate that the opal-A to opal-CT diagenetic transition zone occurs between samples at 688' and 865'. Newlove 76-RD1 compositional trends of opal-A, opal-CT, total silica, total detritus, and pyrite are shown in Figure 22.

Petrophysical Trends

The gamma-ray log of Newlove 76-RD1 displays three distinct trends: (1) consistent gamma-ray values ranging from ~55-65 API units from 700' to 893' (2) significantly varying gamma-ray values from ~30-110 API units with reoccurring gamma-ray cyclic peaks every ~30-70 ft. from 378' to 700' and (3) consistent gamma-ray values ranging from ~45-80 API units from 270' to 377'. These observations are used to distinguish lithostratigraphic units (described later within the section) within Newlove 76-RD1.

An overview of the lithofacies, sedimentary features, and petrophysical trends of Newlove 76-RD1 are shown in Figure 23.

Lithostratigraphic Units

Newlove 76-RD1 is divided into four lithostratiraphic units based on distinct differences in lithofacies, sedimentary features, and/or gamma-ray signatures. The lithostratigraphic units are named A, B, C, and D starting from the deepest (bottom of the core) to the shallowest (top of core) depths of the cored intervals of Newlove 76-RD1.

FIGURE 22. Mineralogical compositional trends of Newlove 76-RD1. Compositional trends shown include opal-A, opal-CT, total silica, total detritus, and pyrite. Solid black squares represents samples that were analyzed by XRD. Solid black lines indicate trends well-supported by large numbers of samples. Dashed lines are interpolated trends across intervals of missing data.

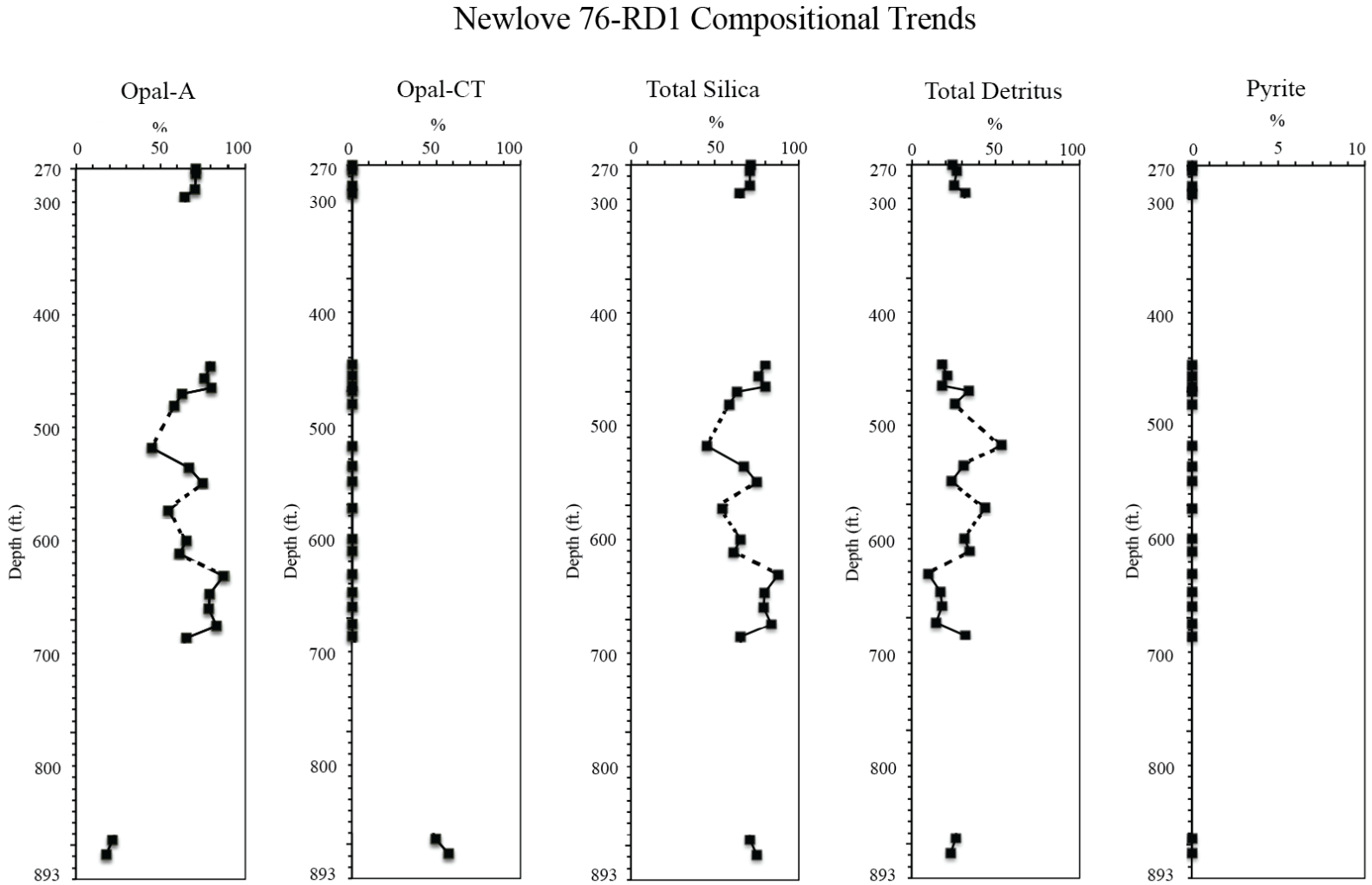
Newlove 76-RD1 Compositional Trends
Opal-A
Opal-CT
Total Silica
Total Detritus
Pyrite
%
0
50
100
5
10
Depth (ft.)
270
300
400
500
600
700
800
893

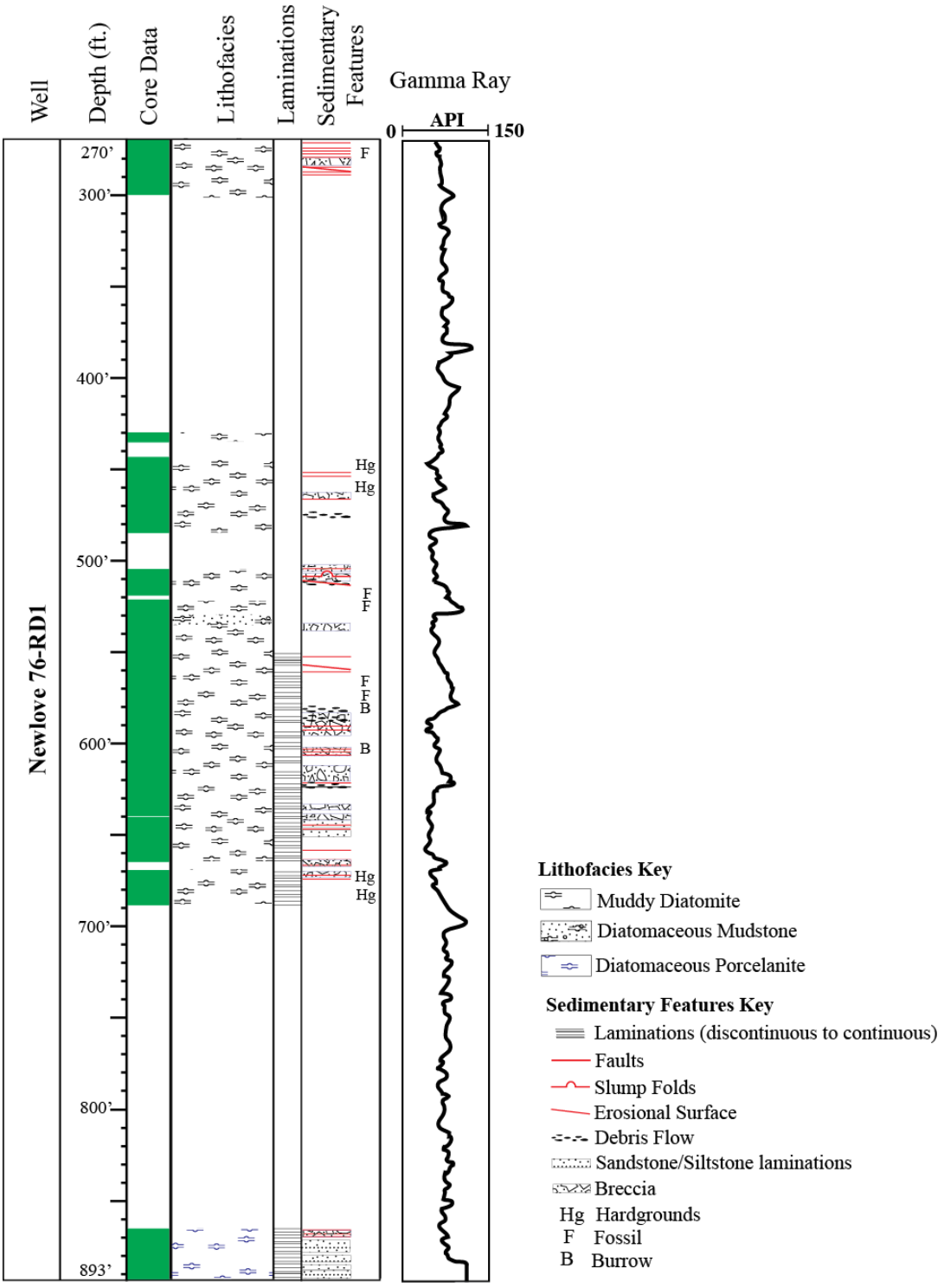

FIGURE 23. Stratigraphic column of Newlove 76-RD1. This figure displays lithofacies, sedimentary features, and a gamma-ray log of Newlove 76-RD1.

The significance of these lithostratigraphic units will be evaluated in the discussion section and is referenced to Figure 24 (unit-labeled integrated stratigraphic column).

Newlove Lithostratigraphic Unit A

This lithostratigraphic unit, spanning depths from 700' to 893' of Newlove 76-RD1, is characterized by being the only unit containing diatomaceous porcelanite. It consists predominantly of light-to-dark brown discontinuous to continuously laminated diatomaceous porcelanite with faults, minor breccia, and is void of debris-flow deposits. The contact between Newlove A and Newlove B is designated at 700' in conjunction with a shift in gamma-ray values that increases from ~65 to 95 API units (interpreted to be the onset of debris flow deposits). The gamma-ray values of Newlove A are fairly consistent without large variations ranging from ~55-65 API units.

Newlove Lithostratigraphic Unit B

Newlove lithostratigraphic B represents depths 550' to 699' and is characterized by alternating light-to-dark brown discontinuously laminated to massive muddy diatomite. Newlove B contains abundant sedimentary features, including: debris-flows deposits, erosional surfaces, faults, hardgrounds, fossils, burrows, slump folds, and discontinuous sandstone and siltstone laminations. The gamma-ray values for Newlove B vary significantly in comparison to Newlove A ranging from ~30-100 API. Gamma-ray highs (ranging from ~60-100 API units) are cyclic reoccurring every ~30-50 ft. The contact between Newlove B and Newlove C is at 550', above which discontinuous laminations are not present.

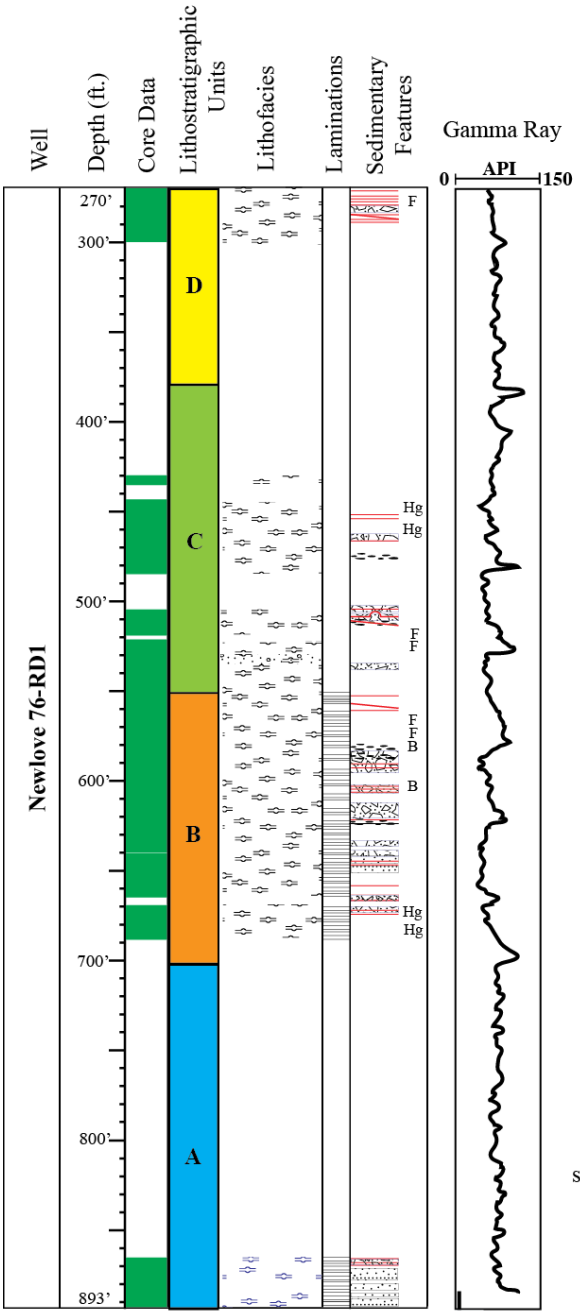

Newlove Lithostratigrahpic Unit D (270'-377')
Mottled light-to-dark brown massive muddy diatomite, fossils, erosional surfaces, hardgrounds, breccia, faults, gamma-ray values average 60 API units

Newlove Lithostratigrahpic Unit C (378'-549')
Dark brown massive muddy diatomite with minor diatomaceous mudstone and cyclic debris-flow deposits, erosional surfaces, faults, hardgrounds, fossils, slump folds, gamma-ray values average 55 API units

Newlove Lithostratigrahpic Unit B (550'-699')
Alternating light-to-dark brown discontinuously laminated muddy diatomite and massive muddy diatomite with cyclic debris-flow deposits, erosional surfaces, faults, fossils, discontinuous sandstone and siltstone laminations, gamma-ray values average 50 API units

Newlove Lithostratigrahpic Unit A (700'-893')
Light-to-dark brown discontinuous to continuous diatomaceous porcelanite, minor small-scale faults, minor breccia, void of debris-flow material, discontinuous sandstone and siltstone laminations, gamma-ray values average 65 API units

FIGURE 24. Integrated stratigraphic column of Newlove 76-RD1. This figure displays lithostratigraphic units, lithofacies, sedimentary features, gamma-ray log, and descriptions of Newlove lithostratigraphic units A, B, C, and D. Symbols as in Figure 23.

Newlove Lithostratigraphic Unit C

Newlove Lithostratigraphic Unit C extends from depths 430' to 549' and is predominantly composed of dark brown massive muddy diatomite with a minor diatomaceous mudstone interval at 534'-539'. Newlove C is compositionally similar to Newlove B, but differentiated by the absence of discontinuous laminations. Newlove C contains similar sedimentary features to Newlove B consisting of erosional surfaces, faults, hardgrounds, fossils, burrows, and slump folds. Newlove C also contains more variable gamma-ray values that range from ~30-110 API units. In addition, gamma-ray highs within this unit are also cyclic, reoccurring approximately every ~40-70 ft. The contact between Newlove C and D is designated at 378', above which there are relatively consistent gamma-ray values without large variations (interpreted as absence of debris-flow deposits).

Newlove Lithostratigraphic Unit D

Newlove Lithostratigraphic Unit D spans depths 270' to 377' and is composed entirely of light-to-dark brown massive muddy diatomite. Sedimentary features include burrows, fossils, breccias, and faults. Newlove D is interpreted to lack clear debris-flow deposits. The gamma-ray values of Newlove D vary between ~45-80 API values.

Summary of Newlove 76-RD1 Results

Overall, Newlove 76-RD1 is chiefly composed of massive to laminated (discontinuous to continuous) muddy diatomite with compositional averages of 65.4% opal-A, 4.8% opal-CT, 26.6% total detritus (7.8% phyllosilicates and 18.9% quartz and feldspars), and <1% pyrite. Newlove 76-RD1 consists of three distinct lithofacies: (1)

muddy diatomite (2) diatomaceous mudstone and (3) diatomaceous porcelanite. Sedimentary features that were identified within Newlove 76-RD1 include slump folds, erosional surfaces, faults, fossils, burrows, hardgrounds, debris-flow deposits breccia, and sandstone/siltstone laminations. In addition, compositional trends reveal that the opal-A to opal-CT diagenetic transition zone occurs between 688' to 865'. Petrophysical trends reveal that Newlove 76-RD1 consists of three distinct trends: (1) consistent gamma-ray values from 700' to 893' (2) significantly varying gamma-ray values from 378' to 699' and (3) consistent gamma-ray values from 270' to 377'. Furthermore, Newlove 76-RD1 is subdivided into four main lithostratigraphic units: Newlove Lithostratigraphic Units A, B, C and D.

Stokes A-30804 Results

Lithofacies

Muddy Diatomite

Muddy diatomite is most prevalent lithofacies within the shallower depths of Stokes A-30804 from 265' to 356'. This lithofacies is light-to-dark brown, massive (Figure 25, A) and contains faults, erosional surfaces, breccia, and fossils. Compositional averages of this lithofacies are 60% opal-A, 0% opal-CT, 38% total detritus (10% phyllosilicates, 28% quartz and feldspars), and 1.5% pyrite. SEM images reveal that this lithology has a low to moderate degree of biofragmentation (Figure 26, A). Gamma-ray averages ~60 API units and ranges from ~40-120 API units.

Porcelaneous Mudstone

Porcelaneous mudstone is the dominant lithofacies within Stokes A-30804. This

lithofacies is commonly represented between 567' to 1,061' and is characterized by light brown-to-dark brown massive to laminated (discontinuous to continuous) mudstone (Figure 25, B, C and D) that contains abundant sedimentary features including erosional surfaces, faults, breccias, fossils, and discontinuous to continuous sandstone and siltstone laminations. The average composition of this lithofacies is 0.6% opal-A, 36% opal-CT, 56% total detritus (22% phyllosilicates and 34% quartz and feldspars), and 1.9% pyrite. Gamma-ray averages ~60 API units and ranges from ~30-95 API units.

Diatomaceous Porcelanite

Diatomaceous porcelanite is represented between 601' to 683' and is commonly found alternating with massive porcelaneous mudstone. It is characterized as a light brown-to-brown massive porcelanite that contains faults, breccia, and erosional or disconformable surfaces. Compositional averages are 7% opal-A, 55% opal-CT, 30% total detritus (10% phyllosilicates and 20% quartz and feldspars), and 2.7% pyrite. Gamma-ray values average ~65 API units and range from ~60-80 API units.

Clayey Diatomaceous Porcelanite

Clayey diatomaceous porcelanite lithofacies represents the deeper depths within Stokes A-30804 (from 1,150' to 1,176'). This lithofacies is characterized by a light brown-to-brown massive to laminated (discontinuous to continuous) diatomaceous porcelanite that contains discontinuous to continuous sandstone and siltstone (Figure 25, E and F). This lithofacies lacks other sedimentary features with the exception of minor faults. SEM photos reveal that this lithofacies contains preserved microfossils (Figure 26, F). On average, this clayey diatomaceous porcelanite is composed of 0%

FIGURE 25. Core photos of lithofacies within Stokes A-30804. Images show (A) muddy diatomite (massive) at 290’ (B) porcelaneous mudstone (massive) at 588’ (C) diatomaceous porcelanite (massive) at 606’ (D) porcelaneous mudstone (discontinuous to continuously laminated) at 779’ (E) clayey diatomaceous porcelanite (massive) at 1,161’ and (F) clayey diatomaceous porcelanite (discontinuous to continuously laminated) at 1,173’.

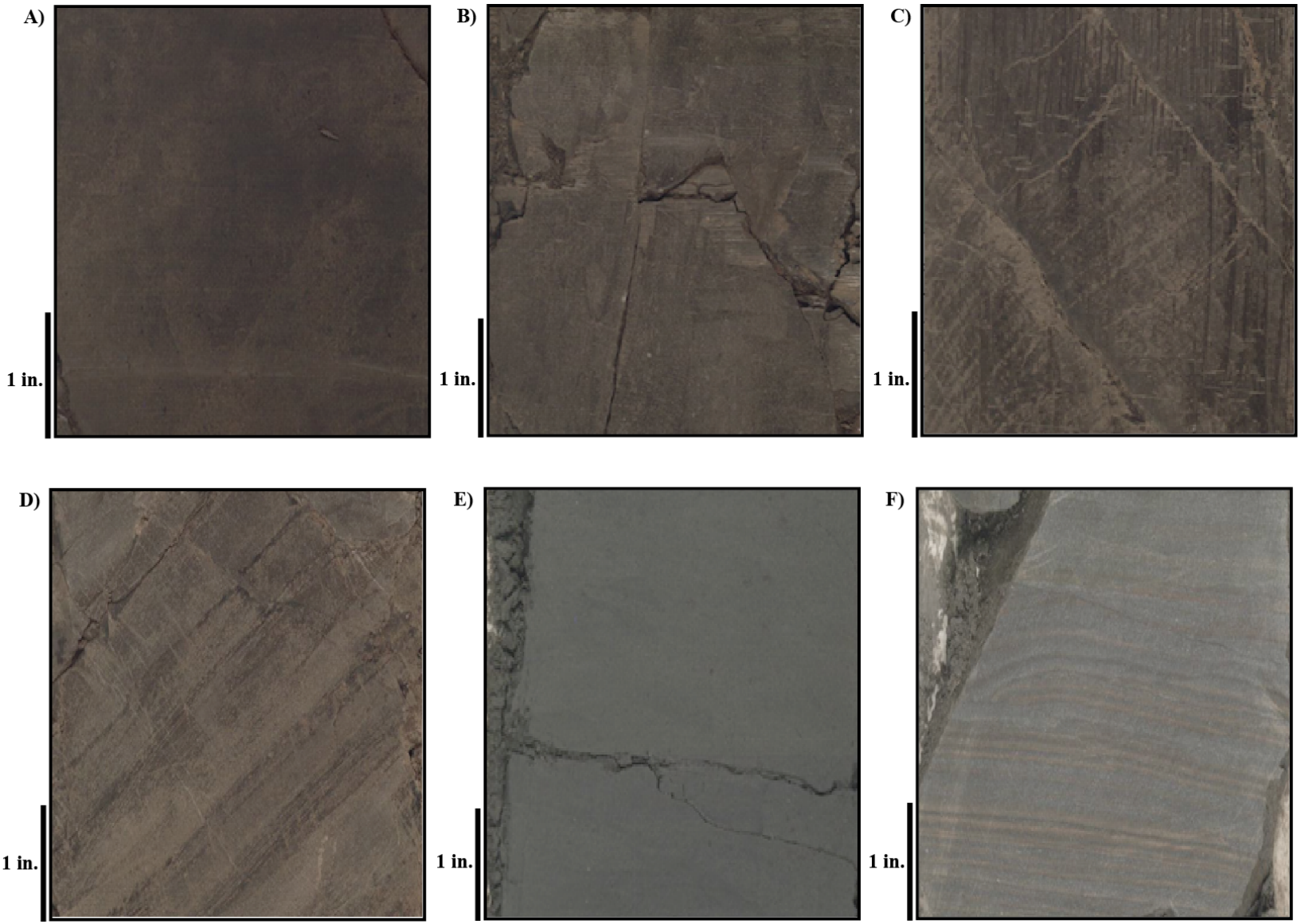
A)
1 in.
B)
1 in.
C)
1 in.
D)
1 in.
E)
1 in.
F)
1 in.

FIGURE 26. SEM images of lithofacies within Stokes A-30804. Images show (A) muddy diatomite (massive) at 335' (B) diatomaceous porcelanite (massive) at 606' (C) porcelaneous mudstone (massive) at 652' (D) porcelaneous mudstone (discontinuously laminated) at 1,000' (E) porcelaneous mudstone (discontinuous to continuously laminated) at 1,040' and (F) clayey diatomaceous porcelanite (continuously laminated) at 1,172' showing microfossil mold.

A)

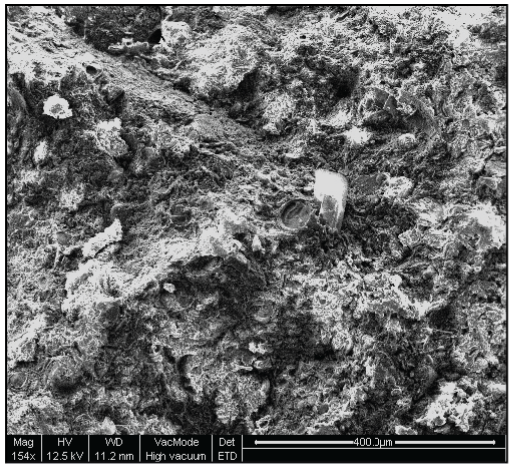

Depth: 335 ft. Magnification: 154x

B)

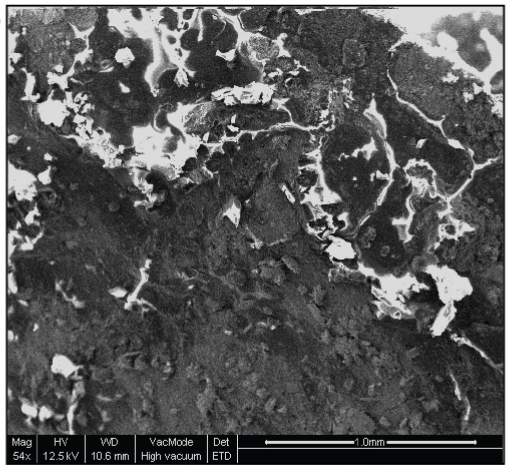

Depth: 606 ft. Magnification: 54x

C)

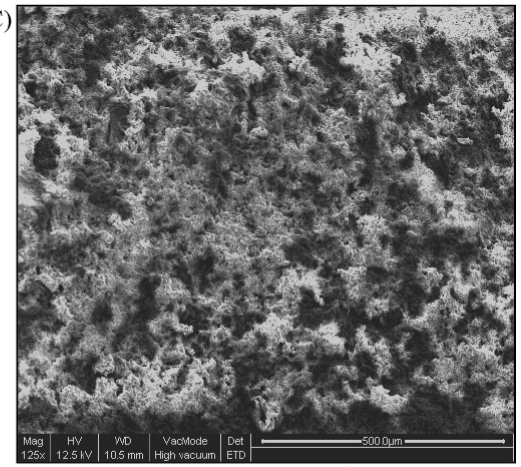

Depth: 652 ft. Magnification: 125x

D)

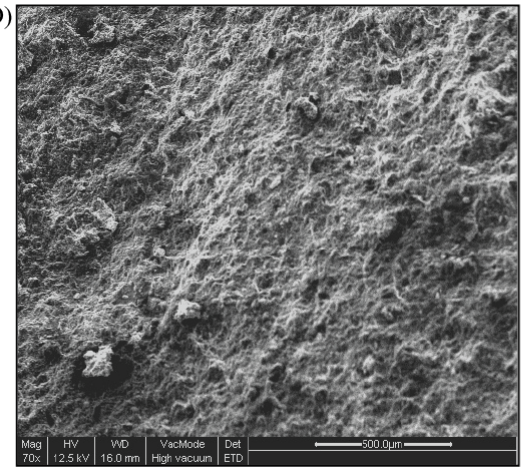

Depth: 1,000 ft. Magnification: 70x

E)

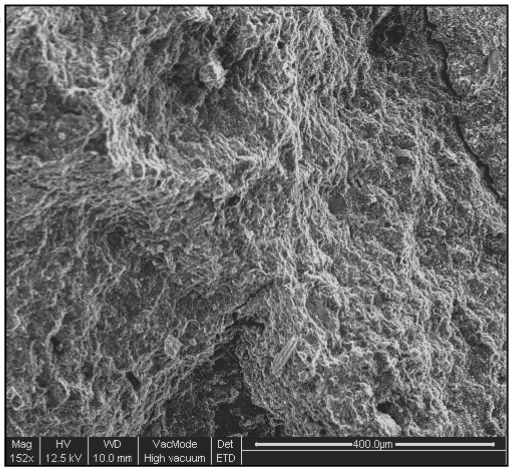

Depth: 1,040 ft. Magnification: 152x

F)

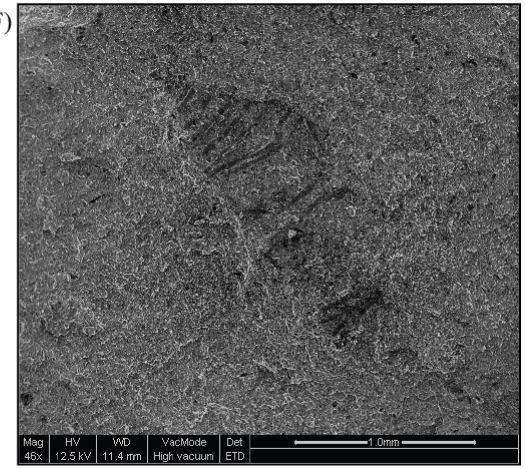

Depth: 1,172 ft. Magnification: 46x

TABLE 2. Summary of lithofacies within Stokes A-30804

Lithofacies	Description
Muddy Diatomite	- Light-to-dark brown and massive - Faults, erosional surfaces, debris-flow deposits and fossils - Averages 60% opal-A, 0% opal-CT, 38% total detritus (10% phyllosilicates and 28% quartz and feldspars), 1.5% pyrite - Gamma-ray values average 60 API units (ranges from 40-120 API units) - Low to moderate degree of biofragmentation (fragmented to fully intact diatoms present)
Porcelaneous Mudstone	- Light brown-to-dark brown and massive to laminated (discontinuous to continuous) - Abundant debris-flow deposits, faults, erosional surfaces, breccia, and fossils - Discontinuous to continuous sandstone and siltstone laminations - Average 0.6% opal-A, 36% opal-CT, 56% total detritus (22% phyllosilicates and 34% quartz and feldspars), 1.9% pyrite - Gamma-ray values average 60 API units (ranges from 30-95 API units)
Diatomaceous Porcelanite	- Light brown-to brown - Faults, breccia, and erosional surfaces - Average 7% opal-A, 55% opal-CT, 30% total detritus (10% phyllosilicates and 20% quartz and feldspars), 2.7% pyrite - Gamma-ray values average 65 API units (ranges from 60-80 API units)
Clayey Diatomaceous Porcelanite	- Light brown to brown and massive to laminated (discontinuous to continuous) - Thin laminated strata with “varve-like” laminations in some strata - Discontinuous to continuous sandstone and siltstone laminations - Absent of debris-flow deposits - Averages 0% opal-A, 51% opal-CT, 43% total detritus (22% phyllosilicates and 21% quartz and feldspars), 3.7% pyrite - Gamma-ray values average 60 API units (ranges from 45-65 API units)

opal-A, 51% opal-CT, 43% total detritus (22% phyllosilicates and 21% quartz and feldspars), and 3.7% pyrite. Gamma ray-values average ~60 API units and range from ~45-65 API units. Descriptions of identified lithofacies within Stokes A-30804 (muddy diatomite, porcelaneous mudstone, diatomaceous porcelanite, and clayey diatomaceous porcelanite) are summarized in Table 2.

Sedimentary Features

Erosional surfaces and faults are abundant throughout Stokes A-30804 and are commonly associated with debris-flow deposits. Erosional surface contacts are chiefly irregular, low-to-high angled, and convoluted (Figure 27, A). Faults are present in all lithofacies within Stokes A-30804. Faults range from the less than 0.1 inch to lengths larger than the viewable core (Figure 27, B). High concentrations of faults or fractured rock typically correlate with observed elevated oil saturations.

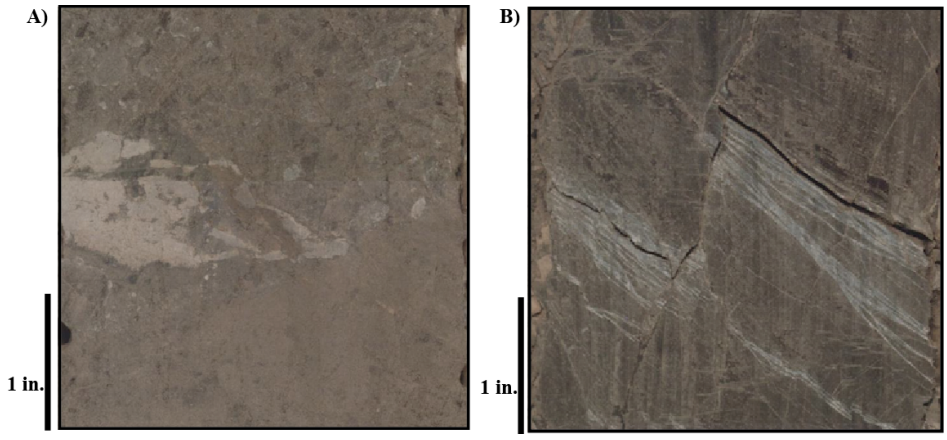

FIGURE 27. Core photo of a sedimentary feature within Stokes A-30804: erosional surface and faults. Images show (A) erosional surface at 672' and (B) faulted strata at 601'.

All (whole and fragmented) fossils in Stokes A-30804 are generally found within debris-flow deposits (Figure 28, A). Fragmented to whole fossils and burrows are typically less than 1 inch in length and are more common within diatomite lithofacies. In several depths, *chondrities* was identified and are ~0.1 inches in width (Figure 28, B)

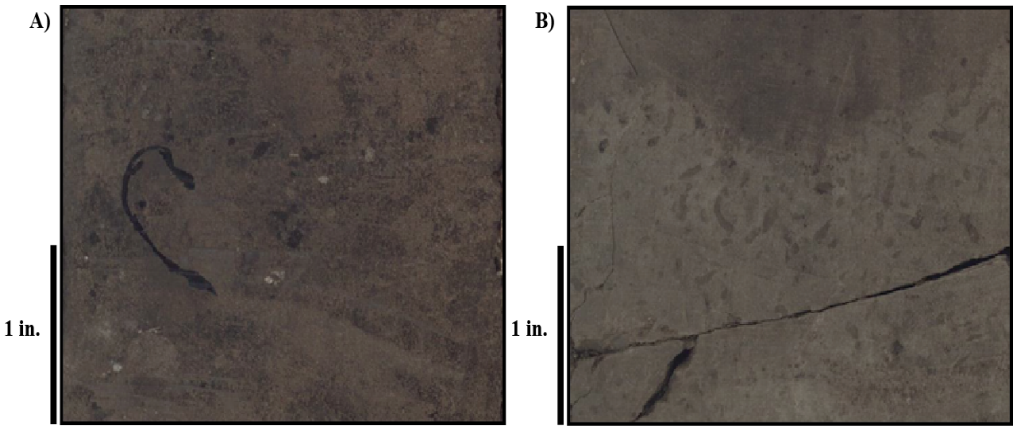

FIGURE 28. Core photo of a sedimentary feature within Stokes A-30804: fossil and burrows. Images show (A) fossil at 272' and (B) burrows (*chondrites)* at 577'.

Debris-flow deposits are the most characteristic sedimentary feature throughout Stokes A-30804 and are commonly associated with erosional surfaces and faults. Debris-flow deposits are primarily composed of poorly to moderately sorted detrital quartz and feldspar subrounded clasts (pebbles to granules). Contacts between debris-flow deposits and adjacent strata are typically irregular, high angled and convoluted (Figure 29, A and B). Some debris-flow deposits are graded. Debris-flow deposits are commonly associated with observed elevated oil saturations.

Intraformational breccias were identified throughout Stokes A-30804 and are commonly associated with erosional surfaces, faults, and debris flow deposits. Brecciated fragments can range from highly brecciated smaller clasts (<0.5 inches) to larger fragments (~2.5 inches) (Figure 30, A and B).

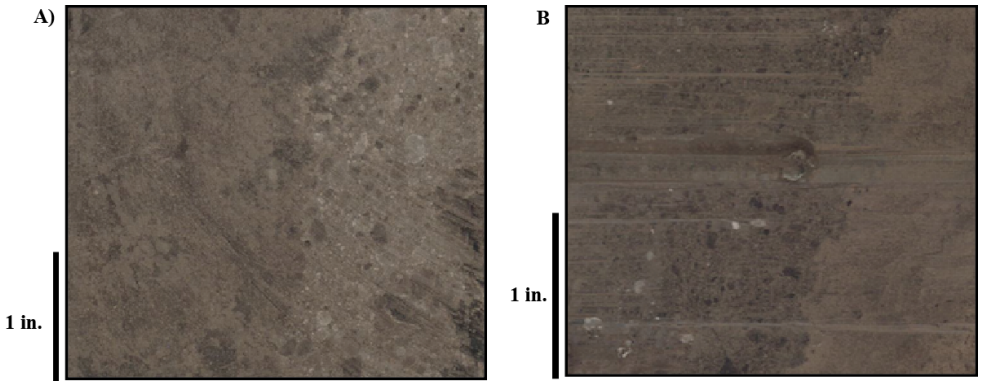

FIGURE 29. Core photo of a sedimentary feature within Stokes A-30804: debris-flow deposit and convoluted irregular contact. Images show debris flow deposits with convoluted irregular contacts at (A) 657' and (B) 309'.

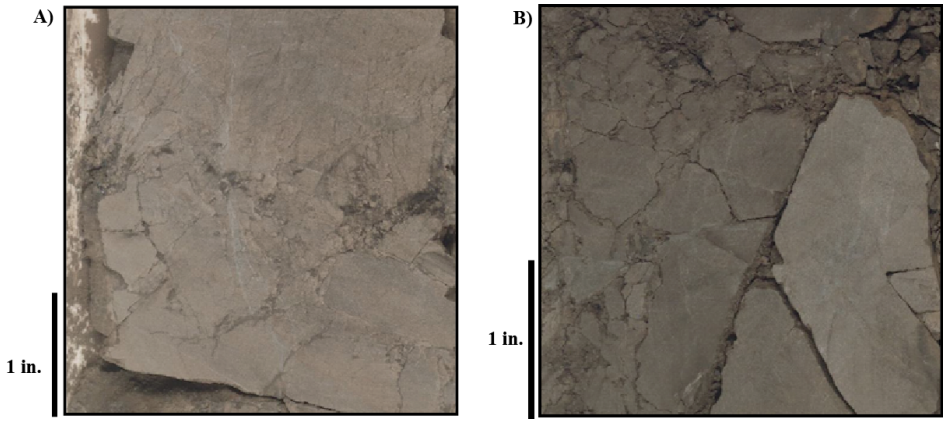

FIGURE 30. Core photo of a sedimentary feature within Stokes A-30804: breccia. Images show (A) breccia at 992' and (B) faulted breccia at 1,010'.

Discontinuous to continuous sandstone and siltstone laminations are prominent in deeper levels within Stokes A-30804. They are characterized as thin laminations (typically <0.2 inches in thickness), fine grained, (Figure 31, A) and typically oxidized to a light orange to tan color. In some cases, laminations are truncated (Figure 31, B). Prominent continuous sandstone and siltstone laminations are more common within diatomaceous porcelanite lithofacies in contrast to porcelanous mudstone.

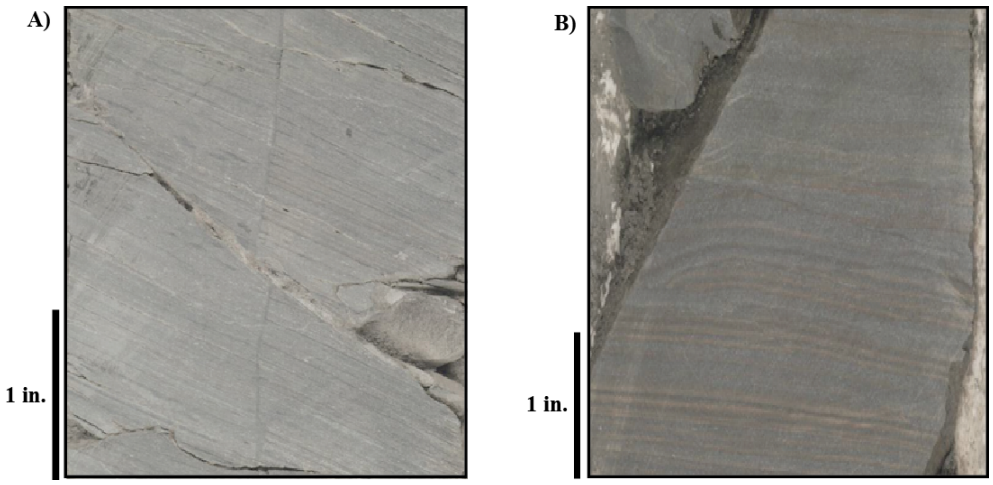

FIGURE 31. Core photo of sedimentary features within Stokes A-30804: sandstone and siltstone laminations. Images show (A) discontinuous to continuous siltstone laminations at 1,152' and (B) continuous truncated siltstone laminations at 1,172'.

Compositional Trends

Overall, combined samples from Stokes A-30804 averaged 17.3% opal-A, 28.6% opal-CT, 48.6% total detritus (18.1% phyllosilicates and 30.4% quartz and feldspars), and 2.1% pyrite shown in Figure 33. In addition, the compositional trends reveal that the

FIGURE 32. Mineralogical compositional trends of Stokes A-30804. Compositional trends shown include opal-A, opal-CT, total silica, total detritus, and pyrite. Solid black squares represents samples that were analyzed by XRD. Solid black lines indicate trends well-supported by large numbers of samples. Dashed lines are interpolated trends across intervals of missing data.

Stokes A-30804 Compositional Trends

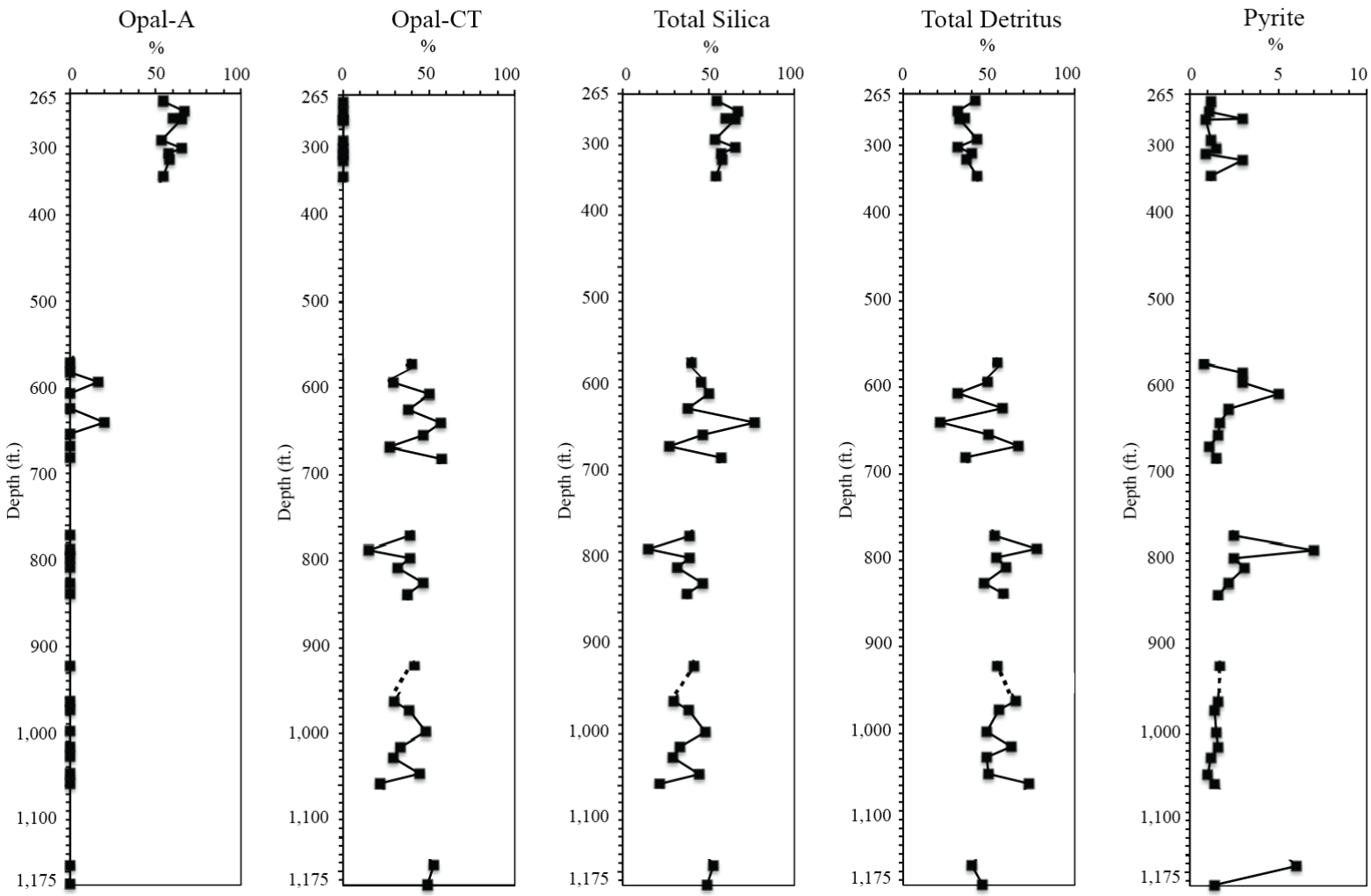

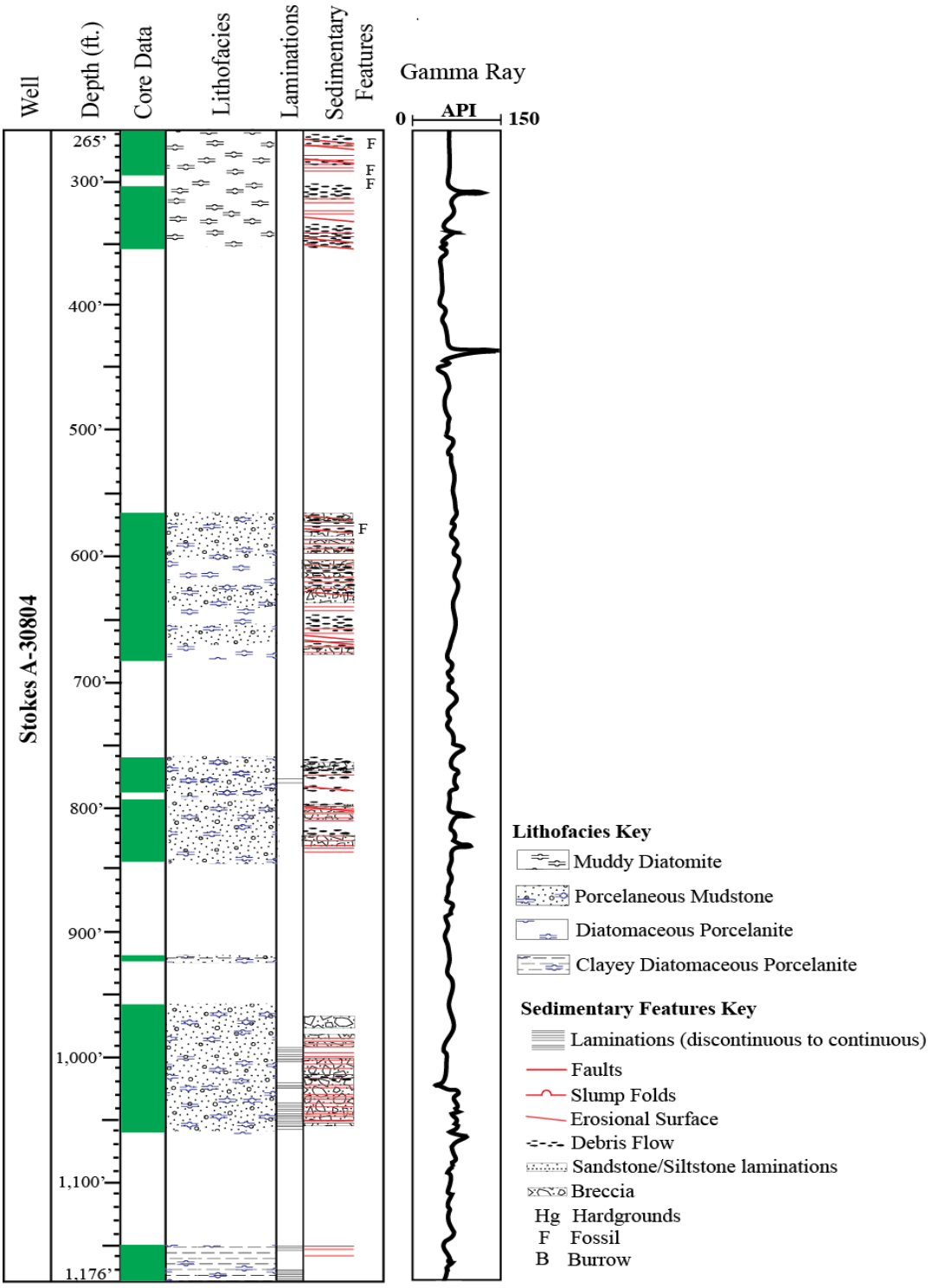

FIGURE 33. Stratigraphic column of Stokes A-30804. This figure displays lithofacies, sedimentary features, and gamma-ray log.

opal-A to opal-CT diagenetic transition zone occurs at a fairly shallow depth between 356' to 567'. Stokes A-30804 compositional trends of opal-A, opal-CT, total silica, total detritus, and pyrite are shown in Figure 32.

Petrophysical Trends

The gamma-ray log of Stokes A-30804 displays predominantly consistent gamma-ray values throughout the entire well typically ranging between ~45-80 API units (except for several gamma-ray spikes interpreted to be caused by phosphatic debris-flow deposits). Thus, it is difficult to identify gamma-ray trends of Stokes A-30804. The only distinct identified gamma-ray shift is from 1,025' to 1,030' in which gamma-ray values increase from 30 API units to 76 API units coinciding with a thinly bedded oil rich debris-flow deposit. Thus, lithofacies and sedimentary features were predominantly used to subdivide Stokes A-30804 into lithostratigraphic units.

An overview of the lithofacies, sedimentary features, and petrophysical trends of Stokes A-30804 are shown in Figure 33.

Core Analysis Trends

Core analyses of selected samples were conducted throughout Stokes A-30804 by Core Laboratories (see methods for procedures) for porosity, oil saturation, and water saturation. Figure 34 displays these results according to depth. The plotted results reveal that the combined selected samples within Stokes A-30804 averages the following values in Table 3 and are illustrated in Figures 35 and 36. Thus, the core analyses reveals that there are distinct variations of porosity, oil saturation, and water saturations between lithofacies. The importance of these data will be elaborated in the discussion.

FIGURE 34. Core analysis trends of Stokes A-30804. Trends include porosity, oil saturation, water saturation, and calculated oil to water ratio. Solid black squares represents samples that were analyzed by Core Laboratories. Solid black lines indicate trends well-supported by large numbers of samples. Dashed lines are interpolated trends across intervals of missing data.

Stokes A-30804 Core Analysis Trends

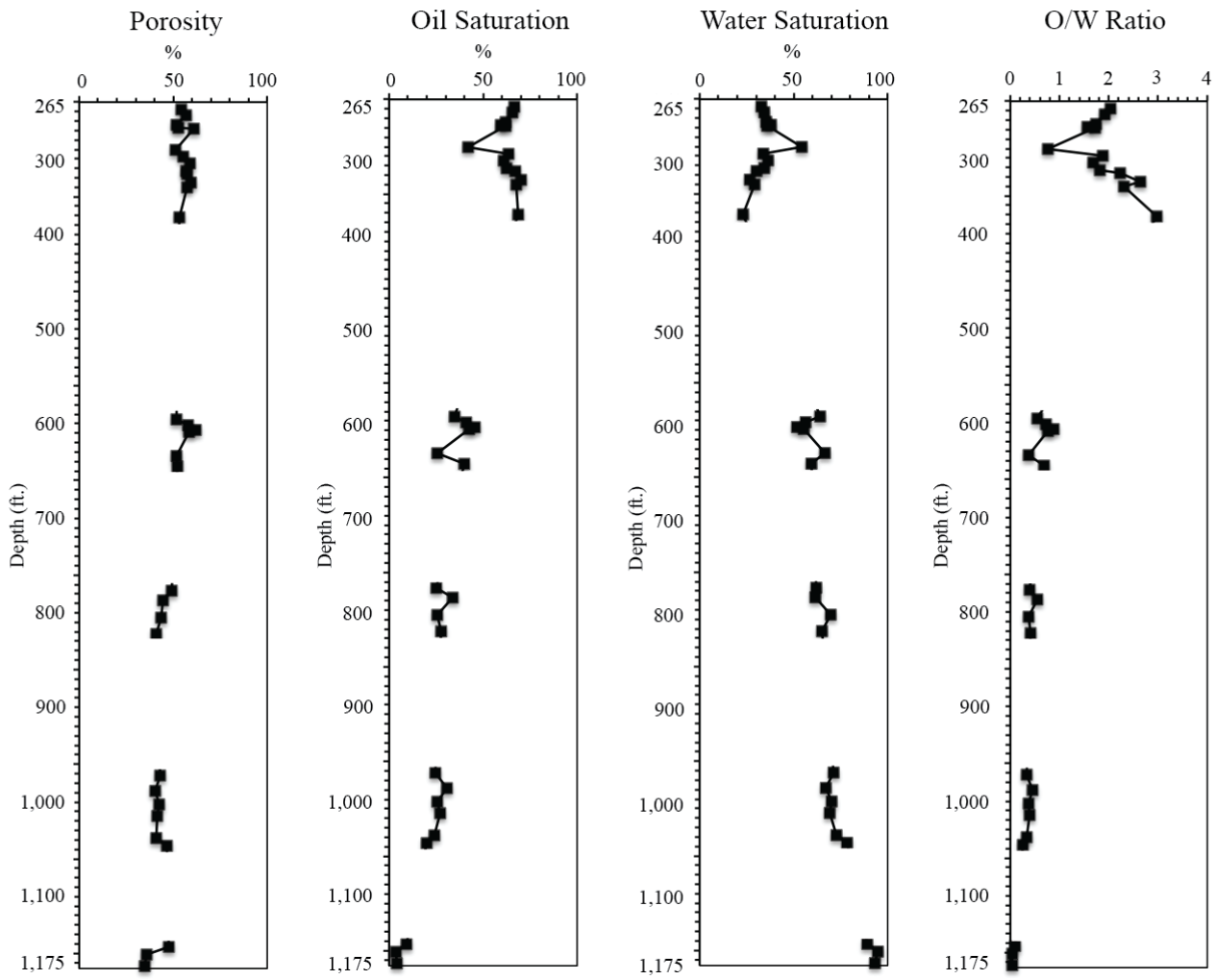

TABLE 3. Statistical averages of porosity, oil and water saturation of lithofacies within Stokes A-30804

Lithofacies	Average Porosity	Average Oil Saturation	Average Water Saturation
Muddy Diatomite	55.9%	52.9%	34.2%
Porcelaneous Mudstone	44.8%	26.9%	68.2%
Diatomaceous Porcelanite	57.7%	42.3%	55.6%
Clayey Diatomaceous Porcelanite	39.6%	5.6%	92.5%

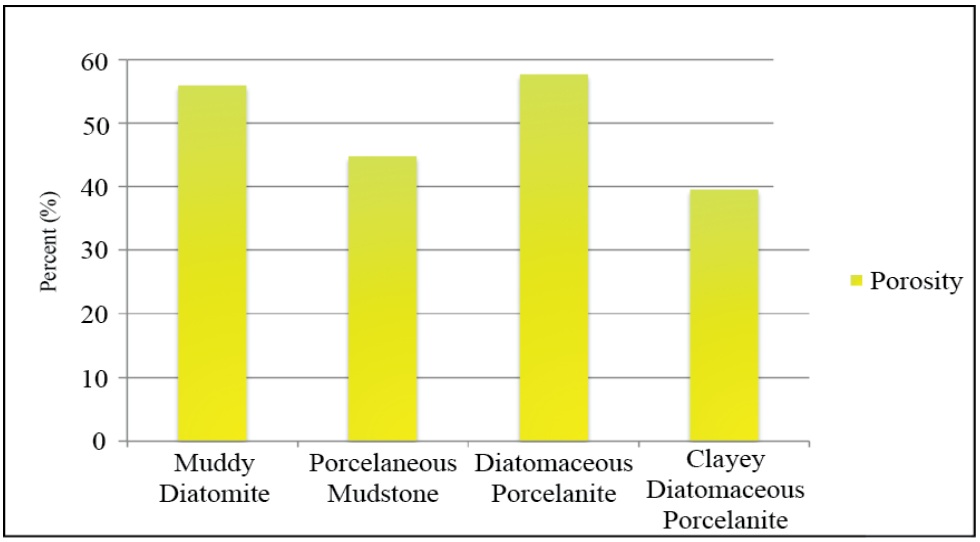

FIGURE 35. Average porosity (%) of lithofacies within Stokes A-30804. Lithofacies include muddy diatomite, porcelaneous mudstone, diatomaceous porcelanite, and clayey diatomaceous porcelanite.

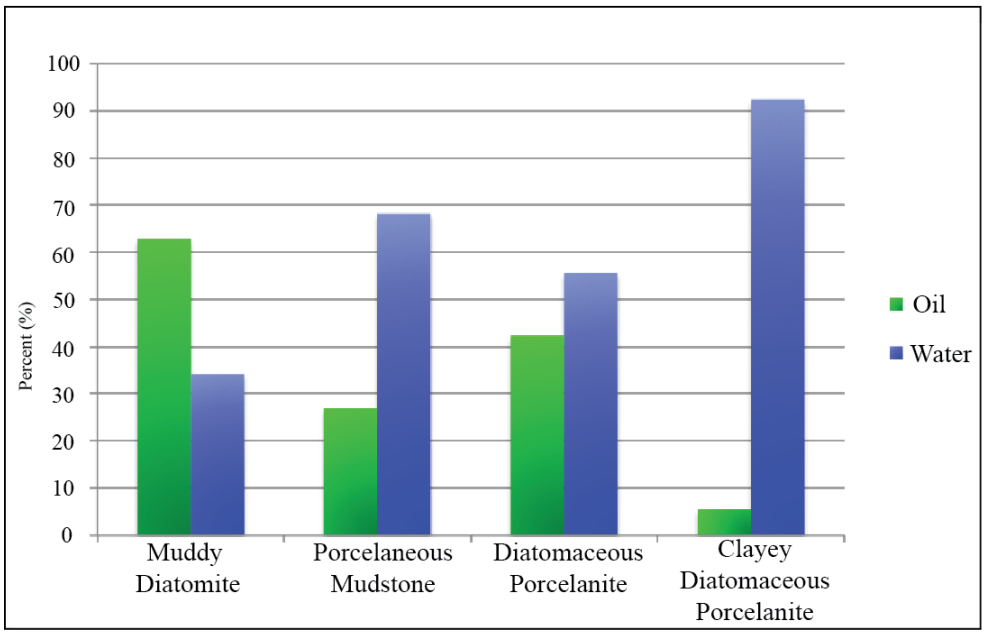

FIGURE 36. Average fluid saturations (%) of lithofacies within Stokes A-30804. Lithofacies include muddy diatomite, porcelaneous mudstone, diatomaceous porcelanite, and clayey diatomaceous porcelanite.

Lithostratigraphic Units

Stokes A-30804 is divided into four lithostratigraphic units based on unique characteristics and changes in lithofacies and sedimentary features. The four units are Stokes Lithostratigraphic Units A, B, C, and D beginning from the bottom (deepest depth) to the top (shallowest depth) of Stokes A-30804. The importance of these lithostratigraphic units will be further elaborated in the discussions and is referenced to Figure 37 (unit-labeled integrated stratigraphic column).

Stokes Lithostratigraphic Unit A

This unit, spanning depths 1,037’ to 1,176’ of Stokes A-30804, is characterized as containing alternating discontinuous to continuous laminated to massive clayey

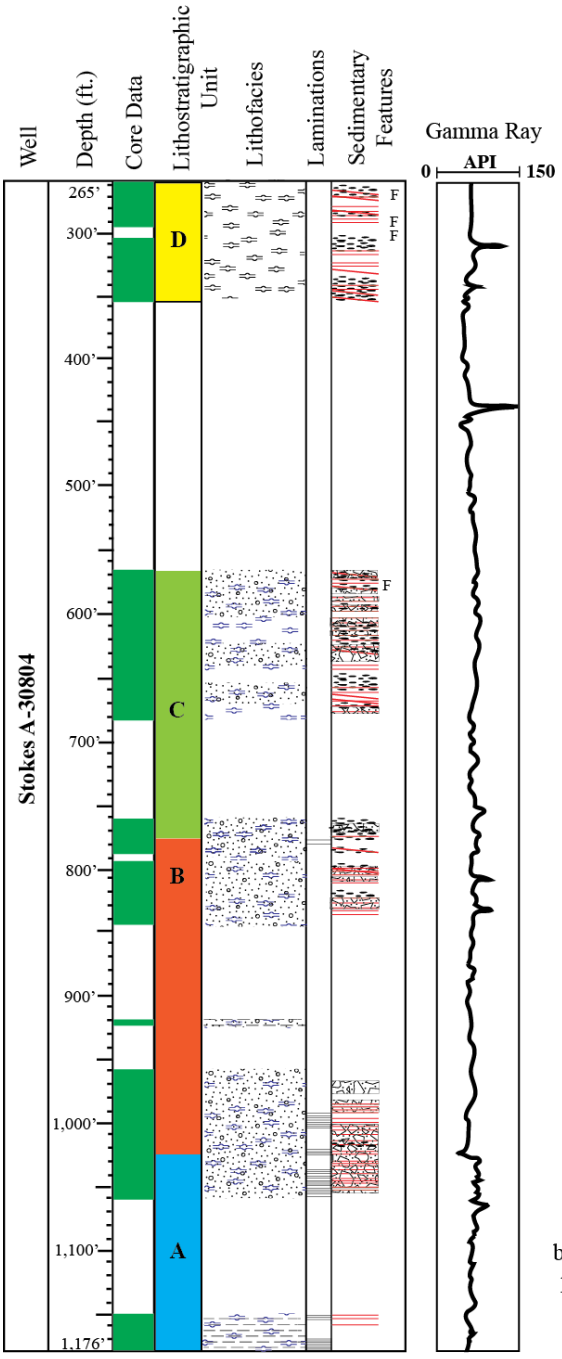

Stokes Lithostratigrahpic Unit D (265'-356')
Light brown massive muddy diatomite, debris flow material, erosional surfaces, faults, breccia, fossils, gamma-ray values average 65 API units

..... ? .....

Opal-A to Opal-CT Transition Zone

..... ? .....

Stokes Lithostratigrahpic Unit C (567'-777')
Alternating light brown diatomaceous porcelanite and clayey porcelaneous mudstone, debris flow material, erosional surfaces, breccia, faults, fossils, gamma-ray values average 60 API units

---

Stokes Lithostratigrahpic Unit B (778'-1,036')
Discontinuously laminated to massive light brown clayey porcelaneous mudstone, debris flow deposits, erosional surfaces, faults, breccia, gamma-ray values average 60 API units

---

Stokes Lithostratigrahpic Unit A (1,037'-1176')
Discontinuous to continuously laminated to massive light brown clayey porcelaneous mudstone and clayey diatomaceous porcelanite, sandstone and siltstone laminations, minor faults, breccia, gamma-ray values average 65 API units

FIGURE 37. Stratigraphic column of Stokes A-30804. This figure displays lithostratigraphic units, lithofacies, sedimentary features, gamma-ray log, and descriptions of Stokes lithostratigraphic units A, B, C, and D. Symbols as in Figure 33.

porcelaneous mudstone and clayey diatomaceous porcelanite. The contact between unit A and B is designated at 1,037' in conjunction with a shift in gamma-ray values (interpreted to be the onset of debris-flow deposits) and the commencement of prominent continuous stratification that is present within unit A. Gamma-ray values of this unit average ~65 API units.

Stokes Lithostratigraphic Unit B

Stokes B ranges from depths 778' to 1,036' and is characterized by alternating light-to-dark brown discontinuously laminated to massive clayey porcelaneous mudstone. These lithofacies are commonly brecciated and contain abundant debris-flow deposits with faults, breccia, and erosional surfaces. Stokes B is differentiated from Stokes A by the presence of debris-flow deposits and less prominent discontinuously laminated strata. The contact between Stokes B and Stokes C is designated at 778' in conjunction with the commencement of laminations. Gamma-ray values for this unit average ~60 API units.

Stokes Lithostratigraphic Unit C

This unit covers depths 567' to 777' of Stokes A-30804 and is characterized by light-to-dark brown alternating diatomaceous porcelanite and clayey porcelaneous mudstone. These lithofacies are intercalated with abundant debris-flow deposits, breccia, and contain fossils. Stokes C is similar in composition to Stokes B, but the major dissimilarity is the absence of discontinuous laminations. The contact between Stokes C and Stokes D cannot be identified as core data is missing from 357' to 566'. This unit averages ~60 API units on the gamma-ray log.

Stokes Lithostratigraphic Unit D

Stokes D spans depths 265' to 356' of Stokes A-30804 and is easily distinguished by light-to-dark brown massive muddy diatomite with debris-flow deposits, absence of opal-CT, and contains erosional surfaces, faults, breccia, and fossils. The average gamma-ray value for Stokes D is ~65 API units.

Summary of Stokes A-30804 Results

Overall, Stokes A-30804 is chiefly composed of massive to laminated (discontinuous to continuous) clayey porcelaneous mudstone and minor diatomaceous porcelanite with compositional averages of 17.3% opal-A, 28.6% opal-CT, 48.6% total detritus (18.1% phyllosilicates and 30.4% quartz and feldspars), and 2.1% pyrite. Stokes A-30804 contains four distinct lithofacies: (1) muddy diatomite (2) porcelaneous mudstone (3) diatomaceous porcelanite and (4) clayey diatomaceous. Sedimentary features that were identified include erosional surfaces, faults, debris-flow deposits, fossils, burrows, breccia, and sandstone/siltstone laminations. Compositional trends reveal that the opal-A to opal-CT transition zone occurs between 356' to 567'. Furthermore, Stokes A-30804 is subdivided into four main units: Stokes Lithostratigraphic Units A, B, C, and D.

CHAPTER 4

DISCUSSION

This chapter will examine: (1) interpretation of depositional environments within lithostratigraphic units of Newlove 76-RD1 and Stokes A-30804 (2) relationship of depositional environment and lithofacies (3) relationship of oxygen-minimum zone and lithofacies (4) relationship of oil saturation and lithofacies of Stokes A-30804 and (5) significance of debris-flow deposits. Interpretations are based primarily on an integrated analysis of core and core-photo descriptions, laboratory analysis, and gamma-ray logs.

Interpretation of Depositional Environments

Newlove 76-RD1

Lithofacies, gamma-ray log, sedimentary structures, and compositional trends of Newlove 76-RD1 indicate that the succession records the following trend in depositional environment: (A) base of slope or basin-floor depositional environment with episodic oscillation between anoxic and oxic conditions (B) slope depositional environment with episodic fluctuation from anoxic to oxic conditions (C) slope depositional environment deposited under oxic conditions and (D) upper-slope depositional environment under oxic conditions (Figure 38). These changes were identified within the lithostratigraphic units of Newlove 76-RD1 and are discussed below.

Newlove Lithostratigraphic Unit A

Newlove A is interpreted to have been deposited on the base of a slope or basin-floor that received minor detrital input (24.9%) under episodic anoxic to oxic conditions. This depositional environment is indicated by the presence of discontinuously laminated diatomaceous porcelanite and the absence of debris-flow deposits. The diatomaceous porcelanite is primarily a hemipelagic low-energy deposit. However, thin, discontinuous sandstone and siltstone laminations preserved in the laminated sediment were likely deposited by infrequent turbidity currents as suggested by their grading and distinctly coarser grain size than the otherwise siliceous mud that made up the porcelanite. Intermittently laminated strata and the absence of fossils suggest a depositional environment with an oscillating, impermanent oxygen-minimum zone (OMZ). Absence of debris-flow deposits discussed below suggests deposition at the base-of-slope or basin floor.

Newlove Lithostratigraphic Unit B

This unit is interpreted to have been deposited on a submarine slope receiving a slightly increased detrital influx (26.5%) under oscillating anoxic to oxic conditions and repeated debris-flow deposits. This environment is indicated by the presence of alternating discontinuously laminated and massive diatomaceous strata deposited in a quiet setting. The presence of debris-flow deposits marks the onset of energetic downslope mass transport, due to decreased slope stability resulting from higher sedimentation rate or related to tectonic uplift. The presence of erosional or truncation surfaces, faults, and slump folds also implies that this environment was increasingly

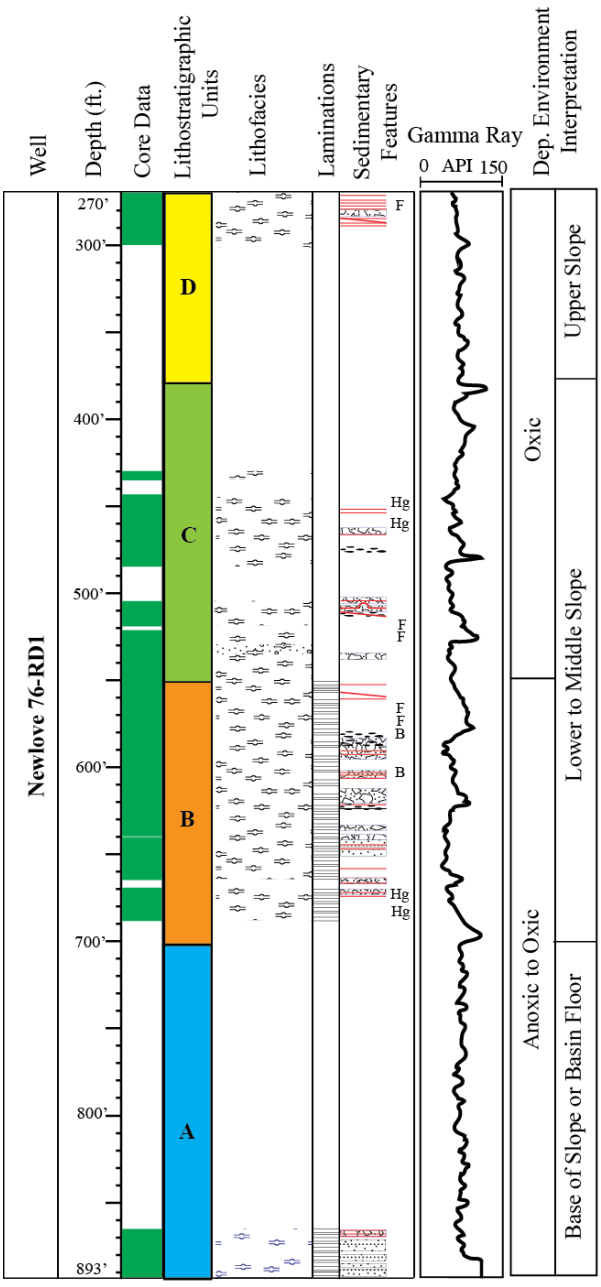

Newlove Lithostratigrahpic Unit D (270'-377')
Upper slope depositional environment with oxic conditions, low detrital influx, no developed oxygen minimum zone

Newlove Lithostratigrahpic C (378'-549')
Slope depositional environment with oxic conditions, repeated debris flow deposits, continuation of downslope mass transport, low to moderate detrital influx, no developed oxygen minimum zone

Newlove Lithostratigrahpic Unit B (550'-699')
Slope depositional environment with oscillating anoxic to oxic conditions, onset of downslope mass transport, repeated debris flow deposits, moderate detrital influx, oscillating weak oxygen minimum zone

Newlove Lithostratigrahpic Unit A (700'-893')
Base of slope or basin floor depositional environment with episodic anoxic to oxic, minor detrital influx, turbidity currents, oscillating impermanent oxygen minimum zone

FIGURE 38. Interpretation of depositional envrionments with integrated stratigraphic column of Newlove 76-RD1. This figure displays lithostratigraphic units, lithofacies, sedimentary features, gamma-ray log, depositional environment interpretations and detailed interpretations of the depositional environments of Newlove A, Newlove B, Newlove C, and Newlove D. Symbols as in Figure 23.

unstable, resulting in higher energy transport mechanisms. The appearance of some fossils and burrows reflects periods of increased oxygenation.

Newlove Lithostratigraphic Unit C

Newlove C is interpreted to have been deposited within an environment similar to Newlove B on a slope setting receiving a moderate detrital influx (28.3%) and debris-flow deposits; however, this unit provides no evidence of deposition within an oxygen-minimum zone. This is indicated by the presence of massive diatomaceous strata and the absence of laminations. In addition, fossils and burrows additionally support the interpretation of an oxic environment located either above the oxygen minimum or during a time when the OMZ was weakened. Debris-flow transport and deposition persisted throughout this unit marking the persistence of a slope setting.

Newlove Lithostratigraphic Unit D

This unit is interpreted to have been deposited on an active upper slope setting receiving lesser amounts of detritus (25.6%) than lithostratigraphic units C and B. The upper-slope setting is indicated by abundant faults, erosional surfaces, and breccia but absence of debris-flows and slumps suggesting that this location was likely where gravity flows and mass movements originated, but were transported away downslope. The absence of laminations, presence of massive strata, and presence of fossils and burrows indicate deposition within an oxic environment, likely consistently above the oxygen-minimum zone.

Stokes A-30804

Sedimentary features, lithofacies, gamma-ray log, and compositional trends in

Stokes A-30804 reveal the following sequence of depositional environments recorded by the stratigraphic succession: (A) base of slope or basin floor depositional environment with episodic anoxic to oxic conditions (B) slope depositional environment with episodic anoxic to oxic conditions and (C) slope depositional environment with oxic conditions (Figure 39). These changes were identified within the lithostratigraphic units of Stokes A-30804 and are discussed below.

Stokes Lithostratigraphic Unit A

This unit is interpreted to have been deposited on the base of a slope or basin-floor that accumulated a high detrital content (52.3%), under largely anoxic conditions, with some oscillations in the strength or position of the oxygen-minimum zone. This setting is indicated by the presence of laminated to massive porcelanite. Thin laminations of sand and silt within laminated lithofacies were likely deposited by relatively infrequent distal turbidity currents. However, the absence of debris-flow deposits found in other units supports the interpretation of a lower gradient environment, possibly on the basin-floor or base-of-slope or in an inter-ridge trough.

Stokes Lithostratigraphic Unit B

Stokes B is interpreted to have been deposited on a slope with episodic anoxic and oxic conditions receiving a high detrital input (57.7%). This setting is evident by the presence of abundant debris-flow deposits intercalated with discontinuously laminated to massive porcelaneous mudstone. The presence of abundant erosional surfaces, faults and breccia suggests deposition in an unstable, steep or tectonically active slope depositional environment.

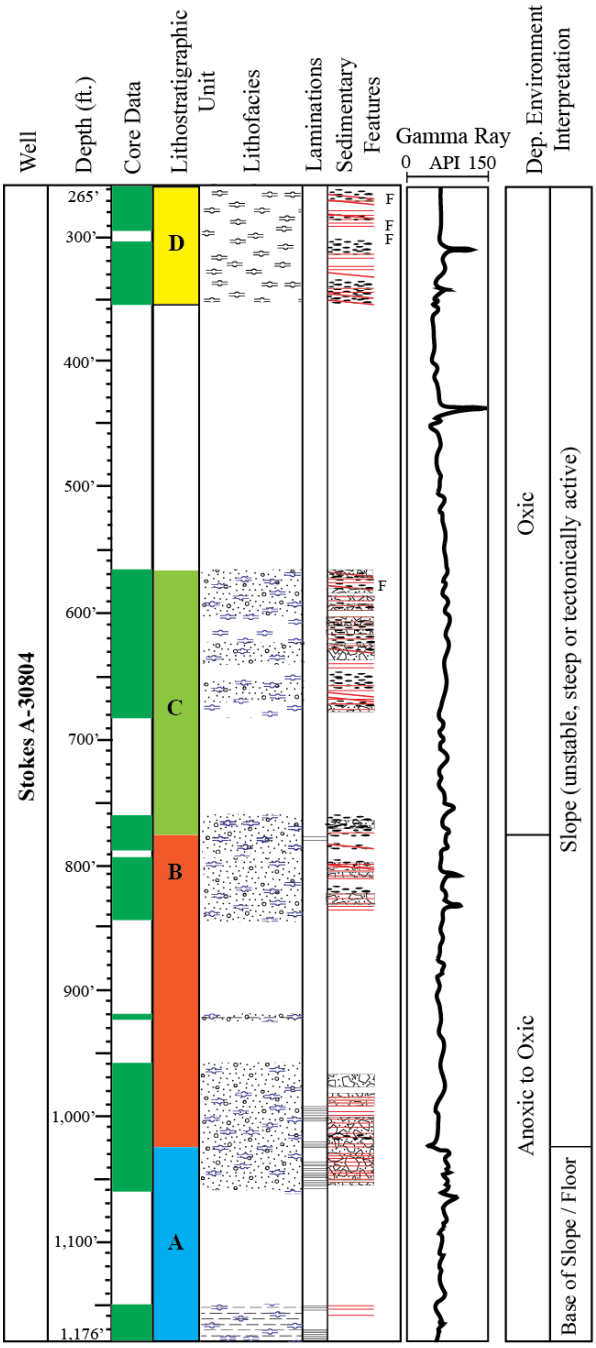

Stokes Lithostratigrahpic Unit D (265'-356')
Slope depositional environment with oxic conditions and debris flow deposits, moderate detrital influx, no developed oxygen minimum zone

Opal-A to Opal-CT Transition Zone

Stokes Lithostratigrahpic Unit C (567'-777')
Slope depositional environment with oxic conditions and debris flow deposits, high detrital influx, no developed oxygen minimum zone

Stokes Lithostratigrahpic Unit B (778'-1,036')
Slope depositional environment with episodic anoxic to oxic conditions and debris flow deposits, high detrital influx, oscillating weak oxygen minimum zone

Stokes Lithostratigrahpic Unit A (1,037'-1176')
Base of slope or basin floor depositional environment with episodic anoxic to oxic conditions, slow accumulation of sediments, high detritual influx, turbidity currents, oscillating weak oxygen minimum zone

FIGURE 39. Interpretation of depositional environments with integrated stratigraphic column of Stokes A-30804. This figure displays the designated lithostratigraphic units, lithofacies, sedimentary features, gamma-ray log, depositional environment interpretations and detailed interpretations of the depositional environments of Stokes A, Stokes B, Stokes C, and Stokes D. Symbols as in Figure 33.

Stokes Lithostratigraphic Unit C

This unit is interpreted to have been deposited within a similar slope depositional environment as Stokes B; however, the absence of laminations and presence of fossils in Stokes C marks the onset of continuously oxic oceanographic conditions. Either the setting was now above the OMZ or the oxygen-minimum zone had weakened by the time that this part of the Sisquoc Formation was deposited. Additionally, the presence of alternating diatomaceous porcelanite and clayey porcelaneous mudstone suggests episodic supply of different proportions of total silica and detritus. Similarly to Stokes B, an abundance of faults, erosional surfaces, breccias, abundant debris-flow deposits, and high detrital content (46.9%) imply tectonic activity or oversteepening by high rates of sedimentation during deposition on a submarine slope.

Stokes Lithostratigraphic Unit D

Stokes D is interpreted to have been deposited within an environment similarly to Stokes C and Stokes B within an unstable slope setting with abundant debris-flow deposits, however, Stokes D received less detritus (37.5%) and higher total silica (60%). The dominant massive muddy diatomite lithofacies within this unit is consistent with deposition under oxic conditions above the oxygen-minimum zone where detrital input was restricted at bathymetric highs, and where macrofauna bioturbated the sediment and left body fossils, yet it still would have been associated with active upwelling and high diatom productivity.

Relationship Between Depositional Environment and Lithofacies

These results provide new insights on the relationship between depositional environment and lithofacies present within Newlove 76-RD1 and Stokes A-30804. The interpretations of depositional environment within lithostratigraphic units of both cores appear to represent a portion of the overall basinal shallowing-upward succession from the bathyal Monterey Formation into the mostly outer-shelfal Foxen Formation. More specifically, these cores are interpreted to primarily represent active slope deposition of the Sisquoc Formation based on evidence of identified sedimentary features (sedimentary faults, erosional surfaces, debris-flow deposits, breccia, hardgrounds, fossils, and burrows) within both cores. In addition, the significant amount of detritus identified within both cores (more dominant in Stokes A-30804 than Newlove 76-RD1) correlates with the overall high-detrital composition of the Sisquoc Formation recorded in previous research (Woodring and Bramlette 1950; Ramirez, 1987; Ramirez, 1990; Ramirez and Garrison, 1995). The shift from the bathyal, distinctly laminated and highly siliceous sediments of the Monterey Formation to the shelfal, massive, and greater detrital composition of the Sisquoc Formation probably resulted from tectonic uplift (during formation of anticlines along the Casmalia-Orcutt trend) and eustatic sea level drops during early the Pliocene through Pleistocene (Ramirez, 1990; Ramirez and Garrison, 1995).

Comparing the predominantly slope-deposited lithofacies identified in Stokes A-30804 and Newlove 76-RD1, it is evident that interpreted variations within this depositional setting caused dissimilar distributions of total silica and total detritus.

Newlove 76-RD1 contains overall higher abundances of total silica (70.2%) and lower total detritus (26.2%) compared to the lower total silica (45.9%) and higher total detritus (48.6%) of Stokes A-30804. These variations between the cores are likely caused by difference in the position on the slope of the depositional environments of Stokes A-30804 and Newlove 76-RD1.

The Pliocene bathymetry of Santa Maria basin was developing into a complex pattern of ridges and troughs during deposition of the Sisquoc Formation due to acceleration of tectonic shortening across the basin (Canfield, 1939; Woodring and Bramlette, 1950; Behl and Ingle, 1995). The position on the slope of the present-day Casmalia Hills during the deposition of sediments within Stokes A-30804 was likely deeper (in comparison to the slope position for deposition of Newlove 76-RD1) and situated on a structurally lower flank of a paleobathemetric high (Figure 40). It is interpreted that inter-ridge troughs provided pathways transporting higher energy deposits, more abundant debris-flow deposits, higher accumulation rate, and higher detrital influx within this system as seen in the Miocene San Joaquin basin (McGuire et al, 1983). This environment would explain the greater accumulation of detritus within Stokes A-30804 compared to Newlove 76-RD1. In contrast, it is likely that the slope during deposition of Newlove 76-RD1 was more gentle, shallower, and situated closer to a paleobathemetric high (Figure 40). This setting would accumulate less detritus as suspensions of these sediments would primarily be transported into the bathymetric lows. This setting results in accumulation of purer diatomaceous sediments (McGuire et al, 1983) and perhaps less indications of mass wasting if the submarine slope flattened into

the bathymetric high. This interpretation would explain the lower abundances of debris flow deposits, lower detritus, and higher total silica compositions at Newlove 76-RD1 compared to Stokes A-30804.

In result, the relationship between the varying slope positions within the depositional environment of Stokes A-30804 and Newlove 76-RD1 are expressed by the differences in dominant lithofacies. Newlove 76-RD1 contains higher abundances of total silica and lower detrital content reflected by its dominant muddy diatomite lithofacies. In contrast, Stokes A-30804 contains lower abundances of total silica and higher detrital

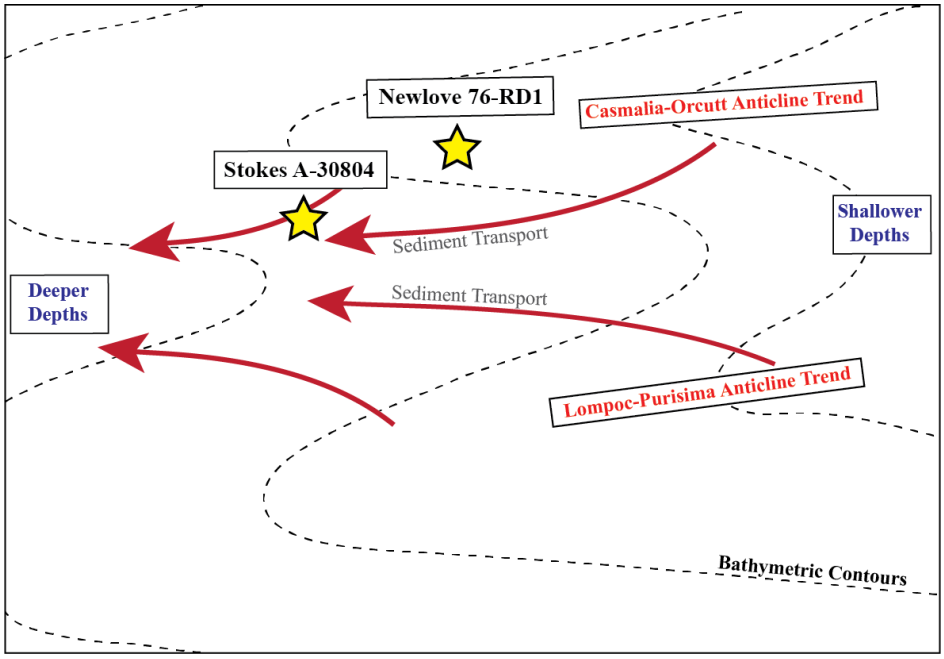

FIGURE 40. Schematic depositional model of Newlove 76-RD1 and Stokes A-30804. This simplified model is roughly approximating the orientation of bathymetric ridges and troughs during Sisquoc Formation deposition (~4 to 5 Ma). Yellow stars indicate the interpreted positions during deposition of deposits within Newlove 76-RD1 and Stokes A-30804.

content reflected by its dominant porcelanous mudstone lithofacies with minor diatomaceous porcelanite and diatomite. In addition, sedimentary features of an unstable slope setting (faults, erosional surfaces, debris-flow deposits, and breccia) are more abundant in Stokes A-30804 than Newlove 76-RD1.

Relationship of Oxygen-Minimum Zone and Lithofacies

Differences in the degree of oxygenation during deposition of Newlove 76-RD1 and Stokes A-30804 are interpreted to have controlled the preservation of laminated or massive lithofacies. Generally, massive strata that lack laminations contain an abundance of macrofaunal fossils and burrows would have been deposited under oxygenated conditions. These high-oxygen conditions prevailed either when the oxygen-minimum zone was weak or absent or when deposition occurred above the oxygen-minimum zone as has been demonstrated for the well-studied Quaternary of the adjacent California Margin (Cannariato and Kennett, 1999). This oxic environment is recorded in several lithostratigraphic units within Newlove 76-RD1 (Newlove C and Newlove D) and Stokes A-30804 (Stokes C and Stokes D). In addition, oxic intervals can be identified within intervals in Newlove A, Newlove B, Stokes A, and Stokes B.

Anoxic conditions prevail in a depositional environment occurring within a well-developed oxygen-minimum zone. An anoxic or dysoxic environment prohibits development of an active benthic marine ecosystem, thus preventing bioturbation and generation of massive or burrow-mottled beds (Behl and Kennett, 1996). Sediment deposited in these environments can preserve thin beds and laminations derived either from fluctuating oceanic/climatic conditions such as varves, or thin sandy or muddy

gravity event deposits (Bramlette, 1946) as characteristic of the laminated lithofacies described in this study. This deposition in this environment is evident in specific intervals within Newlove 76-RD1 (Newlove A and Newlove B) and Stokes A-30804 (Stokes A and Stokes B).

It is likely that major fluctuations in the strength of an oxygen-minimum zone are associated with global and local climate change during the deposition of these diatomaceous sediments as seen for younger geologic time periods along this part of the California Margin (Cannariato and Kennett, 1999). Weakening or the disappearance of an oxygen-minimum zone is likely tied to cooling periods, meanwhile, strengthening

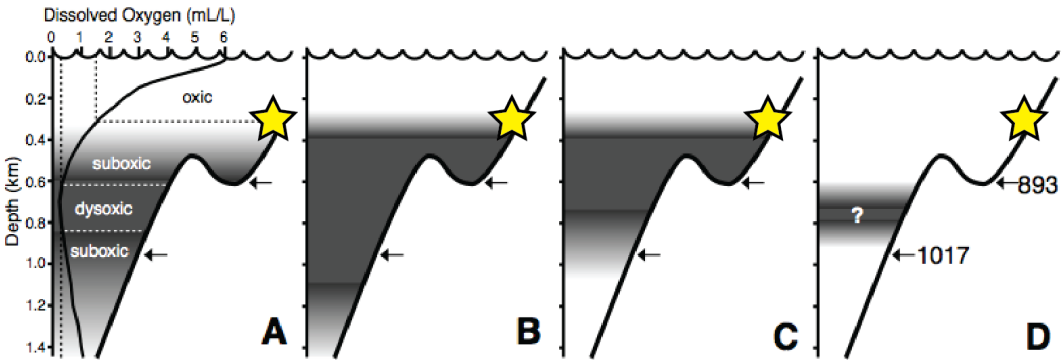

FIGURE 41. Diagrams of reconstructed OMZ fluctuations along NW Pacific margin. This interpretation was based on benthic foraminiferal records from ODP Sites 893 and 1017. Yellow star represents the interpreted possible position of Sisquoc deposition within the Santa Maria basin. (A) modern dissolved-oxygen profile near Site 1017 (B) expanded OMZ in colder temperatures (C) continued expansion of OMZ during colder temperatures and (D) contraction of OMZ during warm periods (modified from Cannariato and Kennett, 1999).

during warmer periods (Cannariato and Kennett, 1999). Figure 41 illustrates a reconstruction of these fluctuations along the northeastern Pacific margin for the Quaternary. It is interpreted that similar oscillations likely occurred locally during the deposition of Pliocene diatomaceous sediments within Newlove 76-RD1 and Stokes A-30804 reflected by the presence of both massive and laminated lithofacies.

Relationship Between Oil Saturation and Lithofacies in Stokes A-30804

Core analysis conducted by Core Laboratories of samples from various depths in Stokes A-30804 (see data and results section for details) show that porosity and oil saturations are distinct for the different lithofacies. The statistical values for porosity and oil saturation of the lithofacies are in Table 4 and are plotted in Figure 42.

TABLE 4. Statistical averages of porosity and oil saturation of lithofacies within Stokes A-30804

Lithofacies	Porosity	Oil Saturation
Muddy Diatomite	55.9%	62.9%
Diatomaceous Porcelanite	57.7%	42.3%
Porcelaneous Mudstone	44.8%	25.9%
Clayey Diatomaceous Porcelanite	39.4%	5.6%

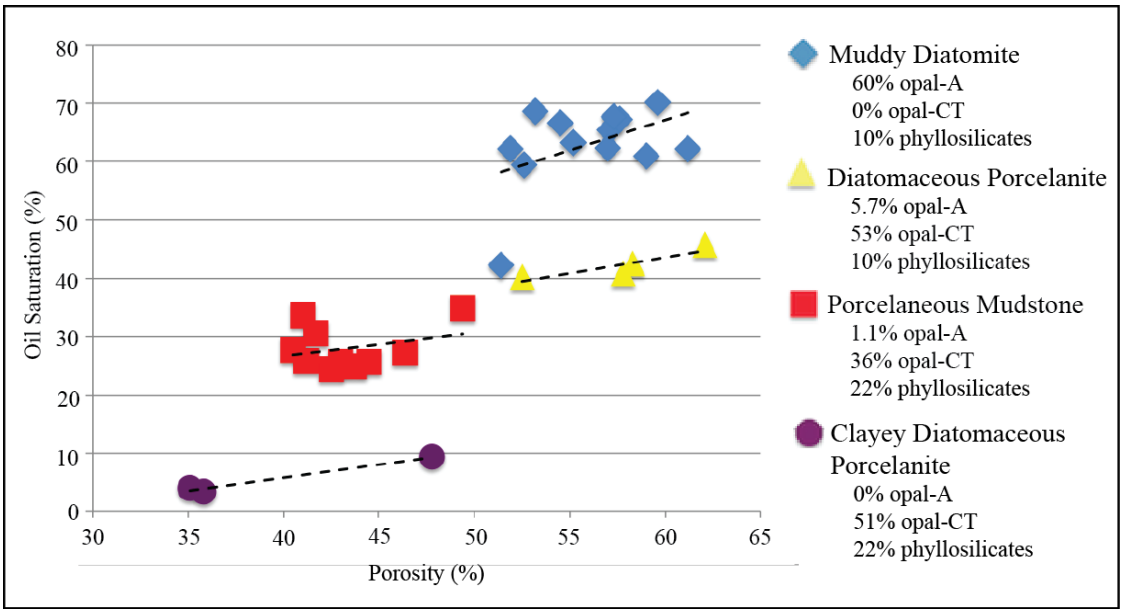

FIGURE 42. Plot of porosity vs. oil saturations of lithofacies within Stokes A-30804. This scatter plot illustrates the oil saturation with respect to porosity of samples separated by lithofacies from Stokes A-30804. Compositional averages of opal-A, opal-CT, and phyllosilicates are given for each lithofacies. Dotted lines represent trends of each dataset. Results of these trends show the following increases of oil saturation (%) per 1% increase of porosity of each lithofacies: muddy diatomite (1.04%), diatomaceous porcelanite (0.55%), porcelaneous mudstone (0.39%), and clayey diatomaceous porcelanite (0.45%).

From these data, the following observations and interpretations can be made:

1. Opal-A dominant lithofacies (muddy diatomite) contains the highest porosities and oil saturation (62.9%). This lithofacies is present in the shallowest depths of Stokes A-30804 and did not undergo opal-CT phase diagenesis as this lithofacies contains no opal-CT.

2. Intermixed opal-A and opal-CT silica phase lithofacies without high abundances of phyllosilicates (diatomaceous porcelanite) contained the second highest oil

saturations (42.3%). Surprisingly, they have equally great porosity as the opal-A-phase muddy diatomite. It is interpreted that the initial stage of diagenesis and precipitation of opal-CT immediately reduces the overall permeability of these rocks hindering oil migration. Reduction of permeability within diatomaceous sediments from opal-A to opal-CT phases has been documented by previous geologic and engineering studies (Hein et al, 1978; Eichhubl and Behl, 1998; Dale et al., 2000). Although permeability data were not calculated for the samples in this research, it is interpreted that the precipitation of opal-CT played a role in reducing permeability of lithofacies within Stokes A-30804 as higher abundances in opal-CT correlate with lower oil saturations (Figure 43).

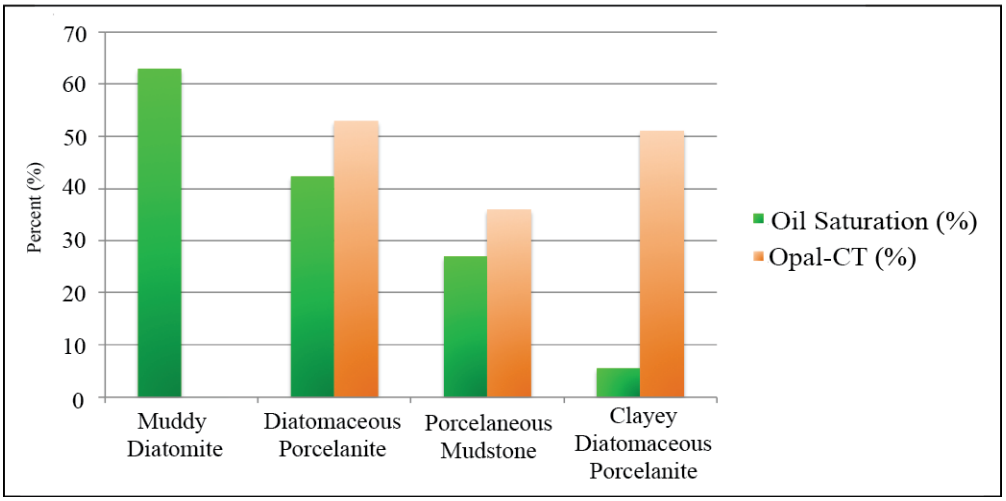

FIGURE 43. Chart of average opal-CT and oil saturations of lithofacies within Stokes A-30804.

3. Phyllosilicate-rich lithofacies (clayey diatomaceous porcelanite and porcelaneous mudstone) contain dramatically lower oil saturations in comparison to phyllosilicate-poor lithofacies (Figure 44). High phyllosilicate content and the presence of opal-CT each likely played a role in decreasing permeability and porosity and resulting in lower oil saturations. Relationship between high phyllosilicate content and decrease in permeability of reservoir rocks has been recorded in recent engineering studies (Yang and Aplin, 2010 and Jiang, 2012). Generally, high abundances of phyllosilicate minerals are detrimental to reservoir quality as they plug pore throats, reduce pore space, and block fluid movement (Jiang, 2012). In addition, the clayey diatomaceous porcelanite

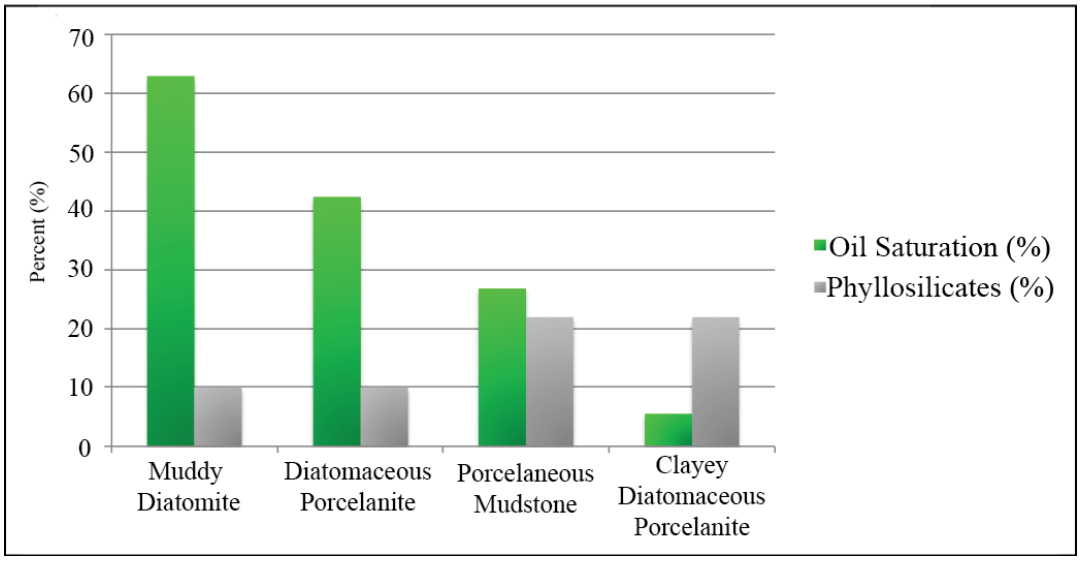

FIGURE 44. Chart of average phyllosilicates and oil saturations of lithofacies within Stokes A-30804

lithofacies is present at the greatest depths of Stokes A-30804 where deeper burial would have lead to greater compaction and degree of opal-CT cementation, both factors contributing to its physical properties and lack of oil saturation.

In addition, percent oil by volume of lithofacies within Stokes A-30804 show a similar pattern illustrating that phyllosilicate-rich lithofacies contain less oil than phyllosilicate-poor lithofacies. Percent oil by volume was calculated by multiplying the porosity of each lithofacies by their oil saturations (%). This calculation revealed the following percent oil by volume of the lithofacies within Stokes A-30804 below (Table 5) and shown in Figure 45.

From these data, it is interpreted that phyllosilicate abundance plays a primary role in decreasing oil saturation, permeability and porosities, with opal-CT having a somewhat lesser secondary role. It should be noted that these relationships are based on a limited number of analyzed samples that may not reveal other significant trends. Thus, more data and samples will provide a more comprehensive understanding of the relationship between oil saturation and lithofacies.

TABLE 5. Statistical averages of percent oil by volume of lithofacies within Stokes A-30804

Lithofacies	Percent Oil by Volume
Muddy Diatomite	35.1%
Diatomaceous Porcelanite	24.9%
Porcelaneous Mudstone	12%
Clayey Diatomaceous Porcelanite	2.2%

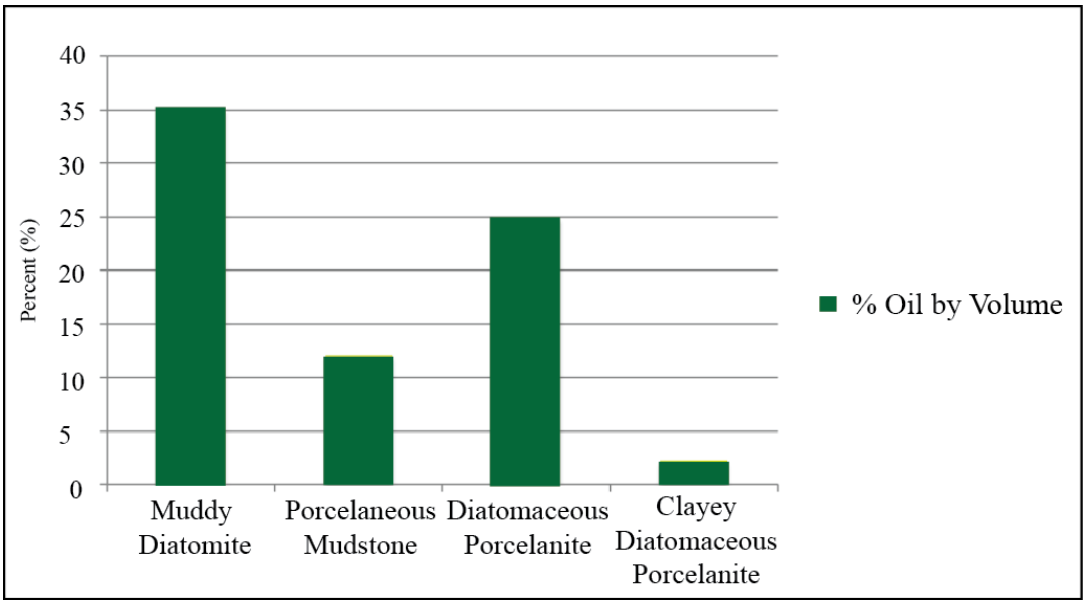

FIGURE 45. Chart of average percent oil by volume of lithofacies within Stokes A03804. Average percent oil by volume was calculated by multiplying the total porosity and percentage of oil saturation.

Petroleum Geologic Significance of Debris-Flow Deposits

Debris-flow deposits were identified throughout Newlove 76-RD1 and Stokes A-30804. Nearly all debris-flow deposits (more abundant in Stokes A-30804) contained elevated visible oil saturation. Increased permeability along these beds suggest that debris-flow strata may have played a role in laterally charging diatomaceous sediment. Farley and Wilson (1983) and Henderson and Ramirez (1990) reported similar trends in high oil concentrations within debris-flow deposits in their cores located within the Casmalia Hills. At this point, it is unknown how laterally continuous these deposits are and it would be important to map their extent and thickness in other wells. If these deposits are thick, laterally and vertically connected with faults, then it is probable that

these debris-flow deposits may be important mechanisms for laterally distributing oil away from faults through otherwise low-permeability diatomaceous and muddy strata. In contrast, if these deposits are not laterally and vertically extensive and connected, then it is probable that fault systems were the primary conduits for oil migration and reservoir charge.

CHAPTER 5

CONCLUSIONS

This research investigated the sedimentology and stratigraphy of two proprietary, industry-acquired cores from the Orcutt (Newlove 76-RD1) and Casmalia Hills (Stokes A-30804) oil fields to better understand the relationships between diatomaceous lithofacies, depositional environment and their possible effects on petroleum reservoirs. Key findings of this research are elaborated below.

1. Five lithofacies were characterized by direct observation, laboratory analysis (x-ray diffraction and scanning electron microscope), and subsurface gamma-ray logs.

A. Newlove 76-RD1 contains three distinct lithofacies: (1) muddy diatomite (2) diatomaceous mudstone and (3) diatomaceous porcelanite.

B. Stokes A-30804 contains four distinct lithofacies: (1) muddy diatomite (2) porcelaneous mudstone (3) diatomaceous porcelanite and (4) clayey diatomaceous porcelanite.

2. Nine sedimentary features provide insight to the depositional environment and are used for interpretation of depositional processes and environments. These include: faults, slump folds, erosional surfaces, debris-flow deposits, sandstone and siltstone laminations, sedimentary breccias, hardgrounds, fossils, and burrows.

3. Quantitative X-ray diffraction determination of opal-A, opal-CT, total silica,

total detritus (phyllosilicates, feldspars and quartz), and pyrite show greater detrital content and diagenesis in Stokes A-30804 than in Newlove 76-RD1.

A. The average composition for Newlove 76-RD1 is 65.4% opal-A, 4.8% opal CT, 26.6% total detritus (7.8% phyllosilicates and 18.9% quartz and feldspars), and <1% pyrite.

B. The average composition for Stokes A-30804 is 17.3% opal-A, 28.6% opal-CT, 48.6% total detritus (18.1% phyllosilicates and 30.4% quartz and feldspars), and 2.1% pyrite.

4. Lithofacies, gamma ray-log, sedimentary structures, and compositional trends of both Newlove 76-RD1 and Stokes A-30804 indicate an upward shallowing succession on the Pliocene slope of the Santa Maria basin from deposition within a fluctuating oxygen-minimum zone to the overlying fully oxygenated waters:

A. Newlove 76-RD1: (A) base of slope or basin-floor depositional environment with episodic oscillation between anoxic and oxic conditions (B) slope depositional environment with episodic fluctuation from anoxic to oxic conditions (C) slope depositional environment deposited under oxic conditions and (D) upper slope depositional environment under oxic conditions.

B. Stokes A-30804: (A) base of slope or basin-floor depositional environment with episodic anoxic to oxic conditions (B) slope depositional environment with episodic anoxic to oxic conditions and (C) slope depositional environment with oxic conditions.

5. Variations of total silica and total detritus between Newlove 76-RD1 (70.2% silica and 26.2% detritus) and Stokes A-30804 (45.9% silica and 48.6% detritus) were

likely caused by different depositional positions on the paleo-slope. The depositional setting of the Stokes well in the Casmalia Hills was likely deeper and situated on a lower flank of a paleobathymetric high, where it was more influenced by debris-flows, and received higher detrital influx transported down inter-ridge troughs. The slope at Orcutt during deposition of sediments within Newlove 76-RD1 was shallower and situated closer to a paleobathymetric high where purer diatomaceous sediments accumulated, as fine terrigenous detrital sediment were primarily transported along and towards surrounding bathymetric lows.

6. Core analysis of a small sample set from Stokes A-30804 revealed the following porosity and oil saturations of lithofacies: muddy diatomite (55.9% porosity and 62.9% oil saturation), diatomaceous porcelanite (57.7% porosity and 42.3% oil saturation), porcelaneous mudstone (44.8% porosity and 25.9% oil saturation), and clayey diatomaceous porcelanite (39.4% porosity and 5.6% oil saturation).

A. Opal-A dominant lithofacies (muddy diatomite) contain the highest porosities (average 60%) and oil saturation (average 62.9%).

B. Intermixed opal-A and opal-CT silica phase lithofacies without high abundances of phyllosilicates (diatomaceous porcelanite) contain the second highest oil saturations (42.3%). The diagenesis and precipitation of opal-CT is interpreted to play an important, but secondary role in reducing permeability and is can be significant in porosity reduction.

C. Phyllosilicate-rich lithofacies (clayey diatomaceous porcelanite and porcelaneous mudstone) contain markedly lower oil saturations (5.6%). Abundant

phyllosilicates apparently plays the most significant role in reducing porosity, permeability, and oil saturation within the lithofacies identified in Stokes A-30804.

7. Debris-flow deposits identified throughout Newlove 76-RD1 and Stokes A-30804 have elevated oil saturations suggesting that debris-flow strata may have played a role in laterally charging the low-permeability diatomaceous sediments.

CHAPTER 6

FUTURE WORK

This research was derived from data from two proprietary, industry-acquired cores from Newlove 76-RD1 and Stokes A-30804. The data were necessarily limited to these two cores and to material available at this time and important questions were raised that were not answered by this study. This research can be extended with the following recommendations for future work to answer these questions.

1. At what precise depth does the opal-A to opal-CT transition occur within Newlove 76-RD1 and Stokes A-30804? What can this tell us about the burial and tectonic history of the Casmalia-Orcutt structure?

The collection of core samples was limited by available core data. Acquiring additional well cuttings, if available, will help fill in gaps of non-existent core data. Conducting x-ray diffraction on these additional samples would help to better distinguish the opal-A to opal-CT diagenetic transition zones, and the degree of diagenetic ordering within Newlove 76-RD1 and Stokes A-30804.

2. What diatom zones do the cores from Newlove 76-RD1 and Stokes A-30804 belong to and what are the ages of the cores?

Detailed diatom biostratigraphy is necessary to understand the approximate ages and diatom zonations of both wells. This will aid in providing a chronostratigraphic

framework for Newlove 76-RD1 and Stokes A-30804 that will permit precise correlation between the sections. Furthermore, diatom biostratigraphy will additionally help with correlations of Newlove 76-RD1 and Stokes A-30804 with other wells.

3. What is the extent and spatial distribution of the interpreted depositional environments and lithofacies within Newlove 76-RD1 and Stokes A-30804?

It is important to understand the lateral extent of the lithofacies identified by this research. One possible way to accomplish this is by correlating and extrapolating the gamma-ray signatures from Newlove 76-RD1 and Stokes A-30804 to other well logs of nearby wells. Combined with chronostratigraphy, this will help establish a paleogeographic or paleoenvironmental reconstruction of evolution of the Casmalia and Orcutt Hills. From a petroleum exploitation perspective, this will help to better predict the locations and trends of the potentially most oil saturated reservoir rocks. A potential petroleum play opportunity may exist if prolific lithofacies are laterally extensive.

4. How much of a role do faults and debris-flow deposits have in oil migration into the diatomaceous sediments within the Casmalia Hills and Orcutt field?

Understanding the connectivity of faults and debris-flow deposits identified within Newlove 76-RD1 and Stokes A-30804 is important as they may play major roles in the petroleum system. It is likely that the higher connectivity of faults and debris-flow deposits correlate with higher oil saturations. In contrast, segregated faults and debris-flows deposits will likely correlate with lower oil saturations. Understanding this relationship can be accomplished by mapping out the faults and debris-flow deposits identified in Newlove 76-RD1 and Stokes A-30804 with other cores available and

extrapolating this data. Petrel or another 3D modeling software can be used to create this proposed model. If applicable, surface faults can be implemented.

5. Does the precipitation of opal-CT and abundance of phyllosilicates decrease permeability within diatomaceous sediments, and if so, how much? How does this effect oil saturation?

Conducting laboratory tests to obtain permeability data from selected samples throughout Newlove 76-RD1 and Stokes A-30804 can aid in better understanding the relationship between the precipitation of opal-CT, phyllosilicate and their effects on permeability. It is likely that the higher opal-CT and phyllosilicate abundances will correlate with lower permeability and oil saturations. Statistical data of these properties will help to better understand this relationship.

6. How are the interpreted depositional environments within Newlove 76-RD1 and Stokes A-30804 comparable with deposition of uppermost Miocene to Pliocene diatomaceous sediments in other places in the Santa Maria basin and other basins throughout California?

Combined with chronostratigraphy, comparing the lithofacies identified in this research to other oil fields in the Santa Maria basin (i.e., Lompoc, Santa Maria Valley, Cat Canyon) will help to better understand the dynamic depositional environments during deposition of diatomaceous sediments of the Santa Maria basin. This can be accomplish by analyzing the stratigraphy and sedimentology of other cores in these additional oil fields and compare the data to Newlove 76-RD1 and Stokes A-30804. In addition, this can be extended to other diatomaceous sediments within other oil fields in other basins

throughout California (i.e., San Joaquin, Salinas, Los Angeles). Comparing and contrasting these sediments will aid in understanding the link between depositional environment, diatomaceous lithofacies, and oil saturation. This is important for the future exploitation of these reservoir rocks.

APPENDICES

APPENDIX A

STOKES A-30804 DEPTHS FOR XRD, SEM, AND

CORE ANALYSIS DATA

APPENDIX A

STOKES A-30804 DEPTHS FOR XRD, SEM, AND CORE ANALYSIS

XRD (ft.)	SEM (ft.)	Core Analysis (ft.)
268	335	268
280	336	274
288	606	284
289	607	287
313	652	288
322	1,000	311
329	1,040	318
336	1,172	325
355		333
571		345
582		350
593		382
607		595
624		602
640		607
654		609
668		634
681		645
771		777
787		787
797		805

808		822
826		972
839		988
922		1,003
963		1,015
973		1,038
998		1,046
1,016		1,153
1,028		1,161
1,047		1,173
1,058		
1,153		
1,175		

APPENDIX B

NEWLOVE 76-RD1 DEPTHS FOR XRD AND SEM

APPENDIX B

NEWLOVE 76-RD1 DEPTHS FOR XRD AND SEM

XRD (ft.)	**SEM (ft.)**
270	275
275	518
288	535
295	553
431	585
446	865
456	
465	
470	
481	
515	
518	
535	
549	
573	
588	
600	
611	
631	
647	
660	
675	

686	
865	
878	

REFERENCES

REFERENCES

Behl, R.J., 1992, Chertification in the Monterey Formation of California and deep-sea sediments of the West Pacific [Ph.D. thesis]: Santa Cruz, University of California, 287 p.

Behl, R. J., 1999, Since Bramlette (1946): The Miocene Monterey Formation of California revisited, GSA Special Paper 338.

Behl, R.J., and Garrison, R.E., 1994, The origin of chert in the Monterey Formation of California (USA), *in* Iijima, A., Abed, A., and Garrison, R., eds., Siliceous, phosphatic and glauconitic sediments of the Tertiary and Mesozoic: Utrecht, International Geological Congress Proceedings, Part C., p. 101-132.

Behl, R.J., and Ingle, J.C., 1995, The Sisquoc/Foxen boundary in the Santa Maria Basin, California: A sedimentary response to the new tectonic regime, *in* Keller, M.A., ed., Evolution of sedimentary basins and onshore oil and gas investigation Santa Maria province: Denver, U.S. Geological Survey Bulletin, 1995-T, U, V, p. V1-V16.

Behl, R. J., and Kennett, J. P., 1996, Brief interstadial events in the Santa Barbara basin, NE Pacific, during the past 60 kyr: Nature, v. 379, p. 243-246.

Behl, R. J., and Ramirez, 2000, Field guide to the geology of the Neogene Santa Maria basin: from rift to uplift: Los Angeles, The Pacific Section Society for Sedimentary Geology, book 86, 56 p.

Bramlette, M. N., 1946, The Monterey Formation of California and the origin of its siliceous rocks: United States Geological Survey, Professional Paper 212, 57 p.

California Division of Oil, Gas, and Geothermal Resources, 2010, annual report: pub. PR06.

Canfield, C.R., 1939, Subsurface stratigraphy of Santa Maria Valley oil field and adjacent parts of Santa Maria Valley, California: American Association of Petroleum Geologists Bulletin, v. 23, p. 45-81.

Cannariato, K.G., and Kennett, J.P., 1999, Climatically related millennial-scale fluctuations in strength of California margin oxygen-minimum zone during the

past 60 k.y.: Geology, v. 27, p. 975-978.

Cole, R.B., and Stanley, R.G., 1998, Volcanic rocks of the Santa Maria Province, California: United States Geological Survey, 1995-R, p. Ri-R35.

Crouch, J.K., and Suppe, J., 1993, Late Cenozoic tectonic evolution of the Los Angeles basin and inner California borderland: A model for core complex-like crustal extension: Geological Society of America Bulletin, v. 105, p. 1415-1434.

Dale, B. A., Narahara, G. M., and Stevens, R. M., 2000, Case history of reservoir subsidence and wellbore damage management in the south Belridge diatomite field: Society of Petroleum Engineers, v.15, p. 50-57.

Dibblee, T.W. Jr., 1989a, Geologic map of the Casmalia and Orcutt Quadrangles: Santa Barbara County, Dibblee Foundation.

Dibblee, T.W. Jr., 1989b, Geologic map of the Point Sal and Guadalupe Quadrangles: Santa Barbara County, Dibblee Foundation.

Durham, D.L., 1973, Diatomite, *in* Brobst, D.A., and Pratt, W.P., eds., United States mineral resources: U.S. Geological Survey Professional Paper 820, p. 191-195.

Eichhubl, P., and Behl, R. J., 1998, Diagenesis, deformation, and fluid flow in the Miocene Monterey Formation, *in* Eichhubl, P., ed., Diagenesis, deformation, and fluid flow in the Miocene Monterey Formation: Pacific Section, SEPM (Society for Sedimentary Geology) Special Publication 83, p. 5-13.

Farley, T., and Wilson, M.L., 1983, Geology of the Airox oil-saturated diatomite deposit, Santa Barbara County, California, *in* Garrison, R.E. et al., eds., Petroleum generation and occurrence in the Miocene Monterey Formation, California: Pacific Section SEPM (Society for Sedimentary Geology) p. 1-15.

Feigl, K.L., King, R.W., and Jordan, T.H., 1990, Geodetic measurement of tectonic deformation in the Santa Maria fold and thrust belt, California: Geophysical Research, v. 95 p. 2679-2699.

Föllmi, K. B., Garrison, R. E., and Grimm, K. A., 1991, Stratification in phosphatic sediments: illustrations from the Neogene of California, *in* Einsele, G., Ricken, W., and Seilacher, A., eds., Cycles and events in stratigraphy: Berlin, Springer-Verlag, p. 492-507.

Gorsline, D.S., and Emery, K.O., 1959, Turbidity currents deposits in San Pedro and

Santa Monica basins off southern California: Geological Society of America Bulletin, v. 70, p. 279-288.

Gorsline, D.S., 1992, The geologic setting of Santa Monica and San Pedro Basins, California continental borderland: Progress in Oceanography, v. 30, p. 1-36.

Gürel, A., and Yildiz, A., 2007, Diatom communities, lithofacies characteristics and paleoenvironmental interpretation of Pliocene diatomite deposits in the Ihlara-Selime plain (Aksaray, Central Anatolia, Turkey): Journal of Asian Earth Sciences, v. 30, p. 170-180.

Hein, J.R., Barron, J.A., Jones, M.G., and Miller, J., 1978, Diagenesis of late Cenozoic diatomaceous deposits and formation of bottom simulating reflector in the southern Bering Sea: Sedimentology, v. 25, p. 155-181.

Henderson, N.C., Jr., and Ramirez, P.C., 1990, Control exerted by lithologic variations and pebbly units on petroleum occurrences in the Pliocene upper Sisquoc Formation, Casmalia Hills, Santa Maria basin, California, *in* Keller, M.A, and McGowen, M.K., eds., Miocene and Oligocene petroleum reservoirs of the Santa Maria and Santa Barbara basins, California: Pacific Section, Society of Economic Paleontologists and Mineralogists Core Workshop Notes, p. 339-400.

Henderson, N.C., Jr., Crawford, A.G., Dunham, J.B., 1984, Relationship of diagenetic dolomite to depositional facies in diatomaceous strata, upper Sisquoc Formation, Casmalia Hills, Santa Barbara Co., California, *in* Garrison, R.E., Kastner, M., and Donald, Z.H., eds, dolomites of the Monterey Formation and other organic-rich units: Pacific Section SEPM, v. 41, p. 119-140.

Hornafius, J.S., 1985, Neogene tectonic rotation of the Santa Ynez Range, western Transverse Ranges, California, suggested by paleomagnetic investigation of the Monterey Formation: Journal of Geophysical Research, v. 90, p. 12,502-12,522.

Hornafius, J. S., Luyendyk, B. P., Terres, R. R., and Kamerling, M. J., 1986, Timing and extent of Neogene rotation in the western Transverse Ranges, California: Geological Society of America Bulletin, v. 97, p. 1476-1487.

Ingle, J. C., Jr., 1981a, Cenozoic depositional history of the northern continental borderland of southern California and the origin of associated Miocene diatomites, *in* Isaacs, C. M., ed., Guide to the Monterey Formation in the California coastal area, Ventura to San Luis Obispo: Los Angeles, Pacific Section, American Association of Petroleum Geologists Special Publication 52, p. 1-8.

Ingle, J. C., Jr., 1981b, Origin of Neogene diatomites around the north Pacific rim, *in* Garrison, R. E., and Douglas, R. G., eds., The Monterey Formation and related siliceous rocks of California: Los Angeles, Pacific Section, Society of Economic Paleontologists and Mineralogists, p. 159-179.

Isaacs, C. M., 1981, Outline of diagenesis in the Monterey Formation examined laterally along the Santa Barbara coast, California, *in* Isaacs, C. M., ed., Guide to the Monterey Formation in the California coastal area, Ventura to San Luis Obispo: Los Angeles, Pacific Section, American Association Petroleum Geologists, p. 25-38.

Isaacs, C. M., 1982, Influence of rock composition on kinetics of silica phase changes in the Monterey Formation, Santa Barbara area, California: Geology, v. 10, p. 304-308.

Isaacs, C. M., 1983, Compositional variation and sequence in the Miocene Monterey Formation, Santa Barbara coastal area, California, *in* Larue, D. K., and Steel, R. J., eds., Cenozoic Marine Sedimentation, Pacific margin, USA. Pacific Section, Society of Economic Paleontologists and Minerologists Special Publication, p. 117-132.

Isaacs, C. M., and Ruellkötter, J., 1999, The Monterey Formation: From rocks to molecules: New York, Columbia University Press, p. 1-30.

Jiang, S., 2012, Clay minerals from the perspective of oil and gas exploration: Clay minerals in nature - their characterization, modification and application, Dr. Martha Valaskova (Ed.), ISBN: 978-953-51-0738-5, InTech, p. 21-38.

Keller, M. A., and Isaacs, C. M., 1985, An evaluation of temperature scales for silica diagenesis in diatomaceous sequence including a new approach based on the Miocene Monterey Formation, California: Geo-Marine Letters, v. 5, p. 31–35.

Luyendyk, B.P., Kamerling, M.J., Terres, R.R., and Hornafius, J.S., 1985, Simple shear of southern California during Neogene time suggested by paleomagnetic declinations: Journal of Geophysical Research, v. 90, p. 12,454-12,466.

Mahood, A.D., and Barron, J.A., 1996, Late Pliocene diatoms in a diatomite from Prydz Bay, East Antarctica: Micropaleontology, v. 42, no. 3, p. 285-302.

McCrory, P. A., Wilson, D. S., Ingle, J. C., and Stanley, R. G., 1995, Neogene geohistory analysis of Santa Maria Basin, California, and its relationship to transfer of Central California to the Pacific Plate: U.S. Geological Survey Bulletin, p. J1-J38.

McGuire, M. D., Bowersox, J. R., and Earnest, L. J., 1983, Diagenetically enhanced entrapment of hydrocarbons—Southern Lost Hills fractured shale pool, Kern County, California, *in* Isaacs, C. M., and Garrison, R. E., eds., Petroleum generation and occurrence in the Miocene Monterey Formation, California: Los Angeles, Pacific Section, Society of Economic Paleontologists and Mineralogists, p. 171–183.

Mees, F., 2002, The nature of calcareous deposits along pan margins in eastern central Namibia: Earth Surf. Process Landforms v. 27, p. 719-735.

Murata, K. J., and Nakata, J. K., 1974, Cristobalitic stage in the diagenesis of diatomaceous shale: Science, v. 184, p. 567-568.

Murata, K. J., and Larson, R. R., 1975, Diagenesis of Miocene siliceous shales, Temblor Range, California: U.S. Geological Survey Journal of Research, v. 3, p. 553-566.

Namson, J., and Davis, T.L., 1990, Late Cenozoic fold and thrust belt of the southern Coast Ranges and Santa Maria basin, California: American Association of Petroleum Geologists v. 74, p. 468-492.

Nicholson, C., Sorlien, C.C., Atwater, T., Crowell, J.C., Luyendyk, B.P., 1994, Microplate capture, rotation of the western Transverse Ranges, and initiation of the San Andreas transform as a low-angle fault system: Geological Society of America, v. 22 p. 491-495.

Pisciotto, K. A., 1981, Diagenetic trends in the siliceous facies of the Monterey Shale in the Santa Maria region, California: Sedimentology, v. 28, p. 547–571.

Pisciotto, K. A., and Garrison, R. E., 1981, Lithofacies and depositional environments of the Monterey Formation, California, *in* Garrison, R. E., and Douglas, R. G., eds., The Monterey Formation and related siliceous rocks of California: Los Angeles, Pacific Section, Society of Economic Paleontologists and Minerologists, p. 97-122.

Pole, M., 1996, Plant macrofossils from the Foulden Hills diatomite (Miocene), Central Otago, New Zealand: Journal of the Royal Society of New Zealand, v. 26:1, p. 1-39.

Ramirez, P.C., 1987, Sedimentary structures and depositional environments of diatomaceous strata of the Sisquoc Formation, Santa Maria area, [abs.]: American Association of Petroleum Geologists Bulletin, v. 71, p. 392.

Ramirez, P.C., 1990, Stratigraphy, sedimentology, and paleoceanographic implications of the Late Miocene to Early Pliocene Sisquoc Formation, Santa Maria area, California [Ph.D. Dissertation]: Santa Cruz, University of California, 401 p.

Ramirez, P.C., and Garrison, R.E., 1995, Stratigraphy of fine grained facies of the Sisquoc Formation, Santa Maria basin, California-Paleoceanographic and Tectonic Implications: U.S. Geological Survey Bulletin 1995-T, U, V, p. U1-U15.

Schnurrenberger, D., Russell, J., Kelts, K., 2003, Classification of lacustrine sediments based on sedimentary components: Journal of Paleolimnology, v. 29, p. 141-154.

Sorlien, C.C., Kamerling, M.J., and Mayerson, D., 1999, Block rotation and termination of the Hosgri strike-slip fault, California, from three-dimensional map restoration: Geology, v. 27, p. 1039-1042.

Stanley, R.G., Johnson, S.Y., Swisher, C.C, Mason, M.A., Obradovich, J.D., Cotton, M.L., Filewicz, M.V. and Vork, D.R., 1996, Age of the Lospe Formation (Early Miocene) and origin of the Santa Maria basin, California: U.S. Geological Survey Bulletin 1995-M, p. M1-M37.

United States Geological Survey, 2012, Assessment of potential additions to conventional oil and gas reserves in discovered fields of the United States from reserve growth, fact sheet, p. 2012-3108.

Woodring, W.P., and M.N. Bramlette, 1950, Geology and paleontology of the Santa Maria district, California: USGS Professional Paper 222, p.185.

Yang, Y., and Aplin, A.C., 2010, A permeability-porosity relationship for mudstones: Marine and Petroleum Geology, v. 27, p. 1692-1697.